Shape-from-Shading Analysis for Reconstructing 3D Object Shape Using an Image Scanner

Hiroyuki Ukida

Abstract

An image scanner is usually used to take 2D images of documents, pictures, photographs, and so on. If 3D shape information is acquired with an image scanner, the shading and geometric distortion in the unfolded book surface image can be restored and an image scanner can be used as a low-cost and easy-to-operate 3D measurement device. This study addresses problems related to the methods of recovering the 3D shape of an object from a scanned image and developing a new advantage for use of an image scanner.

Many shape-recovering methods with use of images have been proposed, such as the stereo method, the shape-from-shading method, the texture analysis method, the shape-from-focus method, etc. Among these methods, the shape-from-shading method, that is a method of reconstruction shape from a shading information in an image, is the most appropriate for a method of recovering object shape from a scanned image. Because an image scanner normally has only one CCD sensor, taking only a single image makes it difficult to use another CCD like an stereo method. But it is possible to recover the object shape from a single image by using the shape-from-shading method. Moreover, having no assumptions about the texture on the object surface makes it possible to pick up various objects as a target.

In implementing a shape-from-shading method, it is necessary to formulate the relation between the shape and shading information. But, the shape-from-shading method is an ill-posed problem because formulating the fundamental relation alone cannot determine the unique surface orientation from one shading measurement. To solve this particular problem and recover shape, therefore, we must take into account the object properties as constraint conditions for the shape reconstruction and formulate the problem based on these conditions. Accordingly, what is going to be important in solving the problem associated with the shape-from-shading method are what object to use as a target, what properties to use to recover its shape, and how to formulate the relation between shape and shading.

The object properties are classified into two types; the photometric and geometric properties. In this study, we pick up two objects whose properties differ with each other as the targets for the shape reconstruction with the use of an image scanner. One of the objects is unfolded book surface and the other, the arbitrary 3D shape whose albedo on the surface is constant like a plaster figure. Since the book surface shape is simple in terms of cross section and is assumed to be a smooth curved one, naturally it leads to the recovery of a simpler 2D cross section shape than 3D shape. However, book surface, because of the interreflections and the non-uniform albedo distribution, presents complex photometric properties. On the other hand, as for the arbitrary 3D shape reconstruction, no-interreflections and a Lambertian surface with constant albedo are assumed. Hence, its photometric properties are simpler than book surface, whereas its geometric properties are complex because there are no constraints for its shape. In this study, we are going to examine shape reconstruction methods for two targets as described above.

To estimate any object shape from its shading information, we must formulate the relation between the shape and its shading. The fundamental model of this relation is a physically-based one concerning the brightness at a certain point on the surface. However, coupled with object properties, the light source in an image scanner is modeled as the linear light source, which naturally complexes the reflectance model. Hence, when

we estimate the object shape using such complex model, we find a method of minimizing the difference of the brightness between actually observed image and the physically-based model to be an effective one. The problem is, however, that this minimization method needs much computation time on account of the physically-based model being the complex non-linear one. Moreover, because the slant, depth, and albedo of the surface in the physically-based model are mutually dependent, a method of merely minimizing brightness cannot always acquire an object shape correctly. Therefore, further consideration has to be paid so as to estimate object shape more efficiently and precisely.

When we assume shape and shading information to be "pattern" data in a region on the surface, not "point" data, we can model the relation between shape and shading as a simple linear transformation, which is to be obtained from samples of actually observed shape and shading patterns. This modeling is called "appearance-based modeling". Under such linear transformation, a shape pattern can be reconstructed from a shading pattern much faster than under the method of minimizing complex physically-based model. But, there is a problem with such linear transformation; this method requires an enormous amount of shape and shading patterns, so they have to be restricted to the subject shape patterns. In other words, we must consider the shape class of the object for this appearance-based model. Therefore, this modeling is appropriate for the reconstruction of book surfaces with limited variation and is not suited to the reconstruction of arbitrary 3D shapes.

In conclusion, under this study as developed hereinafter, we propose methods of (1) the book surface shape reconstruction under the physically-based model and the appearance-based model, and (2) the arbitrary 3D shape reconstruction under the physically-based model.

As far as the problem with the book surface shape reconstruction using the physically-based model, the most important characteristic is the interreflections which are the reflections on one side of the book surface illuminating the other side. In this problem, the brightness of the interreflections must be estimated for the shape reconstruction. But, it depends on both the book surface shape and the albedo distribution. Hence, it is necessary to recover the shape and the albedo on the book surface simultaneously. Moreover, the computational cost of the interreflections become extremely high because the global shape and overall albedo distribution of the book surface are required to compute the interreflections. To get over these problems, and to recover the shape and albedo for their mutual dependency, we propose the iterative and non-linear optimizing algorithm. And we also propose the piecewise descriptions about the book shape and the albedo distribution to reduce the computational costs. By using these methods, the real book surface shape can be reconstructed efficiently and stably. And we also propose the method to restore the geometric and photometric distortions in the book surface image. By using the proposed method, the readability of the book surface can be improved.

To reconstruct the book shape by using the appearance-based model, some shape and shading profile data corresponding to the cross section of the book surface are used as the pattern data. These profiles are preserved in the eigenspaces to reduce the data size, and the book surface shape is reconstructed by the linear interpolation in the eigenspaces from the shading information in the input scanned image. To estimate the book surface shape precisely, we normalize the shape and shading profiles to the shift-invariant profiles, and we use the linear interpolation including the error terms induced by the linear approximation. By using this method, the book surface shape can be reconstructed much faster than

using the physically-based model. Hence, the proposed method is effective for practical applications.

As for the arbitrary 3D shape reconstruction using the physically-based model, because of the characteristics of the linear light source in the image scanner, the surface orientation (two degrees of freedom) and the distance between the light source and the surface should be estimated to recover the shape. Actually, however, they are mutually dependent. Therefore, to add the constraints for the shape reconstruction, we use a color image scanner which has three light sources. The location of each light source is different from the other, so this scanner can take a color image in which the color of the object surface is different from the actual one depending on its shape. From the difference of the surface color, the object shape can be reconstructed by the following two step algorithm; the first is the rough estimation by the iterative computation of the linear equations, and the second is the optimal estimation by non-linear least squares. By using this method, the arbitrary 3D shape can be reconstructed, and its surface color is also restored. This result shows that the image scanner can be used as the shape measurement device.

In this paper, we discuss the 3D shape reconstruction problem from the scanned image. From a viewpoint of the object properties and the relation between the shape and shading, we propose the shape recovering methods to obtain the 2D book surface shapes by using the physically and appearance based model and we also propose the method to reconstruct the arbitrary 3D shape by the physically-based model. This study demonstrates that even if the photometric environment is complicated such as the image scanner, the shape information can be recovered from the shading information in the image.

Contents

Acknowledgements

I would like to thank Professor Takashi Matsuyama in Kyoto University for giving me an opportunity to study this thesis when I was a student in Okayama University and having instructed me till today.

I also wish to thank Professor Toshikazu Wada in Wakayama University and Professor Naoki Asada in Hiroshima City University for giving comments and guidance on my study.

I would like to thank Professor Katsunobu Konishi in Tokushima University for extending me guidance and advice, which were so helpful in developing my thesis.

My thanks also go to Professor Hideki Yamamoto in Okayama University for continuous encouragement and advise.

Special thanks must go to Mr. Masaki Yamamoto who helped proofread the English version of abstract, Chapter 1 and 2 of this paper. (Although of course I am solely responsible for any errors.)

I also appreciate all the help and assistance extended to me by the members of Matsuyama laboratory in Okayama University from 1991 to 1995, and the students of Robotics laboratory in Tokushima University since 1995.

Last but not least, I am most grateful to my family for having spiritually supported me in my study.

Chapter 1

Introduction

Image scanners are usually used to obtain 2D images of documents, pictures, photographs, and so on. When we use a flatbed scanner to take an image of printed papers of a book, the scanned image has the shading and the geometric distortion around the gutter (the binding margin of the book pages) because book papers form curved surface on the image scanner. But, if curved book surface shape is measured, the shading and the geometric distortion can be restored. Moreover, if the image scanner can measure not only the book surface but also other object shape, it will be used as a low-cost and easy-to-operate measurement device. In this study, from the view point of the computer vision, we address the problem of recovering the 3D shape of an object from a scanned image so as to develop a new advantage for the image scanner.

Estimating 3D information from a 2D image is the fundamental problem in the computer vision. In this problem, the 3D information is calculated from various cues in the image such as the color, shading, texture, and so on. As the typical methods, stereo and shape-from-X (X is focus, silhouette, texture or shading, etc.) are proposed. Among these methods, *shape-from-shading* [1], which estimates object shape from the brightness (shading) of the reflection on its surface in observed image, is appropriate for the shape reconstruction using the image scanner. This is because of the following reasons:

- *Stereo method*[2] obtains the depth from the disparity of corresponding points in images taken by two or more cameras. But, the image scanner usually has one CCD image sensor, hence it is impossible to get multiple images like stereo method.

- *Shape-from-focus* estimates the focus position using some images taken by the different focal length, and obtain the depth from the camera to the object[3]. But, the focal length of CCD sensor in the image scanner is usually fixed, hence it is also impossible to apply this method.

- *Shape-from-silhouette* estimates the 3D shape from the outline of the object in the image. In [4], this method is applied for the book shape reconstruction for a scanned image. But, since it is necessary to acquire the outline of the book surface in the scanning, the book size and its arrangement are limited.

- *Shape-from-texture* estimates the 3D shape from the distortion of the texture pattern in the image. As the related study using the image scanner, some methods which estimate the distortion of lines[5] or the size variation of letters at each line[6] in the

document image are proposed. But, in order to apply this method, we must assume the texture pattern. Hence, it is difficult to recover general objects.

By using the shape-from-shading method, we will be able to measure 3D shapes with an off-the-shelf image scanner and an application software; there is no need to develop a new scanner with additional CCD sensors such as stereo method. In addition, the shape-from-shading method is not so tight about the object arrangement and texture pattern. Hence, the shape-from-shading method is appropriate for the shape reconstruction using the image scanner.

In implementing a shape-from-shading method, it is necessary to formulate the relation between the shape and shading information. And, by using this relation, the shape information is obtained from the brightness (shading) information on the surface in the image. But, the brightness of the reflection on the surface is varied with not only the surface shape but also other factors. Hence, the shape-from-shading problem is an ill-posed problem which cannot determine a unique surface shape from only an observed brightness information. In order to solve this problem, it is necessary to use various properties of the object as constraint conditions for problem solving. In other words, it is important that what properties we use to recover its shape and how to analyze the relation between the shape and shading.

The properties used in the shape-from-shading method are classified into two types; the photometric and geometric properties. And these properties are included in both the image scanner and the object for the shape reconstruction. The photometric property of the image scanner is the characteristic of the light source, and the geometric properties are the arrangement of the light source and the CCD sensor and a way of the image projection. The light source of the image scanner is formulated as the moving linear light source model, hence its photometric model is more complex than the parallel light source because the reflection on an object surface is changed by both the surface normal direction and the distance between the light source and the object surface. But, this characteristic implies that we can obtain not only the surface normal vectors (relative shape information) but also the depths of the object (absolute shape information). In order to realize to obtain these shape information, the photometric and geometric properties of the image scanner are assumed to be known a priori. This assumption is reasonable because these properties can be estimated by the calibration of the image scanner.

On the other hand, as the photometric properties of the object itself in the photometric models of the reflection on the object surface, we can consider the following properties:

- The interreflections,
- The reflectance property, and,
- The albedo distribution.

About these properties, if we assume that:

- No interreflections,
- Only the diffuse reflection (Lambertian surface), and,
- The uniform albedo distribution,

then, we can formulate simple photometric model. In other words, assuming these properties makes the ideal condition for the shape-from-shading problem. But, in the real world condition, we must take account into following properties:

- The existence of the interreflections,
- The diffuse and specular reflection, and,
- Non uniform albedo distribution.

Under such conditions, the photometric model become more complex than the ideal one. The geometric properties caused by the object can be also classified into the simple and complex properties, that is,

- Simple geometric property:
  When the object shape can be assumed some mathematical models, the geometric property become simple, because the object shape can be described by a few parameters. In this case, the shape reconstruction is done as the parameter estimation.
- Complex geometric property:
  When the object shape cannot be assumed any models, the geometric property become complex. Because, in order to describe the object shape, we must use the normal vectors or depths at all points on the object surface. In this case, the shape reconstruction is done by estimating the normal vectors or depths all over the surface.

Accordingly, the properties of the shape-from-shading problem caused by the object are classified into the following four types:

Type 1. The photometric and geometric properties are simple.

Type 2. The photometric property is complex and the geometric property is simple.

Type 3. The photometric property is simple and the geometric property is complex.

Type 4. The photometric and geometric properties are complex.

Therefore, in the shape-from-shading problems, we must use appropriate analysis models for each property type. As the analysis models of the relation between the shape and the shading, we employ the following models:

Model A. The physically-based model.

Model B. The appearance-based model.

The physically-based model formulates a physical relation between the reflection and the shape on an object surface. The appearance-based model constructs a shape and shading relation by using observed sample data of shape and shading appearance. Therefore, the shape-from-shading problem is characterized by combining the object properties with the analysis models.

In previous studies of the shape-from-shading problem, the case of type 1 of the object property using model A and B have been discussed. In order to simplify the modeling, these studies usually assume the following conditions:

- The illumination is parallel light source and its brightness is constant.
- The object surface is Lambertian.
- The albedo is constant all over the surface.
- The surface shape is smooth.

But, it is difficult to assume such ideal situation in the real world. In this paper, we propose the shape-from-shading method in case of the type 2 and 3 of the object properties with model A and B as the real world problem. On the other hand, in case of the type 4, because the analysis model becomes very complex in both the model A and B, it is difficult to deal with this case.

As the actual target of the object property type 2 for the shape reconstruction, we deal with the unfolded book surface shape. By using the estimated book shape, the shading and distortion in a book scanned image can be restored, hence it is useful to obtain the book shape. The book surface forms the smooth curved shape, and we can reconstruct only the 2D cross section shape. Hence, the geometric property of the book surface shape is simple. But, to estimate the book shape, we must take into account the interreflections[7], the non-uniform albedo distribution, and the linear light source in the image scanner, hence the photometric properties are very complex. In this paper, we develop the book surface shape reconstruction method by using both the physically and appearance based models.

We also deal with the shape reconstruction of 3D arbitrary shape object as the actual target of the property type 3. This target has no restriction for its shape but assuming a Lambertian surface, an uniform albedo, and no interreflections. Hence, the geometric property of this target is more complex, but the photometric property is simpler than the book surface shape. However, the characteristic of the linear light source in the image scanner is still remained, the photometric property is more complex than the ideal situation. To the type 3 object, we can apply the physically-based model, but cannot apply the appearance-based model. Because the 3D arbitrary shape has no restriction for its shape, we must use an enormous amount of shape and shading appearance data. But, it is difficult to sum up such appearance data to construct the shape and shading relation. Therefore, we develop the 3D arbitrary shape reconstruction method by using the physically-based model.

This paper is organized as follows. First, in chapter 2, we survey the previous shape-from-shading studies from the viewpoint of what characteristics are used for the shape reconstruction methods. And, we show the position of our studies in shape-from-shading methods.

Next, in chapter 3, we describe the characteristics of the image scanner. The most important characteristics of the image scanner is the property of the light source which is modeled as the linear light source. This characteristics makes the photometric models complex, but by using this characteristics, both the slant and the depth of the object surface can be estimated. Moreover, the parallel projection of the image scanner is effective for the shape reconstruction using the appearance-based model.

In chapter 4, we address the book surface shape reconstruction problem using the physically-based model. In this shape-from-shading problem, the most important characteristic is the interreflections which are the reflections on one side of the book surface

and illuminate the other side. In this problem, we must estimate the brightness of interreflections. But, it depends on both the book surface shape and the albedo distribution. Hence, it is necessary to recover the shape and the albedo on the book surface simultaneously. Moreover, the computational cost of the interreflections becomes extremely high because the global shape and albedo distribution are required to compute the interreflections. To get over these problems, and to recover the shape and albedo for their mutual dependency, we propose the iterative and non-linear optimizing algorithm. And, in order to reduce the computational costs, we also propose the piecewise descriptions about the book shape and the albedo distribution. In the experiments, we demonstrate that the real book surface shape can be reconstructed efficiently and stably by the proposed method and the readability of the book surface image can be improved.

In chapter 5, we propose the method to reconstruct the book shape by using the appearance-based model. Here, the relation between the shape and shading is constructed by some shape and shading profile data corresponding to the cross section of the book surface. These profiles are preserved in the eigenspaces to reduce the data size. We propose the method to obtain the shape profile from the input shading profile by using the local linear transformation between the shading and shape eigenspaces which can be regarded as the shape and shading relation. Moreover, to estimate the book surface shape precisely, we also propose the linear interpolation method including the error terms induced by the linear approximation, and the shape and shading profile normalization method which makes them "the shift-invariant profiles" on the scanning plane. We show that the proposed method can reconstruct the book shape in practical time in experiments.

The method for the arbitrary 3D shape reconstruction using the physically-based model is proposed in the chapter 6. Because of the characteristics of the linear light source in the image scanner, it is necessary to estimate the surface orientation and the distance between the light source and the surface to recover the shape. But, from the photometric models of this problem, they are mutually dependent. Therefore, to add the constraints for the shape reconstruction, we use a color image scanner which has three light sources. By using three shading information, in order to estimate the object shape efficiently and precisely, we propose the following two step shape reconstruction algorithm; the first is the rough estimation by the iterative computation of the linear equations, and the second is the optimal estimation by non-linear least squares. As the experimental result, we demonstrate the effectiveness of the proposed method by recovering real object's shape.

And finally, we conclude this study and show the residual problems and the future works in chapter 7.

Chapter 2

Related Works: A Survey of Shape-from-Shading Analysis Methods

In this chapter, we survey the shape-from-shading methods. Here, we classify previous studies from the viewpoint of what characteristics are used for the shape reconstruction. Figure 2.1 and 2.2 show the summary of this chapter. And, we clarify the position of our studies in shape-from-shading methods.

2.1 Shape Reconstruction from a Single Image Using Physically-Based Models

2.1.1 Ideal Condition

Shape reconstruction methods from an image brightness has been studied by Horn[8] in 1970s. The phrase,"shape-from-shading" has also been used since that time. In early shape-from-shading studies, a reflectance model was formulated under ideal conditions as follows:

1. The illumination is parallel and constant brightness (a distant point light source), and the direction of the light source is known,
2. The object surface is Lambertian,
3. The albedo distribution on the surface is uniform and known.

By using these conditions, parameters in the reflectance model can be determined except for the surface slant. Hence, the object shape would be recovered by estimating the surface slant. But, it is difficult to determine two parameters of the surface slant from one image brightness data on the surface. Therefore, Horn added another condition such as:

4. The object surface is smooth.

	Physically-based Model				
	Single Image				Multiple Images
year	Ideal Condition	Constrained Shape	Interreflections	Combining Other Methods	Photometric Stereo
1970	Horn (1975) - characteristic stripes - propagation				
1980	Ikeuchi & Horn (1981) - minimization - occluding boundary Brooks & Horn (1985) - estimate shape and light direction - alternative algorithm Horn & Brooks (1986) - minimization - integrability Frankot & Chellappa (1988) - enforcing integrability Lee (1988) - spline	Pentland (1984) - local spherical shape - estimate light direction Lee & Rosenfeld (1985) - isotropic surface orientation distribution - estimate light direction Asada (1987) - cylindrical shapes Ferrie & Levine (1989) - sphere, elliptic, hyperbolic		Blake et al. (1985) - binocular stereo Malik & Maydan (1989) - line drawing interpretation	Woodham (1980) - three light sources - estimate slants and albedo Ikeuchi (1981,1982) - look up table - glossy object
1990	Vega & Yang (1993) - shading logic	Zeng & Chellappa (1991) - local spherical shape - boundary brightness - estimate light direction, albedo Asada & Nakamura (1993) - cylindrical shapes Wei & Hirzinger (1997) - radial basis functions	Nayar et al. (1990) - shape and albedo Yang et al. (1995) - two surface normals of planes	Choe & Kashyap (1991) - shape from texture Banerjee et al. (1992) - binocular stereo	
2000		Zhao & Chellappa (2001) - symmetric objects			
Chapter 4		◯	◯		
Chapter 5		◯			
Chapter 6					◯

Figure 2.1: Shape-from-shading studies classified by characteristics (part 1).

Physically-based Model					Appearance-based Model
Multiple Images					
Reflectance Properties	Interreflections	Lighting Condition	Non-parallel Light Source	Color	
Iwahori et al. (1988) - Phong's model	Iwahori et al. (1986) - minimization - three light sources		Iwahori et al. (1988) - three and more point light sources - estimate albedo,slants, depths Kamei & Yamaguchi (1988) - two point light sources - surface smoothness		
Nayar et al. (1990) - original diffuse and specular model Tagare & deFigueiredo (1991) - Torrance-Sparrow's model Tagare & deFigueiredo (1993) - m-lobed reflectance map	Cho et al. (1997) - book surface shape - remove interreflections - two light sources	Onn & Bruckstein (1990) - two light sources - smoothness Iwahori et al. (1991) - estimate three light source direction Lee & Kuo (1993) - two light sources - perspective projection Yang et al. (1995) - two light sources - surface normals of polyhedron	Kim & Burger (1991) - four point light sources - textured surface Cho &Minamitani(1993) - three point light sources - using light source direction	Kaneko et al. (1993) - color light sources Christensen & Shapiro (1994) - color surfaces	Murase&Nayar(1994) - pattern recognition - parametric eigen space method Okatani & Deguchi (1995) - quadratic curved surfaces by parametric eigen space method
◯			◯ linear light source, single image		
					◯
			◯ linear light source	◯	

Figure 2.2: Shape-from-shading studies classified by characteristics (part 2).

And, he presented the shape reconstruction method by propagating estimated shape information in [8]. In this method, the surface slant estimation starts from "the singular point" which has the maximum brightness[1] in the image, and then adjacent surface slants are estimated successively along paths called "characteristic stripes" on which the image brightness varies under a condition derived from the surface smoothness, that is, the difference between adjacent surface normals is small.

Ikeuchi and Horn (1981)[9] proposed a method based on the minimization. They formulated an objective functional including terms which are the difference between the observed brightness and the reflectance model, and the difference of adjacent surface slants in the whole image. The surface slants were estimated by minimizing the objective functional using an iterative algorithm. In this method, in order to use the occluding boundary condition[2], the surface slants were transformed to "stereographic coordinates". Horn and Brooks (1986)[10] were also proposed the minimization method. In their study, as the smoothness condition, a penalty term related to the shape integrability was introduced to the objective functional. At a later time, the robustness of the minimization method was reported by Zhang et al. (1999)[49].

Brooks and Horn (1985)[11] also discussed the shape reconstruction in case of unknown light source direction. Since the brightness on the surface is dependent on both the surface shape and the light source direction, they employed an iterative algorithm which estimated surface slants and the light source direction alternatively. Frankot and Chellappa (1988)[12] improved Brooks and Horn's method. In order to recover smooth surfaces, they enforced integrability on the estimated shape in each loop of the iterative algorithm. This method improved the robustness against the noise. On the other hand, Lee (1988)[13] denoted another method in which the estimated shape was approximated to the spline curve. This study used the iterative algorithm on the assumption that the light source direction is known. The uniqueness and convergence of the recovered shape were proved in this study. Vega and Yang (1993)[14] applied three heuristic methods called "Shading Logic" (the weighted neighbor operation, the minor slant adjustment operation, and the normal complementary operation) to improve the stability of Brooks and Horn's method.

2.1.2 Constrained Shape

In the shape-from-shading studies described in previous section, the object shape is represented as a set of the normals (slants) at each point on the surface. But, if a strong constraint about the object shape could be assumed, we will be able to estimate not only the shape but also other properties. Pentland (1984)[15] proposed the method which estimates both the shape and the light source direction by assuming the local spherical shape on the object surface. But, since this method used the first and second derivatives of the image, the estimated shape was not stable against the noise.

Lee and Rosenfeld (1985)[16] estimated the light source direction by assuming the isotropic distribution of the surface orientation. And, they recover the surface normal by using the first and second moments of the image brightness distribution. This method was

[1]The surface normal of this point equals to the direction of the light source.

[2]Under orthogonal projection, the surface normal at the occluding boundary is perpendicular to a view direction.

stabler than Pentland's method. Zeng and Chellappa (1991)[17] proposed the method to obtain the light source direction and the surface albedo by assuming the local spherical shape and using the boundary brightness. The object shape was represented as the surface slants and depth and it was recovered by the iterative algorithm changing the image resolution from coarse to fine.

Asada (1987,1993)[18],[19] showed the methods to recover cylindrical shapes. In these methods, the base (planer) and cylindrical surface were classified by using the analysis of [15]. And then, the cross section shape and the direction of the generating lines on the cylindrical surface were estimated. This method did not need the knowledge of the light source direction and the surface albedo, but the surface normal of the base plane and the direction of the generating lines could not be determined uniquely.

Ferrie and Levine (1989)[20] improved Pentland's method by representing the shape as the mathematical models of the local sphere, elliptic, and hyperbolic. Wei and Hirzinger (1997)[21] used the radial basis functions, which are the sum of two-dimensional Gauss distribution with various parameters, to represent the object shape. They estimated parameters of these functions changing the image resolution from coarse to fine. Zhao and Chellappa (2001)[22] proposed the reconstruction method of symmetric objects such as a human face. This method assumed the symmetry both the shape and albedo distribution and estimated the light source direction, the surface slants and albedos of the object.

2.1.3 Interreflections

When the object shape is concave or some objects are located closely, the surface is illuminated by both the light source and the reflection from other surface. The illuminations from other surface are called "interreflections" or "mutual illuminations". We can not ignore these phenomena for the shape reconstruction in the real world environment.

Nayar et al. (1990)[23] addressed the shape-from-interreflections problem. They pointed out that this problem is "the chicken and egg problem", because the shape estimation needs the interreflections brightness and vice versa. Moreover, if the albedo on the surface is not known, since it also effects the interreflections brightness, the shape and albedo distribution must estimate simultaneously. They formulated the physically-based model taking into account the interreflections, and proposed the method to estimate the shape and albedo alternatively from a single image by the iterative algorithm after "the pseudo shape" was estimated by the photometric stereo method we describe below.

Yang et al. (1995)[24] also addressed the interreflections. They estimated two surface normals of planes constructing concave like a folded paper. They showed the uniqueness of two surface normals by using the interreflections as constraints.

2.1.4 Combining Other Methods

In order to supply the lack of conditions in the shape-from-shading problem, the combinations of the shape-from-shading and other methods are proposed. Blake et al. (1985)[25] and Banerjee et al. (1992)[26] combined the binocular stereo method with the shape-from-shading. In order to apply the stereo method, the albedo on the surface is not constant. These methods, first, obtained "sparse" depth map by the stereo at the edge

part of the region on the surface, and then, "dense" shape in the constant albedo region was recovered by using sparse depth map.

Malik and Maydan (1989)[27] combined the line drawing interpretation with the shape-from-shading. By extracting line parts in image, discontinuous part of the surface could be found and divided into smooth regions in which the shape could be estimated by the shape-from-shading method. The line drawing interpretation could provide convex or concave information for the shape-from-shading. Moreover, from the result of the shape-from-shading, incorrect labeling of the line drawing could be corrected.

Choe and Kashyap (1991)[28] use the shape-from-texture method with the shape-from-shading. In this study, the albedo distribution on the surface was modeled as a sum of the uniform background and the random pattern texture. The input image was divided into small regions. This method estimated the surface normal vectors and the texture parameters by a statistic method in each small region.

2.2 Shape Reconstruction from Multiple Images

2.2.1 Photometric Stereo

As another method to supply the lack of conditions in the shape-from-shading problem, the shape reconstruction from multiple images changing the illumination condition (ex. the light position) was proposed. This method is called "the photometric stereo" and has been discussed by Woodham (1980)[29]. From the physically-based model of the reflection, a set of slants corresponding to a brightness on the surface plots a curved line in the gradient space spanned by two slant parameters. Therefore, if three images (brightness) exist, the surface slants can be determined uniquely as the point crossing three curves. In this method, the assumption of the surface smoothness is not necessary. In [29], the surface slants and albedo were estimated by using three images which were taken under different light positions. Note that in the photometric stereo method, since images are obtained from the same camera position, there is no problem of identifying correspondence between images such as the binocular stereo method.

Ikeuchi (1981,1982)[30],[31] applied a look-up-table (LUT) technique to the photometric stereo. The look-up-table denoted the correspondence of the surface brightness and slants. This table was constructed from images of an object which had known shape. Since this method used observed data, properties of the light source and surface reflectance were not restricted. This experiment showed the glossy object shape reconstruction under the linear light sources.

2.2.2 Reflectance Properties

According to the material of an object, not only the diffuse reflection but also the specular (glossy) reflection are observed. Therefore, the reflectance property on the surface is modeled as a combination of the diffuse and specular components [50],[51],[52]. Since the reflectance property is different with respect to the object, estimating its parameters is also an important problem.

Iwahori et al. (1988)[32] used Phong's model[53] for the reflectance property. They showed the method to estimate the surface slants and the reflectance property parameters

from three images which were obtained by different light positions.

Nayar et al. (1990)[33] employed original reflectance property combining diffuse and specular components. They estimated the reflectance property and the object shape from many images. But this method had conditions with respect to the light source direction, surface normals and the viewing direction, hence, only the cylindrical shape could be recovered.

Tagare and deFigueiredo (1991)[34] employed the Torrance-Sparrow's model[54] for the reflectance property, and estimated the reflectance parameters and the object shape using eight images. And then, they proposed general reflectance property model, called "m-lobed reflectance map"[35], and showed the method of the shape reconstruction using three images.

2.2.3 Interreflections

The photometric stereo method has been also applied to the shape-from-interreflections problem. Iwahori et al. (1986)[36] formulated an objective functional from the physically-based model taking into account the interreflections. The surface shape was estimated by minimizing the objective functional using three images obtained by different light source position.

Cho et al. (1997)[37] recovered the book surface shape from two images. In this method, the effects of the interreflections were removed from the observed images by using their heuristic method, and then the book surface shape was estimated.

2.2.4 Lighting Condition

In order to determine shape parameters (slants or surface normals), the photometric stereo method needs three or more light sources whose positions or directions are known. On the other hand, Onn and Bruckstein (1990)[38] showed a shape reconstruction method using only two light sources. In this method, the surface smoothness was assumed. Lee and Kuo (1993)[39] also proposed a method using two light sources with perspective projection. In their method, an object surface was divided into triangular patches, and the relative depth of nodal points in patches were estimated. Yang et al. (1995)[40] estimated surface normals of a polyhedron using two images. They analyzed locations of two surface plane normals and a line between them in the gradient space, and removed ambiguity of the estimated surface normals.

Iwahori et al. (1991)[41] proposed a shape reconstruction method under the condition that one of two parameters of light source directions were unknown. They used three images and estimated light source directions, albedo, and surface normals by a minimization process.

2.2.5 Non-Parallel Light Source

In the shape-from-shading studies we described above, the light source is modeled as the parallel light source whose intensity is constant. But, there are many different types of light sources in real world. [55] shows modelings of various light sources. For example, the illumination of a fluorescent tube is modeled as a linear light source whose intensity

is attenuating with respect to the distance from the light source, and an incandescent lamp is modeled as a point light source whose intensity is attenuating to the distance squared. In previous shape-from-shading studies, a single distant point light source was approximated to the parallel light source. But, this approximation does not match in real characteristics of the light source. Therefore, the shape-from-shading under non-parallel light source must be discussed.

Iwahori et al. (1988)[42] used three and more point light sources. They estimated the surface albedo, slants, and depths. Because the illuminant intensity of the point light source varies with the distance, both the slants and depths can be estimated. Kamei and Yamaguchi (1988)[43] showed a shape reconstruction method using two point light sources under the surface smoothness assumption.

By using four point light sources, Kim and Burger (1991)[44] proposed a method to estimate albedos, slants, and depths of a textured object surface. They also discussed the alignment of light sources.

Cho and Minamitani (1993)[45] also used three point light sources. But they did not take into account the attenuation of the illumination. They proposed a shape reconstruction method using the difference of the light source direction with an object height.

2.2.6 Color

In the shape-from-shading problem, monocular images are mainly used because the brightness of a surface is main cue for the shape reconstruction. But color information is also used in the shape-from-shading. Kaneko et al. (1993)[46] used color light sources, red, green, and blue. They proposed a shape reconstruction method from a color image obtained by illuminating three color light sources simultaneously. Their method employed a look-up-table technique similar to [30]. By using a white reference sphere, correspondences between color information and surface slants were obtained. The shape reconstruction of colored surface object was also discussed. In this case, the color information was corrected using the white light source.

Christensen and Shapiro (1994)[47] proposed a colored surface shape reconstruction method using three white light sources. In this method, the look-up-table was obtained by the physically-based model for each light source and each object color. And then, the surface slants were estimated from the observed color information using the look-up-table. Since one color information corresponded to many surface slants, they discussed a method how to select the surface slants.

2.3 Appearance-Based Model

The appearance-based model is one of statistical object models using images of object's appearance. This model is often employed in pattern recognition methods. Since appearance images tend to become large data size, they are preserved in their eigenspace to reduce data size. Murase et al. [63] improved this method and proposed "the parametric eigenspace method" which can do both the object recognition and its pose parameters estimation. After this method was reported, the appearance-based model has been used for various parameter estimation process.

Okatani and Deguchi (1995)[48] applied the appearance-based model to the shape-from-shading problem. In this method, various appearance images of quadratic curved surfaces were obtained using the physically-based model, and these images were preserved in the eigenspace with quadratic surface parameters. The surface shape is reconstructed by estimating quadratic surface parameters with the linear interpolation in the eigenspace at each divided rectangular of the input image.

By using the appearance-based model method, the surface shape can be recovered more faster than the physically-based model method. But, in order to estimate various surface shapes, the appearance-based model requires many appearance images. The method in [48] solved such problem by restricting the object shape to the local quadratic surface. Hence, it would be difficult to recover general surface shape by using the appearance-based model. But, if the object shape is restricted under some constraints described in Sect.2.1.2, the appearance-based model is effective for the shape reconstruction.

2.4 Shape from Shading Problem in This Paper

As shown in Fig.2.1 and 2.2, the shape-from-shading problem started from the ideal environment, and its performance has been improved as a result of adopting real world characteristics as coming down in time. In this paper, we also address real world shape-from-shading problems. In chapter 4, we are going to show the method to recover the book surface shape from a single scanned image. The main characteristics of this shape-from-shading problem are *a cylindrical (constrained) book surface*, *interreflections*, *specular reflection* and *the linear light source* in the image scanner. In chapter 5, we propose the shape reconstruction method for *cylindrical book surface* using *the appearance-based model*. And, chapter 6 shows an arbitrary shape reconstruction using *color image* obtained by *three linear light sources*. Hence, the shape-from-shading problems in this paper includes various real world characteristics more than previous studies.

Chapter 3

Image Scanner

In this chapter, we describe characteristics of the image scanner used in this study. First, we show the structure of the image scanner. Next, we describe a formulation of the light source of the scanner. The property of the light source is the most important characteristic in the scanner. And then, we present the effectiveness of the image scanner for the shape-from-shading problem by using the scanner characteristics.

3.1 Structure of Image Scanner

Figure 3.1 shows the structure of the image scanner of our problem. The image scanner consists of the light source L, the linear CCD sensor D, the mirror M and the lens C. They are arranged under the flat scanning plane.

The coordinate system of this scanner is introduced as shown in Fig.3.1. The x-axis is parallel to the sensor D and the y-axis is parallel to the scanning direction. They are arranged on the scanning plane. The z-axis is perpendicular to the scanning plane. It denotes a height on this plane.

The sensor D takes a 1D monochrome image $P^*(x_i)$ along the scanning line S and moves with L, M and C. The sequence $P^*(x_i)$ forms a 2D image $P^*(x_i, y_j)$. Note that while $P^*(x_i)$ is obtained by the perspective projection, the projection along the y-axis is equivalent to the orthogonal projection.

3.2 Light Source

The light source of the image scanner is a long and narrow fluorescent tube and the cover around the tube restrict the illumination to radiate an object on the scanning plane only from the slit (Fig.3.2). Here, we assume that the width of the slit is small and the length of the light source is much longer than objects for the shape reconstruction, the light source is modeled as the linear light source[55], which is a sequence of point light sources.

When the scanning line S locates at y_j on the scanning plane, the illuminant intensity distribution $I_s(y, z, y_j)$ at (y, z) on $y - z$ plane is represented as follows:

$$I_s(y, z, y_j) = \frac{\alpha \cdot I_D(\psi(y, z, y_j))}{\sqrt{(y - (y_j - d_1))^2 + (z + d_2)^2}} + I_e \tag{3.1}$$

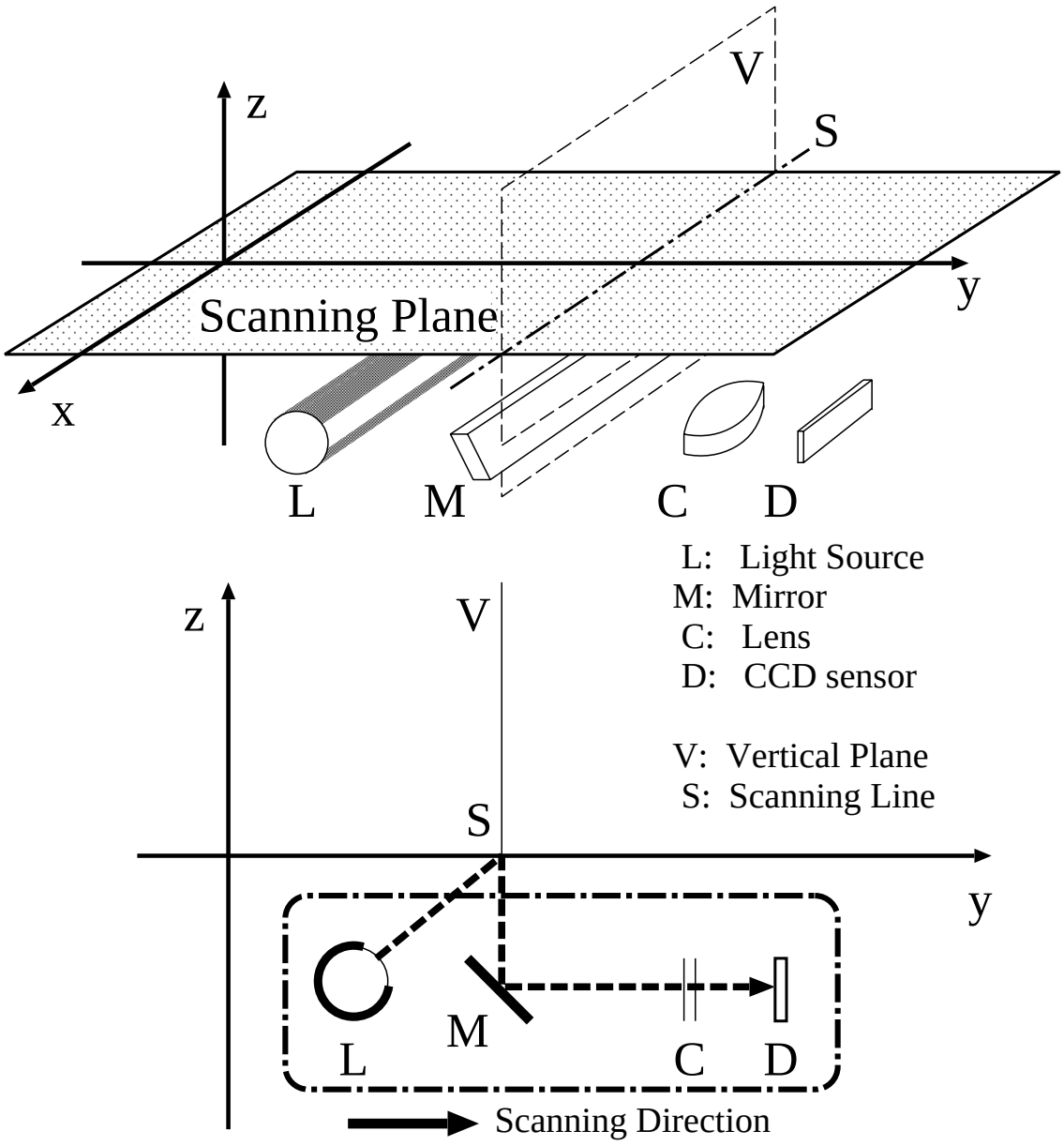

Figure 3.1: Structure of image scanner.

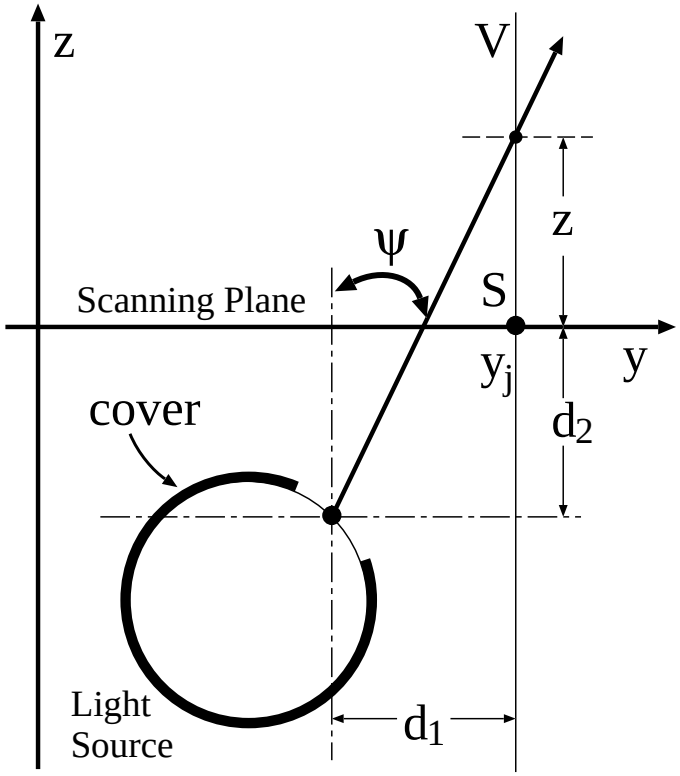

Figure 3.2: Direction and location of light source.

$$\psi(y, z, y_j) \quad = \quad \arctan\left(\frac{y - (y_j - d_1)}{z + d_2}\right) \tag{3.2}$$

where $(y_j - d_1, -d_2)$ denotes the location of the light source on the $y - z$ plane, α the parameter of the illuminant intensity, $\psi(y, z, y_j)$ the angle between the vertical line and the light source direction, $I_D(\psi(y, z, y_j))$ the directional distribution of the illuminant intensity, and I_e the environment light intensity caused by the scattered reflection in the scanner. α, I_e and $(-d_1, -d_2)$ are estimated before the shape reconstruction.

The directional distribution $I_D(\psi(y, z, y_j))$ is caused by the cover around the light source. Because of this property, the light source cannot illuminant isotropically on the $y-z$ plane (Fig.3.3). Since it is difficult to model $I_D(\psi(y, z, y_j))$, its property is estimated from the observed data of the illuminant intensity (Sect.4.6.1).

3.3 Characteristics of Image Scanner

3.3.1 Shape and Depth with Linear Light Source

As shown in Sect.3.2, the light source of the image scanner is modeled as the linear light source, hence the intensity of the reflection on an object surface is changed by both the surface normal direction and the distance between the light source and the object surface.

Figure 3.3: Directional distribution of illumination.

This characteristic makes the physically-based model more complex than the previous shape-from-shading study using the parallel light source.

But, we can calibrate the configuration of the light source and the CCD sensor under the scanning plane and the photometric property of the illumination as shown in later sections (Sect.4.6.1 and Sect.6.4.1). Therefore, by using the property of the linear light source, we can obtain not only the surface normal vectors which can be regarded as the relative shape of the object but also the absolute depth (position) of the object from the physically-based model and the observed intensity of the reflection on the object surface.

3.3.2 Appearance-Based Model and Scanning Projection

The image scanner takes an image of an object on the scanning plane by combined two projections; the perspective projection along x-axis and the parallel projection along y-axis as shown in Sect.3.1. Hence, if the object on the scanning plane moves along x-axis, both the position and the appearance of the object are changed in the scanned image. On the other hand, if it moved along y-axis, the position is also changed but the appearance is not changed in the scanned image.

In the shape reconstruction using the appearance-based model, it is necessary to obtain many sample images which are different appearances of an object. But, if we can arrange object appearances in scanned images at same y position, it is not necessary to obtain sample images changing object y position. Therefore, by using the property of the parallel projection of the image scanner, we can reduce the number of sample images. This is an effective characteristic in the use of the appearance-based model.

In the following chapters, we show the shape reconstruction methods using scanner characteristics.

Chapter 4

Shape Reconstruction of Unfolded Book Surface from a Scanned Image

4.1 Introduction

In this chapter, we formulate the shape reconstruction problem of the book surface from its image taken by the image scanner as the shape-from-shading problem with the physically-based model of the relation between the shading and the shape.

When we copy the printed paper of the book, since it is difficult to contact the whole pages with the scanning plane, the gutter (the binding position of pages) is laid apart from the scanning plane and the printed paper to be copied forms the curved surfaces (Fig.4.1). In such situation, the scanned image has the shading and the geometric distortion around the gutter. But if the 3D shape of the book surface can be estimated, these distortions can be restored, and the readability of the scanned image can be improved without breaking the book pages.

When we treat the book surface shape reconstruction problem as the real world shape-from-shading problem, we can find the following characteristics:

- *Proximal Light Source:* The light source of an image scanner is located very close to the book surface. This implies that the illuminant intensity and the light source direction varies with respect to the location on the book surface.
- *Moving Light Source:* The light source moves during the scanning process.
- *Interreflections:* The light reflected on one side of an unfolded book surface illuminates the other.
- *Specular Reflections:* The book surface is not Lambertian.
- *Nonuniform Albedo Distribution:* The albedo distribution over a printed book surface is not uniform.

In the following sections, we formulate this real world shape-from-shading problem based on an iterative, non-linear optimization scheme. Piecewise models of the 3D shape and albedo distribution are introduced to efficiently and stably computing the shape in practice. We also propose a method of restoring the distorted scanned image based on the

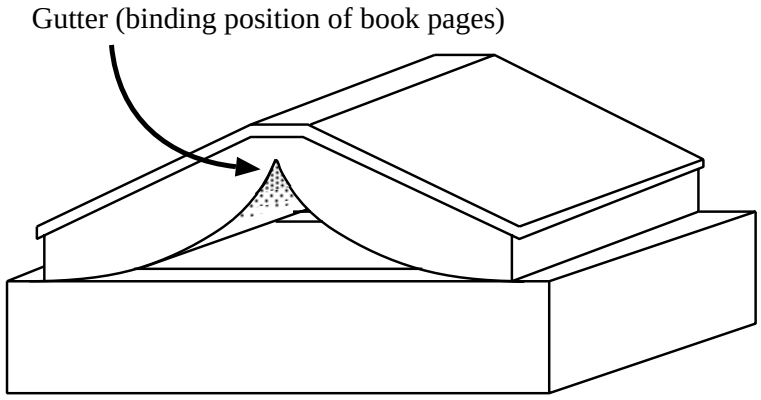

Figure 4.1: Unfolded book surface on flat scanning plane

reconstructed 3D shape and demonstrate the effectiveness and efficiency of the proposed methods with several experiments using scanned images of real books.

4.2 Problem Formulation

Here, we describe a formulation of our shape-from-shading problem under the real world characteristics described in the introduction. First, we begin from the ideal formulation in the following section and modify the formulation step by step to account for the characteristics of our real world problem.

Ideal Environment

Let us consider an *ideal* shape-from-shading problem. Ideally, the following conditions would be satisfied:

- *Distant Light Source:* This implies that the illuminant intensity and the light source direction are constant over the object surface.
- *No Interreflections:* The object surface is illuminated only by the light source.
- *Fixed Light Source Position*
- *Lambertian Surface*
- *Constant Albedos:* The albedo distribution is uniform over the object surface.

The problem under these ideal conditions can be formulated as:

$$I_o(\boldsymbol{x}) = \rho I_s \cos\varphi(\boldsymbol{x}), \tag{4.1}$$

where $\boldsymbol{x}$ denotes a 2D point in the image, $I_o(\boldsymbol{x})$ the reflected light intensity observed at $\boldsymbol{x}$, $\boldsymbol{I}_s$ the illuminant intensity, ρ the albedo on the surface, and $\varphi(\boldsymbol{x})$ the angle between

the light source direction and the surface normal at the 3D point on the object surface corresponding to $\boldsymbol{x}$.

In this case, $\varphi(\boldsymbol{x})$ can easily be calculated for given ρI_s.[1] Then, the shape (i.e., surface normals) of the object surface can be computed from $\varphi(\boldsymbol{x})$ by introducing additional constraints such as those from photometric stereo[29] or the assumption of smooth[8] or cylindrical surface[18].

Proximal Light Source

With a proximal light source, the illuminant intensity is no longer constant over the object surface. The illuminant intensity is now a function of the location of the object surface and that of the light source. We can formulate the problem as follows:

$$I_o(\boldsymbol{x}) = \rho I_s(\boldsymbol{s}(\boldsymbol{x}), \boldsymbol{l}) \cos\varphi(\boldsymbol{x}), \tag{4.2}$$

where $\boldsymbol{l}$ denotes the 3D location of the light source, $\boldsymbol{s}(\boldsymbol{x})$ the 3D point on the object surface corresponding to $\boldsymbol{x}$. If $\varphi(\boldsymbol{x})$ can be computed from $\boldsymbol{s}(\boldsymbol{x})$, we must estimate $\boldsymbol{s}(\boldsymbol{x})$ to recover the object shape. Therefore, the proximal light source transforms the *shape*-from-shading problem into the *depth*-from-shading problem.

Interreflections

The problem under the interreflections is formulated by [23], as:

$$I_o(\boldsymbol{x}) = \rho \left\{ I_s + \int \frac{I_o(\boldsymbol{x}')}{\{d^2(\boldsymbol{s}(\boldsymbol{x}), \boldsymbol{s}(\boldsymbol{x}'))\}} d\boldsymbol{x}' \right\} \cos\varphi(\boldsymbol{x}), \tag{4.3}$$

where $d(\boldsymbol{s}(\boldsymbol{x}), \boldsymbol{s}(\boldsymbol{x}'))$ denotes the distance between $\boldsymbol{s}(\boldsymbol{x})$ and $\boldsymbol{s}(\boldsymbol{x}')$. In this formulation, we assume that

1. The light reflected at $\boldsymbol{s}(\boldsymbol{x}')$ can reach $\boldsymbol{s}(\boldsymbol{x})$ for any combinations of $\boldsymbol{x}$ and $\boldsymbol{x}'$,
2. The light reflected more than twice is sufficiently attenuated to be neglected.

From Eq.(4.3), in order to compute the component of interreflections, the global shape information of the object surface ($\forall \boldsymbol{x}' d(\boldsymbol{x}(\boldsymbol{x}), \boldsymbol{s}(\boldsymbol{x}'))$) is required. Hence, the interreflections make the shape-from-shading problem into the *global shape*-from-shading problem.

Interreflections under Proximal Light Source

Combining the proximal light source and interreflections into one equation, we have:

$$I_o(\boldsymbol{x}) = \rho \left\{ I_s(\boldsymbol{s}(\boldsymbol{x}), \boldsymbol{l}) + \int \frac{I_o(\boldsymbol{x}')}{\{d^2(\boldsymbol{s}(\boldsymbol{x}), \boldsymbol{s}(\boldsymbol{x}'))\}} d\boldsymbol{x}' \right\} \cos\varphi(\boldsymbol{x}). \tag{4.4}$$

This shape-from-shading problem is the *overall depth*-from-shading problem. We must estimate whole depth of the object surface ($\forall \boldsymbol{x} \boldsymbol{s}(\boldsymbol{x})$).

[1] ρI_s can be determined assuming that $\varphi(\boldsymbol{x})$ is equal to zero at $\boldsymbol{x}$ where $I_o(\boldsymbol{x})$ takes the maximum value.

Moving Light Source

Introducing a moving light source[2] into Eq.(4.4), the problem can be formulated as:

$$I_o(\boldsymbol{x}) = \rho \left\{ I_s(\boldsymbol{s}(\boldsymbol{x}), \boldsymbol{l}(\boldsymbol{x})) + \int \frac{I'_o(\boldsymbol{s}(\boldsymbol{x}'), \boldsymbol{l}(\boldsymbol{x}))}{\{d^2(\boldsymbol{s}(\boldsymbol{x}), \boldsymbol{s}(\boldsymbol{x}'))\}} d\boldsymbol{x}' \right\} \cos\varphi(\boldsymbol{x}), \tag{4.5}$$

where $I'_o(\boldsymbol{s}(\boldsymbol{x}'), \boldsymbol{l}(\boldsymbol{x}))$ is the reflected light intensity at $\boldsymbol{s}(\boldsymbol{x}')$:

$$I'_o(\boldsymbol{s}(\boldsymbol{x}'), \boldsymbol{l}(\boldsymbol{x})) = \rho I_s(\boldsymbol{s}(\boldsymbol{x}'), \boldsymbol{l}(\boldsymbol{x})) \cos\varphi(\boldsymbol{x}') \tag{4.6}$$

and $\boldsymbol{l}(\boldsymbol{x})$ denotes the light source location corresponding to $\boldsymbol{x}$. In this case, we must estimate the *overall depth* of the object surface ($\forall \boldsymbol{x} \boldsymbol{s}(\boldsymbol{x})$), too. But, the interreflections are changed under the moving light source, so $I'_o(\boldsymbol{s}(\boldsymbol{x}'), \boldsymbol{l}(\boldsymbol{x}))$ must be calculated at each point on the object surface. Hence, the computational cost becomes more expensive than that under a fixed light source.

The Complete Formulation

Finally, we can formulate our problem by incorporating specular reflection and nonuniform albedo distribution characteristics into Eq.(4.5):

$$I_o(\boldsymbol{x}) = \left\{ I_s(\boldsymbol{s}(\boldsymbol{x}), \boldsymbol{l}(\boldsymbol{x})) + \int \frac{I'_o(\boldsymbol{s}(\boldsymbol{x}'), \boldsymbol{l}(\boldsymbol{x}))}{\{d^2(\boldsymbol{s}(\boldsymbol{x}), \boldsymbol{s}(\boldsymbol{x}'))\}} d\boldsymbol{x}' \right\} \rho(\boldsymbol{s}(\boldsymbol{x})) f(\varphi(\boldsymbol{x}), \boldsymbol{s}(\boldsymbol{x})) \tag{4.7}$$

where

$$I'_o(\boldsymbol{s}(\boldsymbol{x}'), \boldsymbol{l}(\boldsymbol{x})) = \rho(\boldsymbol{s}(\boldsymbol{x}')) I_s(\boldsymbol{s}(\boldsymbol{x}'), \boldsymbol{l}(\boldsymbol{x})) f(\varphi(\boldsymbol{x}'), \boldsymbol{s}(\boldsymbol{x}')), \tag{4.8}$$

$\rho(\boldsymbol{s}(\boldsymbol{x}))$ denotes the albedo and $f(\varphi(\boldsymbol{x}), \boldsymbol{s}(\boldsymbol{x}))$ is the reflectance property at $\boldsymbol{s}(\boldsymbol{x})$. In this problem, the interreflections $I'_o(\boldsymbol{s}(\boldsymbol{x}'), \boldsymbol{l}(\boldsymbol{x}))$ depend on both the object shape (depth) and albedo distribution, hence we must recover the *global depth*($\forall \boldsymbol{x} \boldsymbol{s}(\boldsymbol{x})$) and *overall albedo distribution*($\forall \boldsymbol{x} \rho(\boldsymbol{s}(\boldsymbol{x}))$) on the object surface.

4.3 Solution Scheme

To solve our problem, we must compute the absolute depth ($\forall \boldsymbol{x} \boldsymbol{s}(\boldsymbol{x})$) and albedos ($\forall \boldsymbol{x} \rho(\boldsymbol{s}(\boldsymbol{x}))$) from an observed scanned image. In addition, if the relation between $\boldsymbol{s}(\boldsymbol{x})$ and $\varphi(\boldsymbol{x})$ is not known, we must also compute the global shape information ($\forall \boldsymbol{x} \varphi(\boldsymbol{x})$). To attack this complicated problem, we assume that light source location $\boldsymbol{l}(\boldsymbol{x})$, illuminant intensity $I_s(\boldsymbol{s}, \boldsymbol{l})$ and reflectance ratio $f(\varphi, \boldsymbol{s})$ are known a priori. This assumption is practical because the first two functions represent optical properties of the image scanner and the latter the intrinsic property of the printed paper to be scanned, all of which can be calibrated a priori.

Equation (4.7) can be rewritten as a sum of the direct reflection and interreflections:

$$I_o(\boldsymbol{s}, \varphi, \rho) = \rho \left\{ I_{dir}(\boldsymbol{s}, \varphi) + I_{inter}(\boldsymbol{s}, \varphi, \rho) \right\}, \tag{4.9}$$

[2]As will be described in later, the light source of the image scanner moves synchronously with the scanning sensor, i.e., observation location.

where

$$I_{dir}(\boldsymbol{s},\varphi) = f(\varphi(\boldsymbol{x}),\boldsymbol{s}(\boldsymbol{x}))I_s(\boldsymbol{s}(\boldsymbol{x}),\boldsymbol{l}(\boldsymbol{x})) \quad (4.10)$$

$$I_{inter}(\boldsymbol{s},\varphi,\rho) = f(\varphi(\boldsymbol{x}),\boldsymbol{s}(\boldsymbol{x}))\int \frac{I'_o(\boldsymbol{s}(\boldsymbol{x}'),\boldsymbol{l}(\boldsymbol{x}))}{d^2(\boldsymbol{s}(\boldsymbol{x}),\boldsymbol{s}(\boldsymbol{x}'))}d\boldsymbol{x}'. \quad (4.11)$$

Using these notations and assumptions, we discuss why and how this problem can be solved.

4.3.1 Shape Reconstruction Method under Mutual Dependence

The assumptions we mentioned above reduce the number of unknown parameter functions of our problem to three: depth $\boldsymbol{s}$, shape φ and albedo distribution ρ of the object surface. The problem to be solved can be formulated as that of finding $\boldsymbol{s}$, φ and ρ which minimize the following objective functional:

$$\begin{aligned} F(\boldsymbol{s},\varphi,\rho) &= \|I_o(\boldsymbol{s},\varphi,\rho) - I_o^*\|^2 \\ &= \|\rho\left\{I_{dir}(\boldsymbol{s},\varphi) + I_{inter}(\boldsymbol{s},\varphi,\rho)\right\} - I_o^*\|^2 \end{aligned} \quad (4.12)$$

where I_o^* represents the observed intensity.

But, there are following problems in the minimization of F:

- The computation of I_{inter} in Eq.(4.12) requires $\boldsymbol{s}$, φ and ρ of all over the object surface. This means that there are an enormous of parameters subject to this minimization. Hence, this minimization process takes much computational cost.
- In the computation of I_{inter}, in order to solve $\boldsymbol{s}$, φ and ρ on the surface point $\boldsymbol{x}$, the values of $\boldsymbol{s}$,φ and ρ on another point $\boldsymbol{x}'$ are required, but they are also attempting to solve. Hence, there are mutual dependence in this problem.
- The photometric model (Eq.(4.9)) is affected to $\boldsymbol{s}$, φ and ρ. Hence, if F could be minimized, but $\boldsymbol{s}$, φ and ρ cannot determine uniquely.

For the first problem of the computational cost, we propose the practical solution in Sect.4.5.2. In this section, we discuss the mutual dependence and the uniqueness.

In order to solve the problem including the mutual dependence, it is effective to divide into sub problems and estimate each sub problem iteratively for updating solutions. In our problem, we divide it into the following sub problems:

1. Calculation of the interreflections (I_{inter}),
2. Estimating φ by minimizing F,
3. Estimating $\boldsymbol{s}$,
4. Estimating ρ.

The details of these procedures are follows (Fig.4.2):

1. Let $\boldsymbol{s}_0$, φ_0 and ρ_0 be the initial depth, shape, and albedo estimated by some method, then I_{inter} can be calculated approximately from $\boldsymbol{s}_0$, φ_0 and ρ_0.

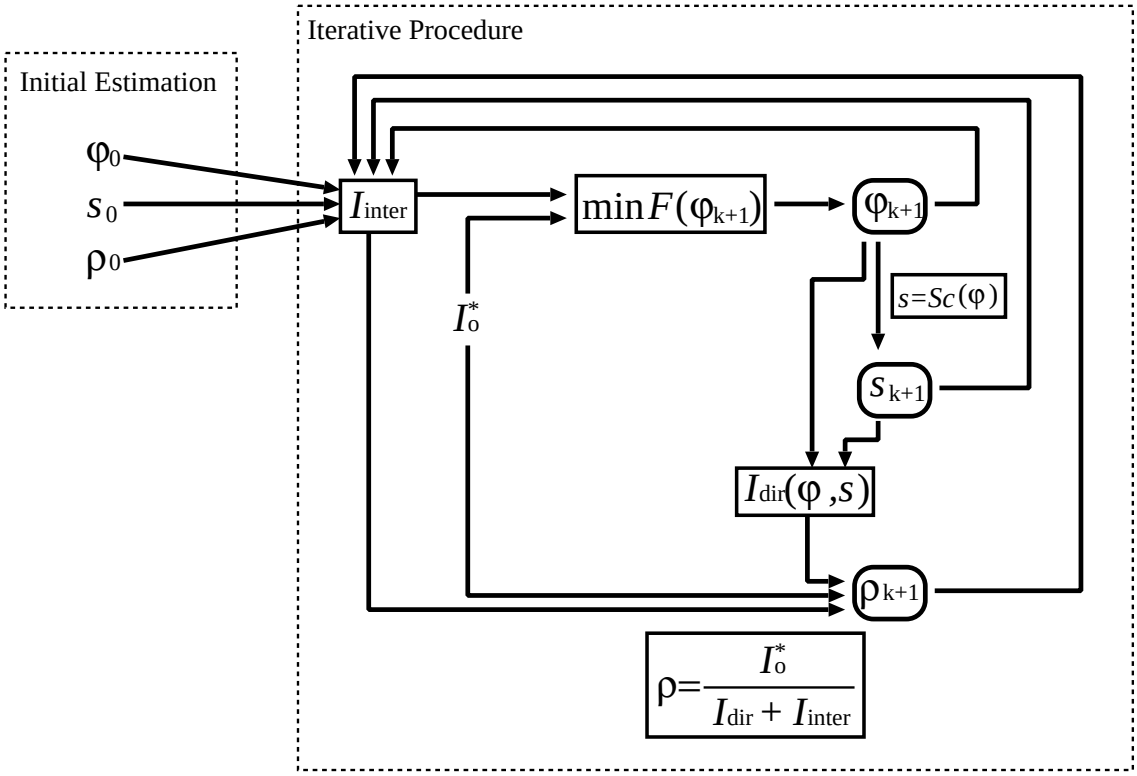

Figure 4.2: Iterative procedure for shape and albedo reconstruction.

2. If the surface smoothness could be assumed, $\boldsymbol{s}$ can be represented by φ. Here, we describe this relation as follows:

$$\boldsymbol{s} = Sc(\varphi). \tag{4.13}$$

From this relation, $\boldsymbol{s}$ is eliminated from Eq.(4.12). Moreover, in this step, ρ can be assumed to be a constant value ρ_k estimated in previous step of iteration. Therefore, the objective functional F can be formulated as follows:

$$F(\varphi_{k+1}) = \|I_o^* - \rho_k I_{dir}(\varphi_{k+1}) - \rho_k I_{inter}\|^2. \tag{4.14}$$

By minimizing F, φ_{k+1} (this denotes the updated parameter of φ) can be estimated.

3. Estimate $\boldsymbol{s}_{k+1}$ from φ_{k+1} by Eq.(4.13).

4. The updated ρ_{k+1} can be estimated by the following calculation:

$$\rho_{k+1} = \frac{I_o^*}{I_{dir}(\varphi_{k+1}) + I_{inter}}. \tag{4.15}$$

Again, I_{inter} can be calculated by φ_{k+1}, $\boldsymbol{s}_{k+1}$ and ρ_{k+1}, and next updated φ, $\boldsymbol{s}$ and ρ are estimated iteratively. By using this method, the optimal φ, $\boldsymbol{s}$ and ρ will be estimated.

But, this method still has the following problems:

- What constrained conditions about the object shape can be used?
- How to estimate the initial shape and albedo?
- Can φ, $\boldsymbol{s}$ and ρ be converged by this method?

For the first problem, strong constrained conditions of the object shape can be employed because we use the book surface shape as the objective shape for the reconstruction in this study. For the second problem, the initial shape and albedo distribution can be estimated by using the photometric models neglecting the interreflections. And the convergence of φ, $\boldsymbol{s}$ and ρ in the third problem can be analyzed by using the shape constrained conditions and the proximal light source properties. The details are shown in next sections.

4.3.2 Solution Using Constraints of Book Surface Shape

In this study, we use the following assumptions about the book surface shape:

- The book surface is a part of cylindrical shape and its cross section shape is smooth except the gutter point.
- In the left and right book surface shape separating at the gutter, the height of the book surface is monotonically increasing or decreasing, and forms downward convex curved surface.
- In both ends of the book surface, the height and slant are equal to 0. This means that these part of the book surface are flat plane.

From these assumptions, $\boldsymbol{s}$ can be represented by φ as shown in later Eq.(4.44), and the following characteristic can be assumed for the interreflections:

- The intensity of the interreflections which illuminate one side of the book surface depend on the shape and albedo distribution of only another side of the book surface.

By using this characteristic, when we estimate only one side of the book surface shape, I_{inter} can be regarded as a fixed value. Hence, as shown in Fig.4.3, since it is no need to take account of the mutual dependence in one side book surface shape reconstruction, we can determine an estimated shape uniquely. But, since the estimated shape depends on the value of I_{inter}, it is difficult to estimate surface shape precisely from approximated I_{inter}. Therefore, we must update I_{inter}, the object shape, and the albedo by the iterative method.

From the discussion we mentioned above, the book surface shape reconstruction algorithm is described as follows:

Initial Estimation: Estimate φ_0 and $\boldsymbol{s}_0$ from I_o^* by using the photometric model without the interreflections (neglecting the term I_{inter} in Eq.(4.9)). And, estimate ρ_0 from φ_0 using Eq.(4.15) in which the term $I_{inter} = 0$.

Step 1: Compute I_{inter} from the estimated φ_k, $\boldsymbol{s}_k$ and ρ_k.

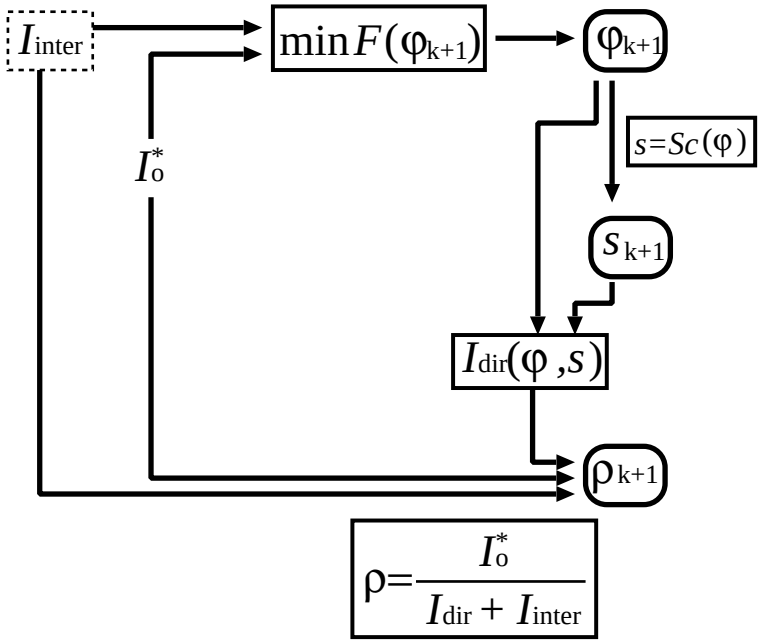

Figure 4.3: Shape and albedo reconstruction under fixed interreflections.

Step 2: Compute φ_{k+1} of one side of the book surface which minimizes the objective functional F using estimated I_{inter}. And then, compute φ_{k+1} of another side of the book surface. After the φ_{k+1} estimation, $\boldsymbol{s}_{k+1}$ are computed by φ_{k+1}.

Step 3: Compute ρ_{k+1} using the estimated $\boldsymbol{s}_{k+1}$, φ_{k+1} and I_{inter}.

Step 4: If the difference between k-th estimated shape and $(k+1)$-th one is small, the estimated shape is converged and stop this procedure. Otherwise, iterate from Step 1.

The detailed algorithm is described in Section 4.5.4.

4.3.3 Analysis of Convergence for Book Surface Shape Reconstruction

Next, we discuss the convergence of the estimated shape by the iterative method. From the book surface shape constraints and the proximal light source property, the following characteristic can be also assumed for the interreflections:

- When the height of the book surface is low in all over one side of the book surface shape, the surface become to be close to the light source and the difference between the surface normals and the light source direction become to be small, hence the intensity of the interreflections from this surface become strong intensity.
- When the height of the book surface is high, the surface become to be apart from the light source and the difference between the surface normal and the light source

direction become to be large, hence the intensity of the interreflections from this surface become weak intensity.

Moreover, the initial shape always has the following characteristics:

- In the initial shape estimated by the photometric model neglecting the interreflections, the height of the initial shape is lower than the actual one, because the observed intensity includes the interreflections, that is, the observed intensity is stronger than that taking no account of the interreflections.

From the qualitative analysis taking account of these characteristics, the estimated book surface shape at each step in iterative procedure changes as shown in Fig.4.4.

Iteration 0 (Initial Estimation). The initial shape is estimated lower than the actual one. Hence, the interreflections of each side of the book surface ($I_{inter}(R)$, $I_{inter}(L)$[3] in Fig.4.4) become stronger than the actual intensity.

Iteration 1. When the interreflections has strong brightness, the term $I_o^* - \rho_k I_{inter}$ in Eq.(4.14) become relatively small. Hence, the estimated shape become higher than the actual one.

And then, the intensity of the interreflections calculated by using this estimated shape are weaker than the actual brightness.

Iteration 2. The calculated intensity of the interreflections in Iteration 1 are weak, but if it is larger than 0, then the estimated shape using this interreflections is higher than the shape estimated in Iteration 0. But, this estimated shape might be lower than the actual one. Hence, the intensity of the interreflections calculated by using this estimated shape are stronger than the actual brightness but weaker than that of Iteration 0.

Iteration3. By using the interreflections calculated in Iteration2, the book surface shape will be estimated lower than that in Iteration 1. But, this estimated shape might be higher than the actual one.

By proceeding above iterative procedure, the estimated shape will become to be converged vibratingly.

Next, we discuss the mathematical analysis of the convergence for the book surface shape to support above qualitative analysis. Here, we employ the following assumptions to make the photometric models simple:

1. The albedo distribution on the book surface is constant and known. This mean that the albedo estimation is not done in the shape reconstruction process.

2. Each cross section shape of the book surface, the right or left side shape, can be described by using one parameter. In practice, we employ the following quadratic

[3]According to the position of the surface, the actual intensity of the interreflections are changed. Hence, the intensity of the interreflections are calculated at each position on the surface.

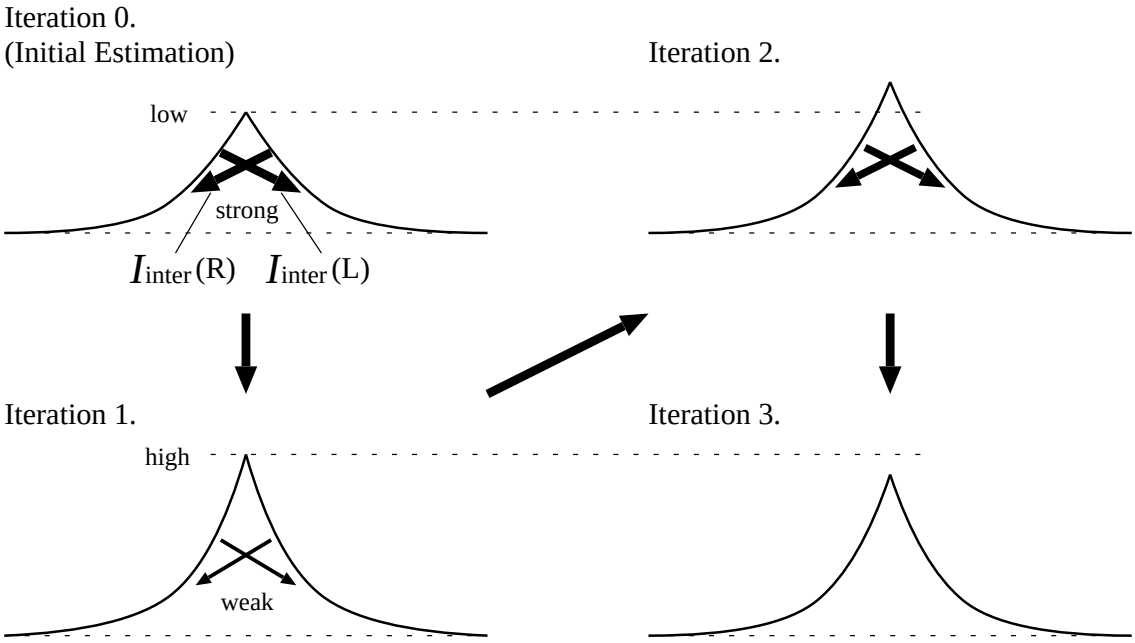

Figure 4.4: Estimated shapes at each iteration.

polynomials[4] as the cross section shape models (Fig.4.5):

$$Z_{pr}(y) = \frac{Z_r}{(y_{r1}-y_{r0})^2}(y-y_{r0})^2, \tag{4.16}$$

$$Z_{pl}(y) = \frac{Z_l}{(y_{l1}-y_{l0})^2}(y-y_{l0})^2, \tag{4.17}$$

where y_{r0} and y_{l0} denote the book surface positions beginning to curve, $y_{r1}(>0)$ and $y_{l1}(<0)$ are the y positions of the gutter point. They are very close to $y=0$. y_{r0}, y_{l0}, y_{r1}, and y_{l1} are assumed to be known. Z_r and Z_l are the heights of the book surface shape at gutter point. We call Z_r and Z_l the shape parameters. These shape models obey the book surface shape assumptions described in the previous section. Z_r and Z_l correspond to $\boldsymbol{s}$, and φ can be represented by $\boldsymbol{s}$ in these shape models.

Similarly to Eq.(4.9), the photometric models on both sides of book surface shapes can be described as follows:

$$rP_w(Z_r, Z_l; y_r) = rI_{dir}(Z_r; y_r) + rI_{inter}(Z_r, Z_l; y_r), \tag{4.18}$$

$$lP_w(Z_r, Z_l; y_l) = lI_{dir}(Z_l; y_l) + lI_{inter}(Z_r, Z_l; y_l), \tag{4.19}$$

where $rI_{dir}()$ and $rI_{inter}()$ denote the direct reflection and interreflections components at $y=y_r(y_r \geq y_{r1})$, and $lI_{dir}()$ and $lI_{inter}()$ also denote them at $y=y_l(y_l \leq y_{l1})$. Since the left and right shape models are different, we employ two photometric models. Note that,

[4]In later section (Sect.4.5.2), we use the piecewise polynomial model as the practical shape model.

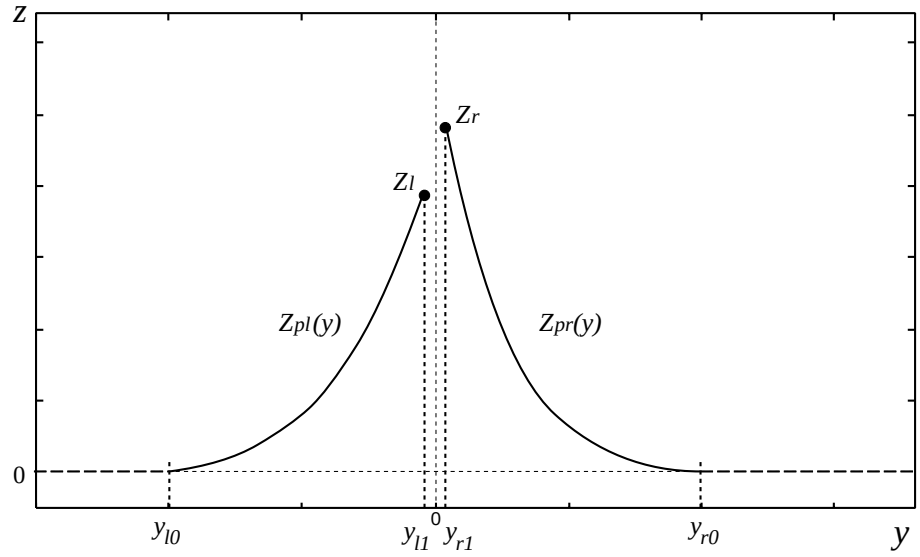

Figure 4.5: Shape model for convergence analysis

the albedo ρ in Eq.(4.9) is omitted in Eq.(4.18) and (4.19), because it can be assumed to be multiplied to $rI_{dir}()$, $rI_{inter}()$, $lI_{dir}()$, and $lI_{inter}()$.

The estimation process of the shape parameters Z_r and Z_l, which is based on the shape reconstruction algorithm in previous section, is described as follows. In this process, Z_r and Z_l are estimated by using the image intensity (the observed data) at $y = y_r$ ($y_{r1} \leq y_r \leq y_{r0}$) and $y = y_l$ ($y_{l0} \leq y_l \leq y_{l1}$). These observed data are represented as $P_w^*(y_r)$ and $P_w^*(y_l)$:

Step 0. Estimate $Z_r^{(0)}$ and $Z_l^{(0)}$, which are the initial values of Z_r and Z_l(the initial shape), by using $P_w^*(y_r)$, $P_w^*(y_l)$ and the photometric models ($rI_{dir}()$ and $lI_{dir}()$) taking no account of the interreflections. In this step, the method to estimate $Z_r^{(0)}$ and $Z_l^{(0)}$ is not restricted. Since they are estimated by $rI_{dir}()$ and $lI_{dir}()$, the following relations can be assumed:

$$P_w^*(y_r) = rI_{dir}(Z_r^{(0)}; y_r), \tag{4.20}$$

$$P_w^*(y_l) = lI_{dir}(Z_l^{(0)}; y_l). \tag{4.21}$$

Step 1. Before estimating i-th Z_r and Z_l, that is $Z_r^{(i)}$ and $Z_l^{(i)}$, calculate the interreflections rI_{inter} and lI_{inter} using $Z_r^{(i-1)}$ and $Z_l^{(i-1)}$.

Step 2. Estimate $Z_r^{(i)}$ and $Z_l^{(i)}$ from $P_w^*(y_r)$, $P_w^*(y_l)$, rI_{inter}, and lI_{inter} using the photometric models (Eq.(4.18),(4.19)).

Step 3. Iterate from Step 1 until $Z_r^{(i)}$ and $Z_l^{(i)}$ are converged.

Next, we derive the recurrence relations of $Z_r^{(i)}$ and $Z_l^{(i)}$ in the above iterative process. In the following, we denote that $P_w^*(y_r) = P_{wr}^*$, $P_w^*(y_l) = P_{wl}^*$, $Z_r^{(0)} = Z_{r0}$, and $Z_l^{(0)} = Z_{l0}$.

The descriptions of y_r and y_l in the photometric models are omitted. In order to derive these relations, first, we approximate $rI_{dir}(Z_r)$ of Eq.(4.18) to the linear equation around $Z_r = Z_{r0}$:

$$rI_{dir}(Z_r) = rI_{dir}{}'(Z_{r0})(Z_r - Z_{r0}) + rI_{dir}(Z_{r0}), \tag{4.22}$$

where $rI_{dir}{}'(Z_r)$ is the first order derivative of $rI_{dir}(Z_r)$ with respect to Z_r. By assigning Eq.(4.22) to Eq.(4.18), the relation of $Z_r^{(i)}$, $Z_r^{(i-1)}$ and $Z_l^{(i-1)}$ in Step 2 becomes:

$$P_{wr}^* = rI_{dir}{}'(Z_{r0})(Z_r^{(i)} - Z_{r0}) + rI_{dir}(Z_{r0}) + rI_{inter}(Z_r^{(i-1)}, Z_l^{(i-1)}). \tag{4.23}$$

From Eq.(4.23), $Z_r^{(i)}$ is represented as:

$$Z_r^{(i)} = \frac{P_{wr}^* - rI_{dir}(Z_{r0}) - rI_{inter}(Z_r^{(i-1)}, Z_l^{(i-1)})}{rI_{dir}{}'(Z_{r0})} + Z_{r0}. \tag{4.24}$$

In order to simplify Eq.(4.24), we also approximate $rI_{inter}(Z_r, Z_l)$ to the linear equation around $Z_r = Z_{r0}$ and $Z_l = Z_{l0}$:

$$\begin{aligned} rI_{inter}(Z_r, Z_l) &= \frac{\partial rI_{inter}(Z_{r0}, Z_{l0})}{\partial Z_r}(Z_r - Z_{r0}) + \frac{\partial rI_{inter}(Z_{r0}, Z_{l0})}{\partial Z_l}(Z_l - Z_{l0}) \\ &\quad + rI_{inter}(Z_{r0}, Z_{l0}). \end{aligned} \tag{4.25}$$

By using Eq.(4.25) and Eq.(4.24), $Z_r^{(i)}$ can be rewritten to Eq.(4.26). In the same way, $Z_l^{(i)}$ can be also represented by the photometric models of the left side of the book surface:

$$Z_r^{(i)} = a_{rr} Z_r^{(i-1)} + a_{rl} Z_l^{(i-1)} + b_r, \tag{4.26}$$

$$Z_l^{(i)} = a_{lr} Z_r^{(i-1)} + a_{ll} Z_l^{(i-1)} + b_l, \tag{4.27}$$

where

$$\left.\begin{aligned} a_{rr} &= -\frac{\frac{\partial rI_{inter}(Z_{r0}, Z_{l0})}{\partial Z_r}}{rI_{dir}{}'(Z_{r0})}, \quad a_{rl} = -\frac{\frac{\partial rI_{inter}(Z_{r0}, Z_{l0})}{\partial Z_l}}{rI_{dir}{}'(Z_{r0})}, \\ a_{lr} &= -\frac{\frac{\partial lI_{inter}(Z_{r0}, Z_{l0})}{\partial Z_r}}{lI_{dir}{}'(Z_{l0})}, \quad a_{ll} = -\frac{\frac{\partial lI_{inter}(Z_{r0}, Z_{l0})}{\partial Z_l}}{lI_{dir}{}'(Z_{l0})}, \end{aligned}\right\} \tag{4.28}$$

$$\begin{aligned} b_r &= \frac{1}{rI_{dir}{}'(Z_{r0})}\left(\frac{\partial rI_{inter}(Z_{r0}, Z_{l0})}{\partial Z_r} Z_{r0} + \frac{\partial rI_{inter}(Z_{r0}, Z_{l0})}{\partial Z_l} Z_{l0} - rI_{inter}(Z_{r0}, Z_{l0})\right) \\ &\quad + Z_{r0}, \end{aligned} \tag{4.29}$$

$$\begin{aligned} b_l &= \frac{1}{lI_{dir}{}'(Z_{l0})}\left(\frac{\partial lI_{inter}(Z_{r0}, Z_{l0})}{\partial Z_r} Z_{r0} + \frac{\partial lI_{inter}(Z_{r0}, Z_{l0})}{\partial Z_l} Z_{l0} - lI_{inter}(Z_{r0}, Z_{l0})\right) \\ &\quad + Z_{l0}, \end{aligned} \tag{4.30}$$

and $lI_{dir}{}'()$ is the first order derivative of $lI_{dir}()$ with respect to Z_l. b_r and b_l are simplified by using the relations of Eq.(4.20) and Eq.(4.21).

By using the following equations:

$$\boldsymbol{Z}^{(i)} = \begin{bmatrix} Z_r^{(i)} \\ Z_l^{(i)} \end{bmatrix}, \boldsymbol{A} = \begin{bmatrix} a_{rr} & a_{rl} \\ a_{lr} & a_{ll} \end{bmatrix}, \boldsymbol{B} = \begin{bmatrix} b_r \\ b_l \end{bmatrix}, \tag{4.31}$$

Eq.(4.26),(4.27) can be rewritten as:

$$\boldsymbol{Z}^{(i)} = \boldsymbol{A} \cdot \boldsymbol{Z}^{(i-1)} + \boldsymbol{B}. \tag{4.32}$$

Therefore, $\boldsymbol{Z}^{(i)}$ is represented as:

$$\boldsymbol{Z}^{(i)} = \boldsymbol{A}^i \cdot \boldsymbol{Z}^{(0)} + \sum_{k=1}^{i-1} \boldsymbol{A}^k \cdot \boldsymbol{B} + \boldsymbol{B}, \quad \left(\boldsymbol{Z}^{(0)} = \begin{bmatrix} Z_{r0} \\ Z_{l0} \end{bmatrix} \right). \tag{4.33}$$

Let λ_1 and λ_2 as the eigen values of $\boldsymbol{A}$, $\boldsymbol{\Lambda}$= $\begin{bmatrix} \lambda_1 & 0 \\ 0 & \lambda_2 \end{bmatrix}$ (the diagonal matrix), $\boldsymbol{E}$ as a matrix constructed by the eigen vectors correspond to λ_1 and λ_2. Since the eigen values of $\boldsymbol{A}$ are the solutions of the characteristic equation of $\boldsymbol{A}$, they can be obtained by:

$$\lambda = \frac{a_{rr} + a_{ll} \pm \sqrt{(a_{rr} - a_{ll})^2 + 4a_{rl}a_{lr}}}{2}. \tag{4.34}$$

Since $\boldsymbol{A} = \boldsymbol{E} \cdot \boldsymbol{\Lambda} \cdot \boldsymbol{E}^{-1}$, $\boldsymbol{A}^i$ is represented as:

$$\boldsymbol{A}^i = \boldsymbol{E} \cdot \boldsymbol{\Lambda}^i \cdot \boldsymbol{E}^{-1} = \boldsymbol{E} \cdot \begin{bmatrix} {\lambda_1}^i & 0 \\ 0 & {\lambda_2}^i \end{bmatrix} \cdot \boldsymbol{E}^{-1}. \tag{4.35}$$

Therefore, if the conditions:

$$|\lambda_1| < 1 \ \text{ and } \ |\lambda_2| < 1 \tag{4.36}$$

can be satisfied, $\boldsymbol{A}^i = \boldsymbol{O}$ in $i \to \infty$ and Eq.(4.33) can converge to:

$$\begin{aligned} \boldsymbol{Z}^{(\infty)} &= \boldsymbol{E} \cdot \sum_{k=1}^{\infty} \boldsymbol{\Lambda}^k \cdot \boldsymbol{E}^{-1} \cdot \boldsymbol{B} + \boldsymbol{B} \\ &= \boldsymbol{E} \cdot \begin{bmatrix} \frac{\lambda_1}{1-\lambda_1} & 0 \\ 0 & \frac{\lambda_2}{1-\lambda_2} \end{bmatrix} \cdot \boldsymbol{E}^{-1} \cdot \boldsymbol{B} + \boldsymbol{B}. \end{aligned} \tag{4.37}$$

Note that, the shape parameters obtained by Eq.(4.37) are not the true values but approximate to them. The accuracy of the estimated shape parameters depend on the approximations of the linear equations of $rI_{dir}()$, $rI_{inter}()$, $lI_{dir}()$, and $lI_{inter}()$ with respect to the actual non-linear photometric models.

Next, we analyze the behavior of $Z_r^{(i)}$ and $Z_l^{(i)}$ in the convergence process. By using Eq.(4.20) and Eq.(4.21), $Z_r^{(1)}$ can be represented as:

$$Z_r^{(1)} = Z_{r0} - \frac{rI_{inter}(Z_{r0}, Z_{l0})}{{rI_{dir}}'(Z_{r0})}. \tag{4.38}$$

In generally, since ${rI_{dir}}'(Z_{r0}) < 0$ and $rI_{inter}(Z_{r0}, Z_{l0}) > 0$ when the interreflections exist at $y = y_r$,

$$Z_r^{(1)} - Z_{r0} = -\frac{rI_{inter}(Z_{r0}, Z_{l0})}{{rI_{dir}}'(Z_{r0})} > 0. \tag{4.39}$$

Hence,

$$Z_r^{(1)} - Z_{r0} > 0. \tag{4.40}$$

In the same way,

$$Z_l^{(1)} - Z_{l0} > 0. \tag{4.41}$$

From Eq.(4.32), we can derive the following relation:

$$\boldsymbol{Z}^{(i)} - \boldsymbol{Z}^{(i-1)} = \boldsymbol{A} \cdot \left(\boldsymbol{Z}^{(i-1)} - \boldsymbol{Z}^{(i-2)} \right). \tag{4.42}$$

Therefore, if all elements of $\boldsymbol{A}$ are negative, that is,

$$a_{rr}, a_{rl}, a_{lr}, a_{ll} < 0, \tag{4.43}$$

then the sign of $(\boldsymbol{Z}^{(i)} - \boldsymbol{Z}^{(i-1)})$ is opposite to that of $(\boldsymbol{Z}^{(i-1)} - \boldsymbol{Z}^{(i-2)})$. This means that:

- If $\boldsymbol{Z}^{(i-1)} > \boldsymbol{Z}^{(i-2)}$, then $\boldsymbol{Z}^{(i)} < \boldsymbol{Z}^{(i-1)}$,
- If $\boldsymbol{Z}^{(i-1)} < \boldsymbol{Z}^{(i-2)}$, then $\boldsymbol{Z}^{(i)} > \boldsymbol{Z}^{(i-1)}$.

Therefore, in the iterative process for the shape reconstruction, the estimated shape parameters (the heights of the book shape) repeat up and down, and become to be converged.

From the discussion we mentioned above, in order to show the convergence of the estimated shape, we must examine the eigen values (λ_1, λ_2) of $\boldsymbol{A}$ in Eq.(4.31) whether $|\lambda_1|$ and $|\lambda_2|$ are smaller than 1. As shown in Eq.(4.34), λ_1 and λ_2 can be represented by a_{rr}, a_{rl}, a_{lr}, and a_{ll} which are the elements of $\boldsymbol{A}$. In addition, the behavior of the estimated shape in the iterative process is determined by the signs of a_{rr}, a_{rl}, a_{lr}, and a_{ll}. As shown in Eq.(4.28), a_{rr}, a_{rl}, a_{lr}, and a_{ll} are formulated by using the derivatives of the photometric models of the direct reflection and interreflections. However, as shown in later section, since the formulations of the practical photometric models are very complex, it is difficult to represent a_{rr}, a_{rl}, a_{lr}, and a_{ll} using the parameters of the practical models. Moreover, if the values of parameters are not known, it is also difficult to confirm the conditions, $|\lambda_1|, |\lambda_2| < 1$, and the signs of elements in $\boldsymbol{A}$. Hence, in order to evaluate the convergence of the shape reconstruction, we calculate the values of $\boldsymbol{A}$, λ_1, and λ_2 by using the actual scanner image and the photometric parameters. This experimental result will be shown in Sect.4.6.4.

4.4 Book Surface

We discussed the basic solution scheme of our problem to compute the shape, depth and albedo distribution of the unfolded book surface. Here we specify our problem by describing the practical conditions of copying an unfolded book surface by an image scanner.

4.4.1 Cross Section Shape of Book Surface

The unfolded book surface is laid on the flat scanning plane as shown in Fig.4.6. For the geometric configuration of the book surface, we use the following assumptions which are introduced in Sect.4.3.2:

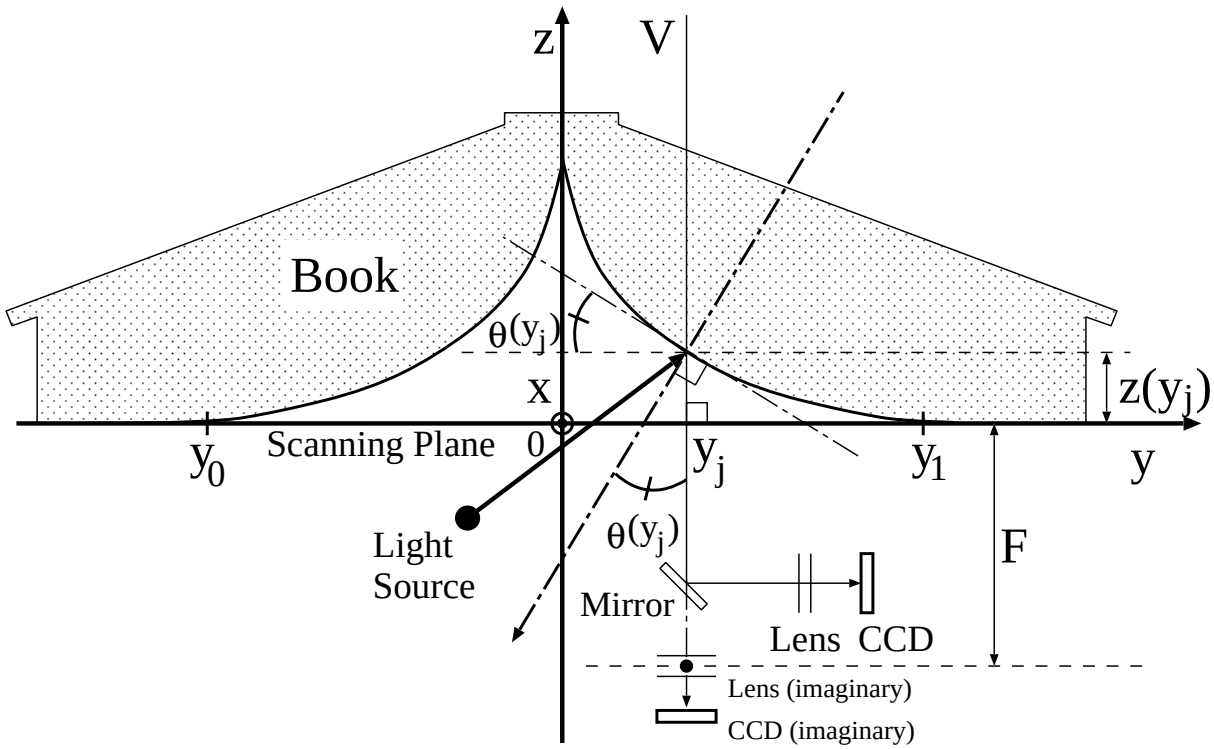

Figure 4.6: Book surface cross section.

- The book surface is cylindrical (constant cross section) and its cross section shape on the $y-z$ plane is smooth except for the gutter point separating the book pages.
- The unfolded book surface is aligned on the scanning plane so that the center line separating the book pages is parallel to and lies just above the x-axis. Hence, the cross section is constant along the x-axis.
- Both end of the book surface touch the scanning plane. That is, we can neglect the term I_{inter} in Eq.(4.15) and albedos can be estimated at the end of the book surface without iterative computation.

With these assumptions, φ and $\boldsymbol{s}$ are reduced to 1D functions of y.

In Fig.4.6, $z(y_j)$ is the distance between the scanning plane and the book surface. This is the practical representation of $\boldsymbol{s}$. When the book surface contact with the scanning plane at $y = y_0$ and $y = y_1$, it is represented as follows:

$$z(y_j) = \begin{cases} 0 & (y_j \le y_0, y_1 \le y_j) \\ \displaystyle\int_{y_1}^{y_j} \tan\theta(y)\, dy & (0 < y_j < y_1) \\ \displaystyle\int_{y_0}^{y_j} \tan|\theta(y)|\, dy & (y_0 < y_j < 0) \end{cases} \tag{4.44}$$

where $\theta(y_j)$ is the slant angle of the book surface. That is, $\theta(y_j)$ is the practical representation of φ and Eq.(4.44) corresponds to $Sc(\varphi)$ in Eq.(4.13).

4.4.2 Reflectance Property

To represent both the diffuse and specular components of the reflected light, we employ Phong's model[53],[56] as the reflectance property of the book surface. This property is represented as follows:

$$f(\boldsymbol{n}, \boldsymbol{l}, \boldsymbol{v}) = s\cos\varphi(\boldsymbol{n}, \boldsymbol{l}) + (1-s)\cos^n\delta(\boldsymbol{n}, \boldsymbol{l}, \boldsymbol{v}), \tag{4.45}$$

where $\boldsymbol{n}$ denotes the surface normal, $\boldsymbol{l}$ the direction of the illumination, and $\boldsymbol{v}$ the view point direction, φ the angle between $\boldsymbol{n}$ and $\boldsymbol{l}$, and δ the angle between $\boldsymbol{v}$ and the direction of the regular reflection. s is the ratio of the diffuse component to the reflection and n is the "lobe" parameter of the specular component.

4.5 Shape Reconstruction of Book Surface

4.5.1 Photometric Model

The relationship between the image intensity (pixel value) and the reflected light intensity is represented as follows:

$$\begin{aligned} P(x_i, y_j) &= aI_o(x_i, y_j) + \Delta \\ &= a\rho(x_i, y_j)\left\{I_{dir}(x_i, y_j) + I_{inter}(x_i, y_j)\right\} + \Delta, \end{aligned} \tag{4.46}$$

where

- $P(x_i, y_j)$:the image intensity at (x_i, y_j) in the scanned image.
- a, Δ: The gain and the bias of the photo-electric transformation in the image scanner respectively.
- $\rho(x_i, y_j)$: The albedo on the book surface corresponding to the pixel at (x_i, y_j) in the scanned image.
- $I_{dir}(x_i, y_j)$: The reflected light component corresponding to the direct illumination from the light source.
- $I_{inter}(x_i, y_j)$: The reflected light component corresponding to the indirect illumination from the opposite side of the book surface.

$I_{dir}(x_i, y_j)$ and $I_{inter}(x_i, y_j)$ are represented as follows:

$$I_{dir}(x_i, y_j) = I_s(y_j, z(y_j), y_j) f(\boldsymbol{n}_1, \boldsymbol{l}_1, \boldsymbol{v}_1), \tag{4.47}$$

$$I_{inter}(x_i, y_j) = A \sum_{y=y_{\min}}^{y_{\max}} \left[V(y, y_j) \cdot I_s(y, z(y), y_j) \sum_{x=x_{\min}}^{x_{\max}} \rho(x, y) \frac{f(\boldsymbol{n}_2, \boldsymbol{l}_2, \boldsymbol{v}_2) f(\boldsymbol{n}_1, \boldsymbol{l}_3, \boldsymbol{v}_1)}{d^2(x, y, x_i, y_j)} \right], \tag{4.48}$$

where

- $z(y_j)$: The distance between the scanning plane and the book surface (Eq.(4.44)).

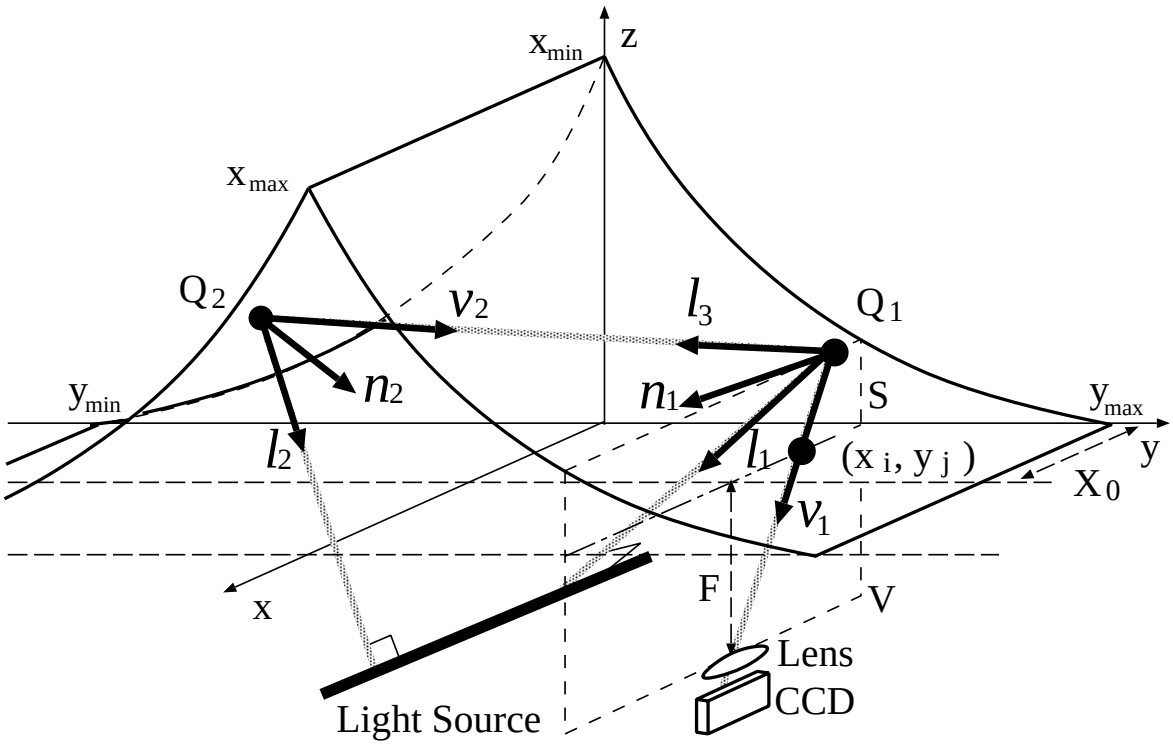

Figure 4.7: Interreflections on book surface.

- $I_s(y, z, y_j)$: The illuminant intensity (Eq.(3.2)).
- $f(\boldsymbol{n}, \boldsymbol{l}, \boldsymbol{v})$: The reflectance property of the book surface (Eq.(4.45)). $\boldsymbol{n}$, $\boldsymbol{l}$, $\boldsymbol{v}$ are corresponding to $\boldsymbol{n}_1$, $\boldsymbol{l}_1$, $\boldsymbol{v}_1$, ..., etc. as shown in Fig.4.7.
- A: The area size of a pixel in the image.
- $V(y, y_j)$ (the visibility function): Let Q_1 be the point on the book surface corresponding to (x_i, y_j) on the scanned image and Q_2 the another point corresponding to (x, y) (Fig.4.7). If the light reflected at Q_2 can reach Q_1 then this function takes 1, otherwise 0.

In the experiments, the parameters a, Δ, d_1, d_2, I_e, s, n and $I_D(\psi)$ are estimated a priori using calibrated images of white flat slopes with known slants.

Since most of the book surface has the unprinted white background, we can assume that pixel values $P_w^*(y_j)$ corresponding to the background can be obtained from the observed image $P^*(x_i, y_j)$ as the maximum along each row y_j:

$$P_w^*(y_j) = \max_{x_i} P^*(x_i, y_j) \tag{4.49}$$

The photometric model of the white background with the constant albedo ρ_w is represented as follows:

$$P_w(y_j) = a\rho_w \left\{ I_{dir}(x(y_j), y_j) + I_{inter}(x(y_j), y_j) \right\} + \Delta, \tag{4.50}$$

where $x(y_j)$ denotes the location of the white background at y_j.

4.5.2 Piecewise Shape and Albedo Approximation

Under the practical conditions described in the previous section, the problem now becomes that of estimating the shape $\theta(y_j)$, the depth $z(y_j)$ and the albedo $\rho(x_i, y_j)$ which minimize the total error between the observed image intensity $P^*(x_i, y_j)$ and the image intensity model $P(x_i, y_j)$ represented by Eq.(4.46). The depth $z(y_j)$ can be calculated from $\theta(y_j)$ by Eq.(4.44) and the albedo $\rho(x_i, y_j)$ from $\theta(y_j)$, $z(y_j)$ and $P^*(x_i, y_j)$ by the following formulation obtained from Eq.(4.46):

$$\rho(x_i, y_j) = \frac{P^*(x_i, y_j) - \Delta}{a\left\{I_{dir}(x_i, y_j) + I_{inter}(x_i, y_j)\right\}}. \tag{4.51}$$

Hence, the problem is essentially equivalent to estimating optimal $\theta(y_j)$ which minimize the total error.

This estimation problem can be formulated as a non-linear optimization problem in N-dimensional space, where N represents the number of sampling points along the y-axis. To compute the numerical solution of this problem, simultaneous equations with an $N \times N$ coefficient matrix must be solved iteratively. In practice, however, there are thousands of sampling points, and hence, such a naive computation becomes extremely expensive. Moreover, local noise in an image introduces errors into $\theta(y_j)$, which are accumulated by Eq.(4.44) and lead to global errors in $z(y_j)$.

To improve the computational efficiency and the stability, we employ the following two piecewise approximations of the book surface.

2D Piecewise Polynomial Model Fitting

This method represents the 2D cross section by m quadratic polynomials. The y-axis is partitioned into m uniform intervals and the depth $Z_p(y)$ at y in the p-th interval is represented as follow:

$$Z_p(y) = \frac{z'_p - z'_{p-1}}{2(y^\Delta_p - y^\Delta_{p-1})}(y - y^\Delta_{p-1})^2 + z'_{p-1}(y - y^\Delta_{p-1}) + z_{p-1}, \tag{4.52}$$

where y^Δ_p $(p = 0, 1, ..., m)$ denotes the end point of a uniform interval of Δ pixels($y^\Delta_p = y_{p\times\Delta}$),

$$z_p = z(y^\Delta_p), \quad z'_p = \frac{2(z_p - z_{p-1})}{y^\Delta_p - y^\Delta_{p-1}} - z'_{p-1}$$

and $z_0 = z'_0 = 0$ (just on the scanning plane). By using this model, the number of parameters to describe the cross section shape is reduce to m, also z_p can be regarded as the independent parameter of this problem instead of θ_i.

The optimal number of polynomials m is evaluated by Minimum Description Length (MDL) criterion[57]. In MDL criterion, we define an objective functional for a given model as the sum of lengths describing observed data and the model itself, and select the optimal model in case of that the objective functional has minimum value.

When the observed data $P^*_w(y_j)$ are given, the objective functional $L(m)$ for the number of polynomials m is formulated as follows:

$$L(m) = L_P(\mathbf{P}_w|m) + L_M(m) \tag{4.53}$$

where, $\mathbf{P}_w$ denotes the set of the observed data = $\{\forall j\ P_w^*(y_j)\}$, $L_P(\mathbf{P}_w|m)$ the description length of the observed data and $L_M(m)$ the description length of the model.

Let $\hat{\boldsymbol{\zeta}}_m = \{\hat{z}_1, \ldots, \hat{z}_m\}$ as the estimated shape parameters using m polynomials. $L_P(\mathbf{P}_w|m)$ is obtained as follows:

$$L_P(\mathbf{P}_w|m) = \frac{1}{\log_e 2}\left\{\frac{n}{2}\log_e 2\pi\hat{\sigma}^2 + \frac{n}{2}\right\}, \tag{4.54}$$

where n denotes the number of $P_w^*(y_j)$, and,

$$\hat{\mu} = \frac{1}{n}\sum_{j=1}^{n} e(y_j)\ , \quad \hat{\sigma}^2 = \frac{1}{n}\sum_{j=1}^{n}(e(y_j) - \hat{\mu})^2\ , \quad e(y_j) = P_w^*(y_j) - P_w(y_j; \hat{\boldsymbol{\zeta}}_m)\ , \tag{4.55}$$

and $P_w(y_j; \hat{\boldsymbol{\zeta}}_m)$ is the image intensity computed from Eq.(4.50) using $\hat{\boldsymbol{\zeta}}_m$.

$L_M(m)$ is obtained as follows:

$$L_M(m) = \sum_{p=1} m \log_2 |y_p^{\Delta}| + \log_2(|\hat{z}_p|/\hat{\delta}_p), \tag{4.56}$$

where, y_p^{Δ} is assumed to be integer and $\hat{\delta}_p$ is the quantization step given by the following equation[57]:

$$\hat{\delta}_p = \sqrt{\left.\frac{12}{\partial^2 L_P/\partial z_p^2}\right|_{z_p=\hat{z}_p}}\ . \tag{4.57}$$

The optimal number of polynomials under the MDL criterion are estimated by the following algorithm:

Step 1. Let $m = 1$ as the initial value.

Step 2. Estimate shape parameters $\hat{\boldsymbol{\zeta}}_m$ using m polynomials, and evaluate $L(m)$. If $L(m)$ has minimum value, then let $\hat{m} = m$.

Step 3. If the condition $L_M(m) > L(\hat{m})$ is satisfied, then stop. $\hat{m}$ is the optimal number of polynomials. If this condition is not satisfied, then increment m and go to step 2.

3D Tessellation of the Book Surface

This method approximates the 3D book surface by piecewise planar rectangles with constant albedos. The constant albedo is estimated by averaging the albedos in its rectangle. As shown in Fig.4.8, this tessellation is constructed to the recovered book surface. Hence, before this tessellation, the albedo distribution is restored by using the method described in next Sect.4.5.3.

By using this tessellation, the computational cost of the interreflections are reduced. In this method, we assume that, in all over a rectangle region, the slant of the book surface shape and the illuminant intensity have constant values respectively, which are equal to the values at the center of the rectangle. From this assumption, the sum of the reflection intensities at each point in a rectangle equals to the product of the rectangle area by the reflection intensity at the center of rectangle with the average albedo. Using this

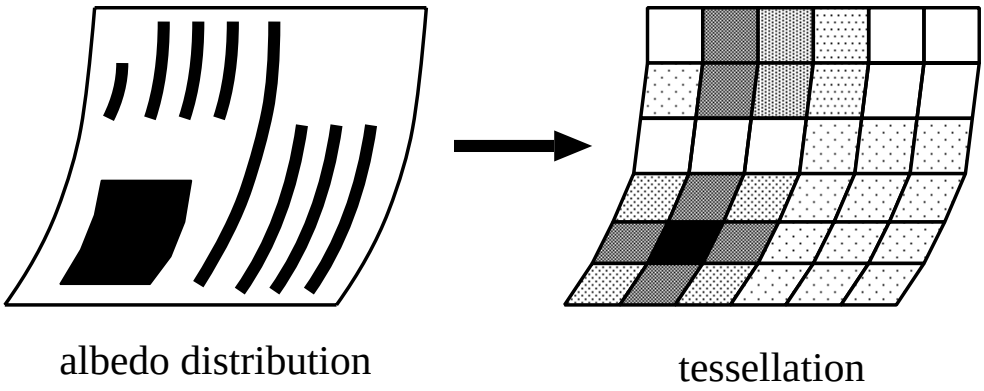

Figure 4.8: Tessellation of albedo distribution.

approximation, the computation time of $I_{inter}(x_i, y_j)$ can be reduced from the number of surface points to the number of rectangles.

The problem of the tessellation method is how to determine the size of rectangles. The rectangular size might be determined by the trade-off between the computational cost of the interreflections and the accuracy of the estimated shape. But, it is clear that the optimal rectangular size is different from the book surface shape, hence it is difficult to determine the optimal rectangular size beforehand. Moreover, this method has another problem about the rectangular configuration, ex. isotropic or anti-isotropic division. These problems are examined quantitatively in the experiments (Sect.4.6).

4.5.3 Restoration of Geometric Distortion

The albedo obtained from Eq.(4.51) is corresponding to the pixel (x_i, y_j) in the scanned image. On the other hand, in order to recover the surface shape, the albedos all over the book surface is necessary. But the scanned image is geometrically distorted because of the following reasons:

- Since 1D images $P^*(y_j)$ along x-axis are obtained by the perspective projection, the higher the book surface located from the scanning plane, the smaller the 1D image is projected.
- Also along y-axis, the scanned image is reduced because the curved book surface is taken by the orthogonal projection.

Hence, the distorted scanned image should be restored to the undistorted book surface image. We use the following restoration methods:

- *Restore the distortion caused by the perspective projection (along x-axis):*
  Let $z(y_j)$ be the height of the book surface at (x_i, y_j) in the scanned image, X_i the x coordinate on the book surface corresponding to (x_i, y_j), is represented as follow:

$$X_i = \frac{z(y_j) + F}{F}(x_i - X_0) + X_0, \tag{4.58}$$

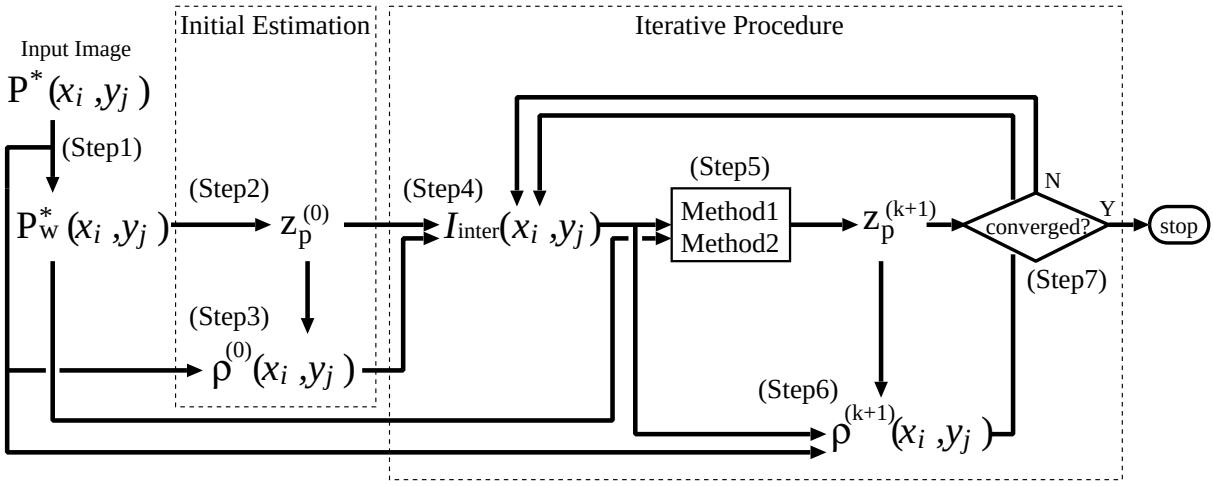

Figure 4.9: Shape reconstruction algorithm.

where F denotes the length from the scanning plane to the focal point of the lens C, X_0 is the x coordinate of the focal point (Fig.4.7). From this relation, 1D image $P^*(y_j)$ can be expanded.

- *Restore the distortion caused by the orthogonal projection (along y-axis):*
  Let $\theta(y_j)$ be the slant angle of the book surface along y-axis at (x_i, y_j) in the scanned image. In this case, $1/\cos\theta(y_j)$ is the length of the book surface corresponding to the width of one pixel at (x_i, y_j). Hence, the distortion can be restored by expanding $1/\cos\theta(y_j)$ pixels per one pixel along y-axis.

These restorations are used at Step. 3 and 6 in the next shape reconstruction algorithm. In the image expansion, we use the linear interpolation.

4.5.4 Shape Reconstruction Method

We use the following iterative algorithm to recover the cross section shape of the book surface (Fig.4.9):

Step 1. Extract $P^*_w(y_j)$ from $P^*(x_i, y_j)$.

[**Initial Estimation**]

Step 2. Estimate the initial shape by using the photometric model ignoring $I_{inter}(x_i, y_j)$ in Eq.(4.46). In this estimation, the optimal number of intervals m is also calculated based on the MDL criterion described in Sect.4.5.2.

Step 3. Recover the albedo distribution $\rho^{(0)}(x_i, y_j)$ and the geometric distortion using the initial shape and the observed image $P^*(x_i, y_j)$.

[**Shape Reconstruction under Interreflections**]

Step 4. Calculate $I_{inter}(x_i, y_j)$ using the tessellated book surface model.

Step 5. Calculate the depth $z_p^{(k+1)}$ which minimize the total square errors between $P_w(y_j)$ and $P_w^*(y_j)$ for the $I_{inter}(x_i, y_j)$ obtained at Step 4.

The computation of $z_p^{(k+1)}$ is realized by Method 1 followed by Method 2.

Method 1. Calculate z_p sequentially by minimizing the function G in each interval:

$$G(p, z_p) = \sum_{y_j=y_{p-1}^{\Delta}}^{y_p^{\Delta}} \left\{P_w^*(y_j) - P_w(y_j)\right\}^2. \tag{4.59}$$

Method 2. Calculate all z_p simultaneously by minimizing the function:

$$H(z_1, ..., z_m) = \sum_{p=1}^{m} G(p, z_p). \tag{4.60}$$

The results of Method 1 are also used as the initial estimates of z_p in Method 2.

Step 6. Recover the albedo distribution $\rho^{(k+1)}(x_i, y_j)$and the geometric distortion using the 3D shape estimated at Step 5, the $I_{inter}(x_i, y_j)$ obtained at Step 4 and $P^*(x_i, y_j)$.

Step 7. If the values $z_p^{(k+1)}$ converge, then the algorithm is terminated. Otherwise goto Step 4.

4.5.5 Enhancement of Image Restoration

By using Eq.(4.51) and the restoration of the geometric distortion described above, the albedo distribution is almost recovered. But, the clearness and readability of the image is not improved so much because of the following reasons:

- The albedo distribution near the gutter become low contrast between the white background and the black letters.
- Because of the linear interpolation for the image restoration (Sect.4.5.3), the edge part of the letter is blurred.
- The length of the linear light source is actually limited. But, since this characteristic is not included in the photometric model, the shading is remained along the x-axis.

To improve these problems, we use the following methods:

- Enhance the contrast between the albedos at printed and unprinted areas.
- Interpolate the albedos by the cubic convolution.
- Remove the shading along the x-axis using the light source model which length is limited.

These methods could be used in Step 3 and 6 of the shape reconstruction algorithm. But, since the computation time of the shape reconstruction will be increased, these methods are applied to the finally image restoration.

4.6 Experiments

In this section, we show the experimental results of the shape reconstruction and the image restoration by using the proposed method. First, we show the methods to estimate the photometric parameters of the image scanner. Next, the ability of the shape reconstruction is evaluated by using an artificial 3D model (Sect.4.6.2 $\sim$ Sect.4.6.6), and the effectiveness of the proposed method is demonstrated by a real book surface image (Sect.4.6.7).

4.6.1 Scanner Calibration

In this section, we describe the methods to estimate the parameters in the photometric model of the image scanner.

Focal length and position

The focal length and its position of x coordinate in the image scanner is obtained from an image of lines drawn on the slope surface model (Fig.4.10). First, we extract lines segments in the obtained image as shown Fig.4.11, where $(x_0^{(i)}, y_0)$ and $(x_{max}^{(i)}, y_{max})$ $(1 \leq i \leq N)$ are end point coordinates of each line segment. We assume that the model surface height (z) equals to 0 at $y = y_0$.

Next, we estimate the focal length F and x coordinate X_0 using the relation between F, X_0 and end point coordinates of each line segment by the perspective projection as follows (Fig.4.12):

$$X_0 + \frac{x_0^{(i)} - x_{max}^{(i)}}{(y_{max} - y_0)\tan(\theta)} F = x_{max}^{(i)} \tag{4.61}$$

where θ is the angle between the scanning plane and the slope surface. By using this relation, F and X_0 are estimated by linear least squares. From Eq.(4.61), we can formulate this relation for all line segments:

$$\begin{bmatrix} 1 & a_1 \\ 1 & a_2 \\ \vdots & \\ 1 & a_N \end{bmatrix} \begin{bmatrix} X_0 \\ F \end{bmatrix} = \begin{bmatrix} b_1 \\ b_2 \\ \vdots \\ b_N \end{bmatrix} \tag{4.62}$$

where

$$a_i = \frac{x_0^{(i)} - x_{max}^{(i)}}{(y_{max} - y_0)\tan(\theta)}, \tag{4.63}$$

$$b_i = x_{max}^{(i)}. \tag{4.64}$$

Hence, F and X_0 are estimated by:

$$\begin{bmatrix} X_0 \\ F \end{bmatrix} = \frac{1}{N\sum_{i=1}^{N} a_i^2 - \left(\sum_{i=1}^{N} a_i\right)^2} \begin{bmatrix} \sum_{i=1}^{N} a_i^2 \sum_{i=1}^{N} b_i - \sum_{i=1}^{N} a_i \sum_{i=1}^{N} a_i b_i \\ -\sum_{i=1}^{N} a_i \sum_{i=1}^{N} b_i + N \sum_{i=1}^{N} a_i b_i \end{bmatrix}. \tag{4.65}$$

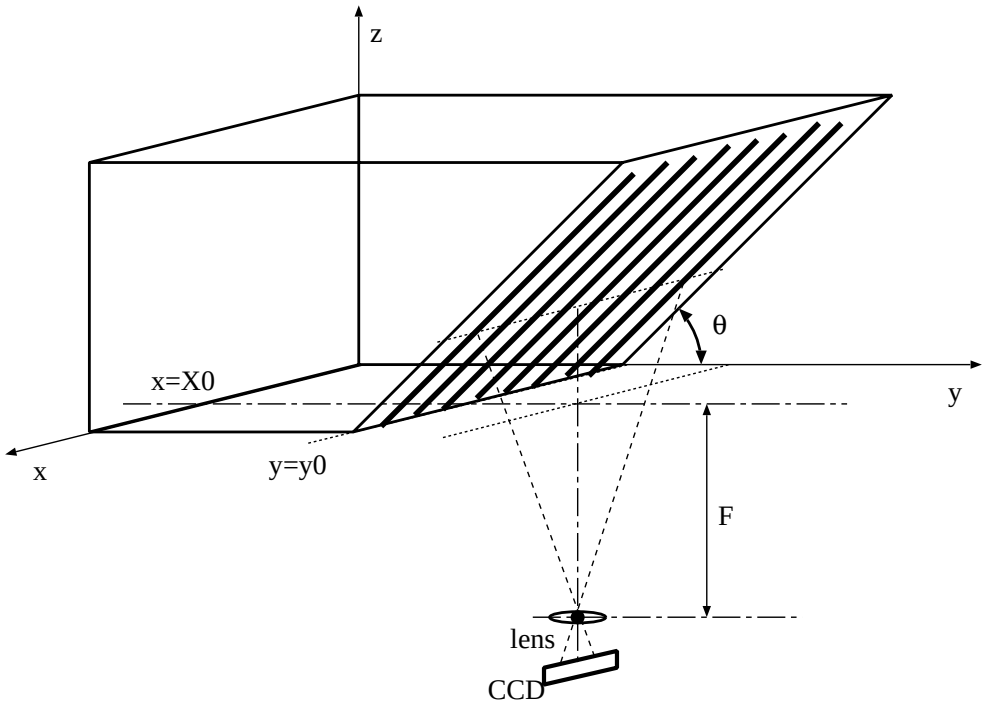

Figure 4.10: Slope model for estimation of focal length and position.

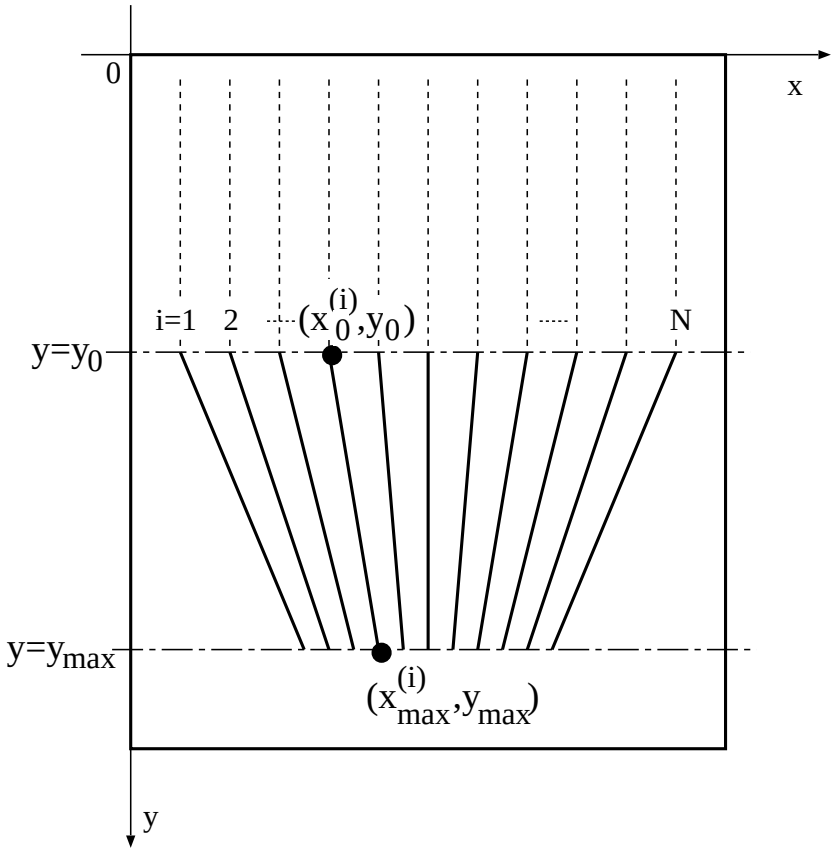

Figure 4.11: Line segments on slope model image.

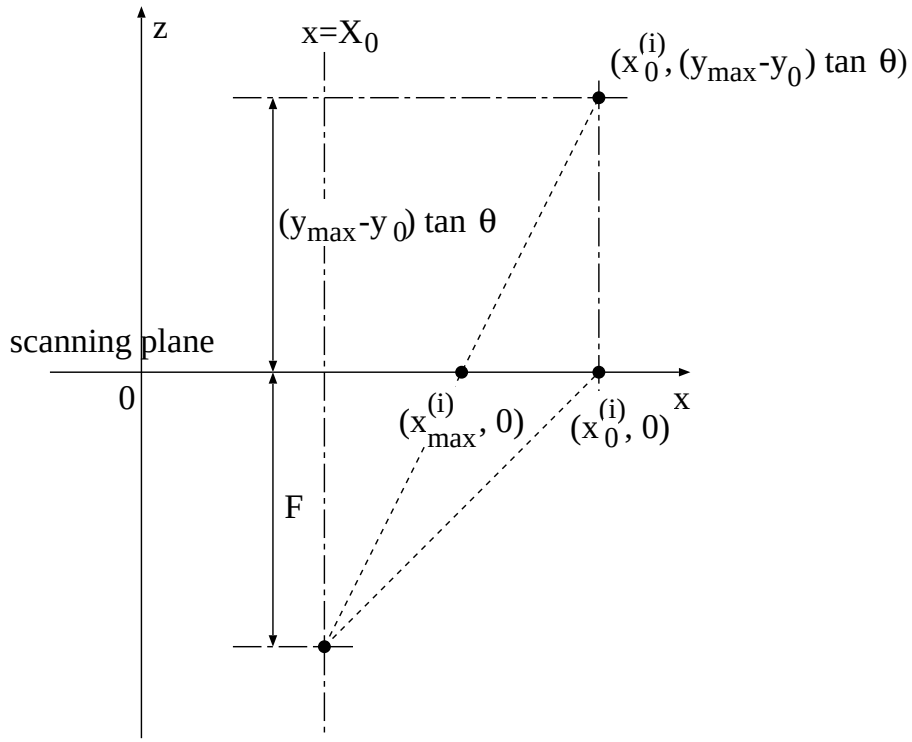

Figure 4.12: Perspective projection of a line segment on slope model in $x - z$ plane.

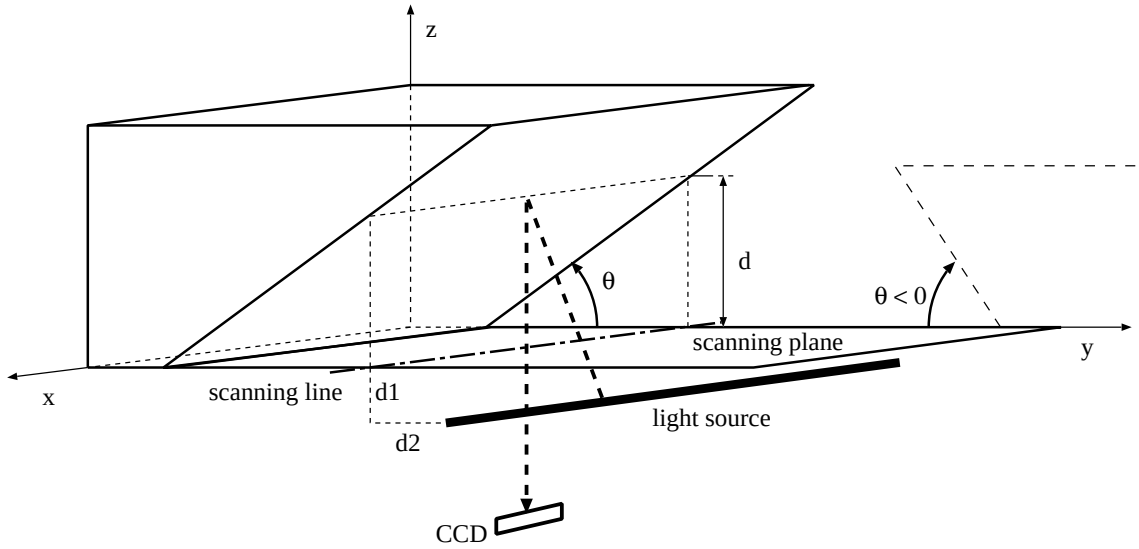

Figure 4.13: Slope model for photometric parameter estimation.

Photometric parameters

The parameters a, ρ_w, α, I_e, d_1, d_2, s, n and Δ in the photometric models are estimated by using the slope surface model. A white paper is put on this surface, and several images of this surface are acquired (Fig.4.13). At each image, the slant angle θ is different to each other. In this experiment, we use $\theta = \pm 10$, ± 20, ± 27.5, ± 35, ± 46, ± 54, and ± 59 which are determined by the image resolutions. The images in case of $\theta < 0$ are acquired by turning the slope surface model on the scanning plane.

The photometric parameters are estimated by the following procedure:

Step 1. Extract the intensities $P_w^*(z, \theta)$ on the white slope surface in observed images.

Step 2. Estimate s, n, Δ and the distribution of the illuminant intensity $\hat{I}_s(z_i)$ $(1 \leq i \leq m)$ by minimizing the following objective functional:

$$\sum_{\theta, z_i} \left\{ P_w^*(\theta, z_i) - \hat{I}_s(z_i) \cdot (s \cos(\theta - \psi(z_i)) - (1 - s) \cos^n(2\theta - \psi(z_i)) - \Delta \right\}^2 \quad (4.66)$$

where m is the number of illuminant intensity to compute, and we use the specific measurements for d_1 and d_2. Figure 4.14 shows $\hat{I}_s(z_i)$ estimated in this experiment.

Step 3. Estimate the light source parameters $a \cdot \rho_w \cdot \alpha$, I_e, d_1 and d_2 from $\hat{I}_s(z_i)$ by minimizing the following objective functional:

$$\sum_{z_i} \left\{ \hat{I}_s(z_i) - \frac{a \cdot \rho_w \cdot \alpha}{\sqrt{(d_1)^2 + (z_i + d_2)^2}} + a \cdot \rho_w \cdot I_e \right\}^2 \quad (4.67)$$

In this method, $a \cdot \rho_w \cdot \alpha$ and $a \cdot \rho_w \cdot I_e$ cannot be obtained separately.

Step 4. By using the estimated parameters above procedures as the initial values, we estimate all photometric parameters by minimizing the following objective functional:

$$\sum_{\theta, d} \{ P_w^*(\theta, d) - P_w(\theta, d) \}^2 \quad (4.68)$$

where the term $I_D(\psi)$ (the directional distribution of the illumination) is neglected in $P_w(\theta, d)$.

Step 5. Estimate $I_D(\psi)$ using d_1 and d_2 estimated in step 4 by the method described in next section.

Step 6. Estimate all photometric parameters again by minimizing the objective functional in Eq.(4.68). In this step, $I_D(\psi)$ estimated in step 5 is used in $P_w(\theta, d)$.

Step 7. Iterate from step 5 and 6 until the estimated parameters are converged.

Directional distribution of illumination

In this section, we describe the method to measure the directional distribution of the illumination $I_D(\psi)$. First, as shown in Fig.4.15, the white Lambertian surface plane is stood up on the scanning plane. This plane is arranged to perpendicularly to both the scanning plane and the linear light source. This Lambertian surface is illuminated by the linear light source in the image scanner, and the image of its surface is taken by the external camera. The optical axis of this camera is parallel to the Lambertian surface normal.

The intensity of the reflection on the Lambertian surface is formulated as follows (Fig.4.16):

$$P(\psi, r) = \rho \cdot \alpha \cdot I_D(\psi) \int_{L_0}^{L} \frac{x}{\sqrt[3]{x^2 + r^2}} dx, \tag{4.69}$$

where

$$L_0 = \frac{r \cdot \cos\psi \cdot d_1}{r \cdot \cos\psi - d_2}. \tag{4.70}$$

From this formulation, we obtain

$$P(\psi, r) = \rho \cdot \alpha \cdot I_D(\psi) \left(\frac{1}{\sqrt{L_0^2 + r^2}} - \frac{1}{\sqrt{L^2 + r^2}} \right). \tag{4.71}$$

If the light source location (d_1, d_2) is known, $\rho \cdot \alpha \cdot I_D(\psi, r)$ can be calculated from the observed intensity $P^*(\psi, r)$ in the image.

$I_D(\psi)$ is computed by averaging $\rho \cdot \alpha \cdot I_D(\psi, r)$ for r, normalizing to $0 \leq I_D(\psi) \leq 1$ and smoothing to reduce noise. The estimated $I_D(\psi)$ is shown in Fig.4.17.

Albedo on white background

The albedo on the white background (ρ_w) is estimated from a scanned image existing the interreflections using known shape objects whose surface is put the white paper. We calculate ρ_w from the photometric model, known shape parameter and the observed intensity including high interreflections:

$$\rho_w(x_i, y_j) = \frac{P_w^*(x_i, y_j) - I_{dir}(x_i, y_j) - \Delta}{I_{inter}(x_i, y_j)}, \tag{4.72}$$

where (x_i, y_j) is the point on the image. ρ_w is estimated by averaging $\rho_w(x_i, y_j)$.

By using these methods, the estimated values of the photometric parameters are:

$$\begin{array}{lll} a \cdot \alpha = 431.07, & d_1 = 6.94[\text{mm}], & d_2 = 12.16[\text{mm}], \\ \Delta = -5.75, & a \cdot I_e = 0.0, & \\ s = 0.94, & n = 2.24, & \rho_w = 0.014 \end{array} \tag{4.73}$$

These parameters are used in the following experiments.

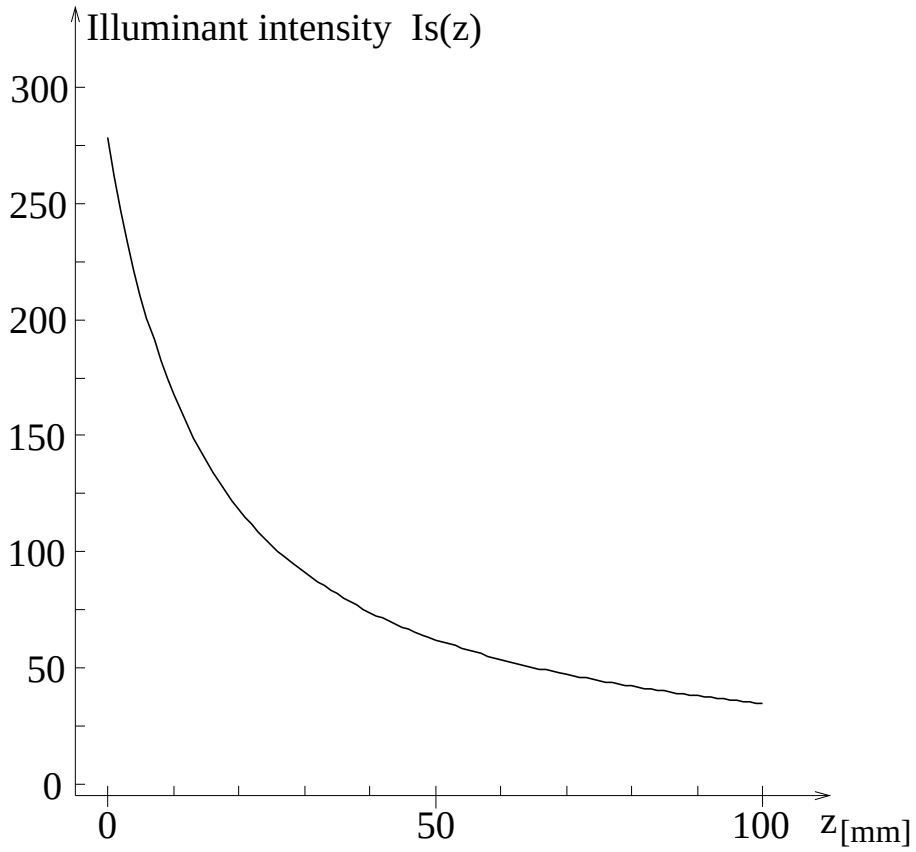

Figure 4.14: Estimated illuminant intensity distribution $\hat{I}_s(z_i)$.

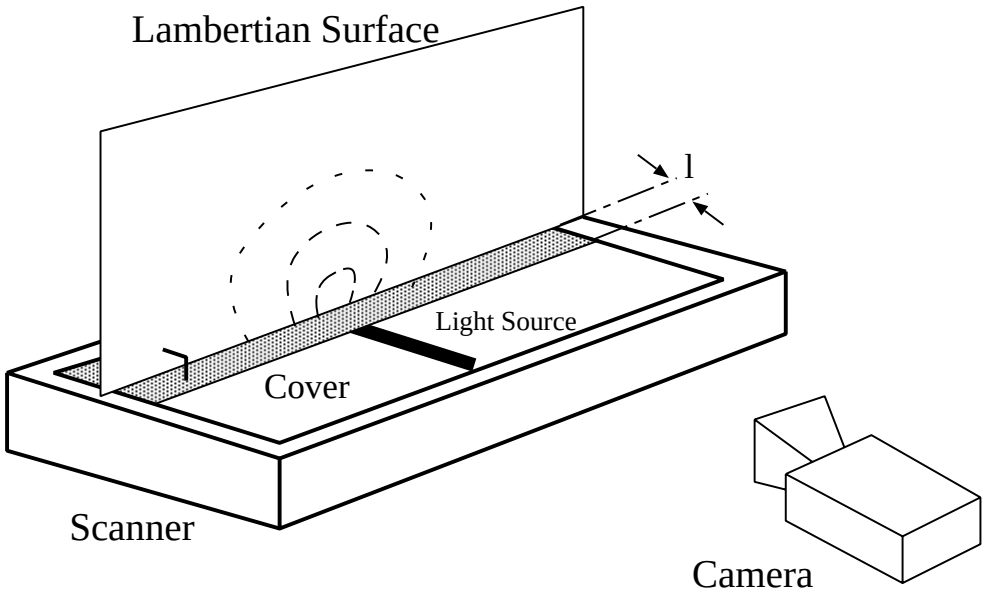

Figure 4.15: Experimental set up for measuring illumination distribution.

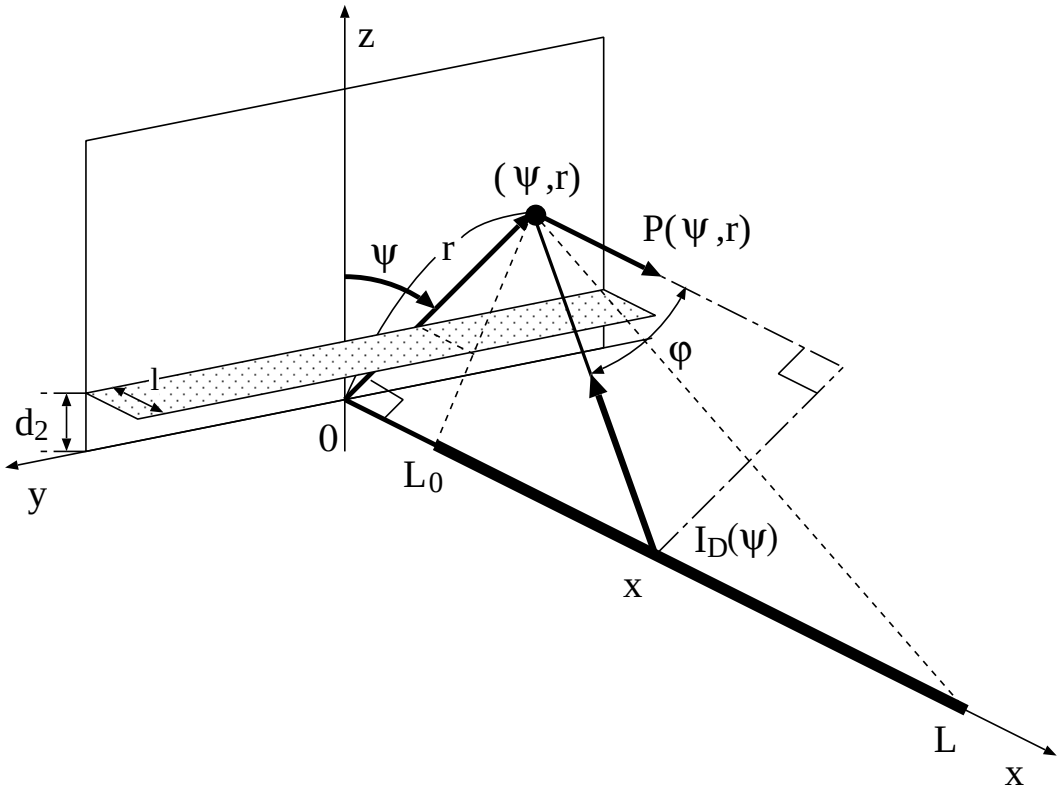

Figure 4.16: Photometric model of illumination distribution.

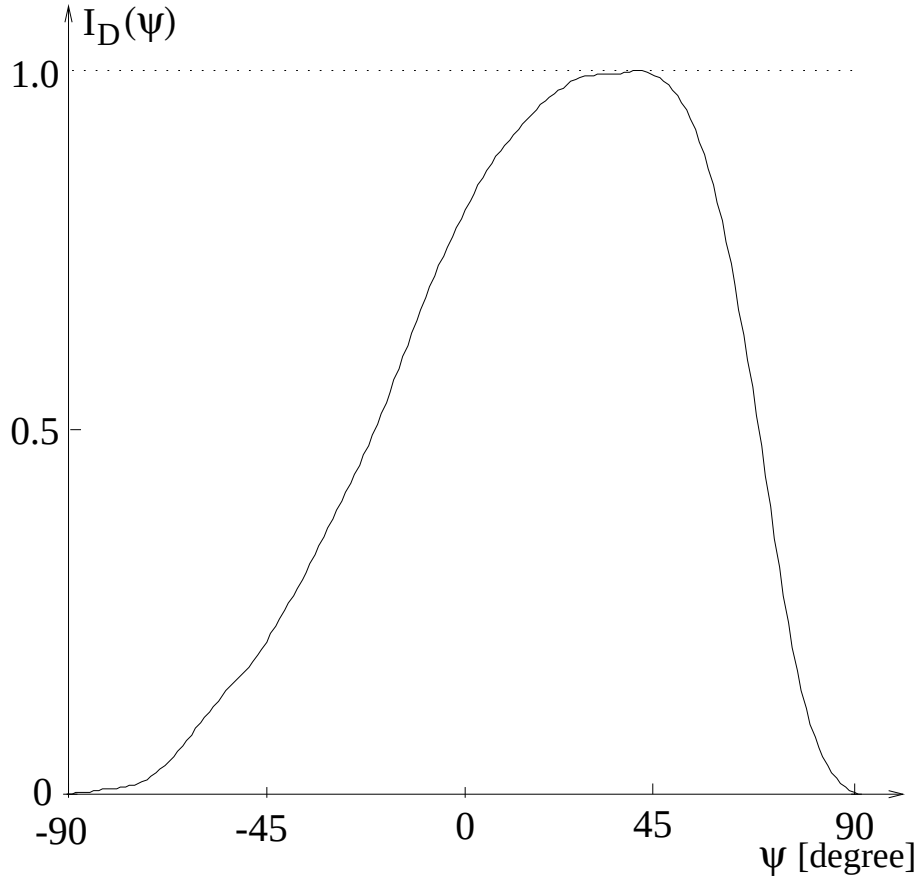

Figure 4.17: Estimated illumination distribution.

4.6.2 Scanned Image of Book Surface Model

In this experiment, an artificial 3D model with a known cylindrical shape is used instead of the book. The undistorted document image is put on its surface. While scanning the image, the image scanner and the model are covered with a black box to avoid the illumination from the outside.

Figure 4.18 shows the input image of the book surface model. In this image, we notice that the shading and the geometric distortion have occurred around the gutter. In Fig.4.19, the bold lines denote the intensity profile $P_w^*(y)$ of the white background in Fig.4.18. The dashed lines are also the intensity profiles without the interreflections. These distributions are obtained from scanned images by arranging the model at $y > 0$ or $y < 0$ respectively. The differences of the bold and dashed lines are equivalent to the pixel values of the interreflections $I_{inter}(x(y_j), y_j)$.

4.6.3 Shape Reconstruction Using Piecewise Polynomial Model

First, we show the comparison of the shape estimation error and the computation time using the piecewise polynomial model fitting and the full point-wise estimation. In this experiment, half of the 3D model ($y > 0$) is used so the interreflections are ignored. In case of the polynomial model, the optimal number of polynomials obtained by the MDL criterion was 15.

Table 4.1 shows the computation time (on a SPARC Station 10) and the mean error of the estimation using the piecewise polynomial model fitting and the full point-wise estimation. This result demonstrates that the piecewise shape approximation drastically reduces the computation time. Moreover, the accuracy of the estimation is improved, because the piecewise approximation provides stability against noise.

Table 4.1: Effectiveness of the piecewise polynomial model fitting.

	number of parameters	time ([min.])	error [mm]
piecewise	15	1 (1.18)	0.94
point-wise	480	233 (276.17)	1.28

4.6.4 Convergence of Book Surface Shape

Next, we show the experimental results of the convergence of the estimated shape. As shown in Sect.4.3.3, the conditions of the convergence are:

$$|\lambda_1| < 1 \ \text{ and } \ |\lambda_2| < 1, \tag{4.74}$$

for λ_1 and λ_2 which are the eigen values of $\boldsymbol{A}$ in Eq.(4.32). The behavior of the estimated shape in the iterative shape reconstruction process is also determined by the signs of elements in $\boldsymbol{A}$. However, since it is difficult to formulate λ_1, λ_2 and $\boldsymbol{A}$ using the photometric models, we evaluate the actual values of them with the scanner image and the photometric parameters under the following conditions:

Figure 4.18: Observed image (artificial model).

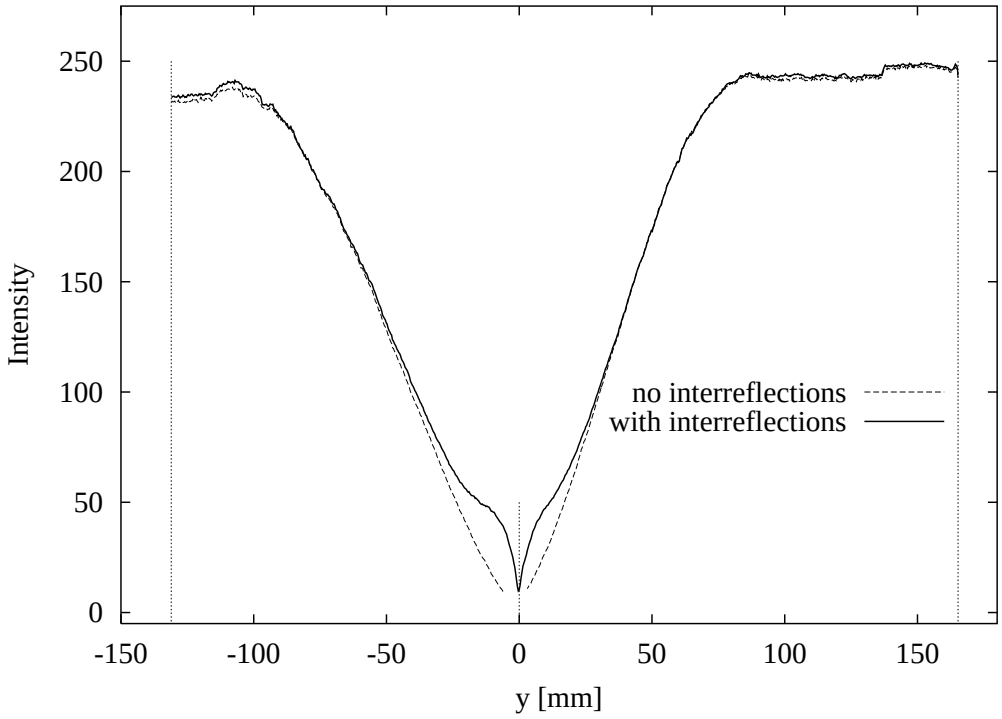

Figure 4.19: Image intensity $P_w^*(y_j)$ at non-printed region.

- As the observed image intensity, we use the intensity profile of the white background as shown in Fig.4.19. In the analysis of the convergence, the albedo distribution is assumed to be constant, so we use the synthesized scanner image such as the intensity profile distributing along x-axis.

- Equations (4.16) and (4.17) are used as the shape models.

- Equations (4.18) and (4.19) are used as the photometric models. These models are constructed by Eqs. (4.47) and (4.48).

- The values of parameters in Eq.(4.73) are used as the photometric parameters.

- The differential coefficients in matrix $\boldsymbol{A}$ are calculated by the central difference as follows:

$$rI_{dir}{}'(Z_{r0}) = \frac{rI_{dir}(Z_{r0}+h) - rI_{dir}(Z_{r0}-h)}{2h} \tag{4.75}$$

$$\frac{\partial rI_{inter}(Z_{r0}, Z_{l0})}{\partial Z_r} = \frac{rI_{inter}(Z_{r0}+h, Z_{l0}) - rI_{inter}(Z_{r0}-h, Z_{l0})}{2h} \tag{4.76}$$

$$\frac{\partial rI_{inter}(Z_{r0}, Z_{l0})}{\partial Z_l} = \frac{rI_{inter}(Z_{r0}, Z_{l0}+h) - rI_{inter}(Z_{r0}, Z_{l0}-h)}{2h} \tag{4.77}$$

$$lI_{dir}{}'(Z_{l0}) = \frac{lI_{dir}(Z_{l0}+h) - lI_{dir}(Z_{l0}-h)}{2h} \tag{4.78}$$

Table 4.2: Calculated matrix elements and eigen values (Z_{r0}= 48.78, Z_{l0}= 39.09[mm])

y_r	y_l	a_{rr}	a_{rl}	a_{lr}	a_{ll}	λ_1	λ_2
3.387	−3.387	0.0000	0.0000	−0.3767	0.8455	0.4228	−0.4228
6.773	−6.773	0.0000	0.0000	−0.2320	0.5641	0.2820	−0.2820
10.160	−10.160	0.0027	0.2800	−0.1528	0.3712	—	—
13.547	−13.547	0.0565	−0.0051	−0.1019	0.2611	0.1305	−0.0792
16.933	−16.933	0.1043	−0.0467	−0.0689	0.1965	0.1019	−0.0444
20.320	−20.320	0.0888	−0.0394	−0.0472	0.1487	0.0772	−0.0279
23.707	−23.707	0.0645	−0.0249	−0.0326	0.1133	0.0573	−0.0177
27.093	−27.093	0.0454	−0.0152	−0.0227	0.0855	0.0424	−0.0122
30.480	−30.480	0.0313	−0.0089	−0.0161	0.0616	0.0305	−0.0081
33.867	−33.867	0.0221	−0.0058	−0.0107	0.0427	0.0211	−0.0047

$$\frac{\partial lI_{inter}(Z_{r0}, Z_{l0})}{\partial Z_r} = \frac{lI_{inter}(Z_{r0}+h, Z_{l0}) - lI_{inter}(Z_{r0}-h, Z_{l0})}{2h} \quad (4.79)$$

$$\frac{\partial lI_{inter}(Z_{r0}, Z_{l0})}{\partial Z_l} = \frac{lI_{inter}(Z_{r0}, Z_{l0}+h) - lI_{inter}(Z_{r0}, Z_{l0}-h)}{2h} \quad (4.80)$$

In the above calculations, the interreflections are estimated by the tessellation constructed by 40×40 same size rectangulars per one side of the book surface.

- In the shape model (Eq.(4.16), (4.17)), y_{r0}, y_{r1}, y_{l0}, and y_{l1} are assumed to be fixed. Here, we use $y_{r0} = 101.6$, $y_{r1} = 1.52$, $y_{l0} = -101.6$, and $y_{l1} = -1.52$[mm].

$\boldsymbol{A}$, λ_1, and λ_2 are evaluated by giving the y coordinates of the observed data (y_r, y_l) and the initial shape parameters (Z_{r0}, Z_{l0}) as shown in Fig.4.20. Table 4.2 shows the values of a_{rr}, a_{rl}, a_{lr}, a_{ll}, λ_1, and λ_2 under Z_{r0}= 48.78, Z_{l0}= 39.09[mm][5], $y_r = 3.387 \sim 33.87$[mm] (interval: 3.387[mm][6]), and $y_l = -y_r$ (the symmetric position).

In Table 4.2, in case of $y_r = 10.160$, the eigen values are obtained as the imaginary solutions. In case of $y_r = 3.387$ and 6.773, a_{rr} and a_{rl} become to 0 because of the difference of height between the left and right shape. In case of $y_r \geq 13.547$, all values of $|\lambda_1|$ and $|\lambda_2|$ is smaller than 1, hence we can see that the estimated shapes can converge. But, in case of $y_r \geq 13.547$, the values of elements of $\boldsymbol{A}$ become $a_{rr}, a_{ll} > 0$ and $a_{rl}, a_{lr} < 0$. This means that the estimated shapes do not always change vibratingly in the iterative shape reconstruction process.

Next, we show another results of experiments because the initial shape parameters (Z_{r0}, Z_{l0}) are not always obtained same values in Table 4.2 what method is used to estimate these parameters. Here, we examine another 250 cases of Z_{r0}, Z_{l0}, y_r, and y_l as follows:

- Z_{r0} and Z_{l0} are assigned from 30 to 50[mm] (interval: 5[mm]) at each. The combination of Z_{r0} and Z_{l0} are 25 cases.

[5]These heights are the initial shapes in the next experiments.

[6]3.387[mm] = 10 [dots] in 75 [dpi] image data.

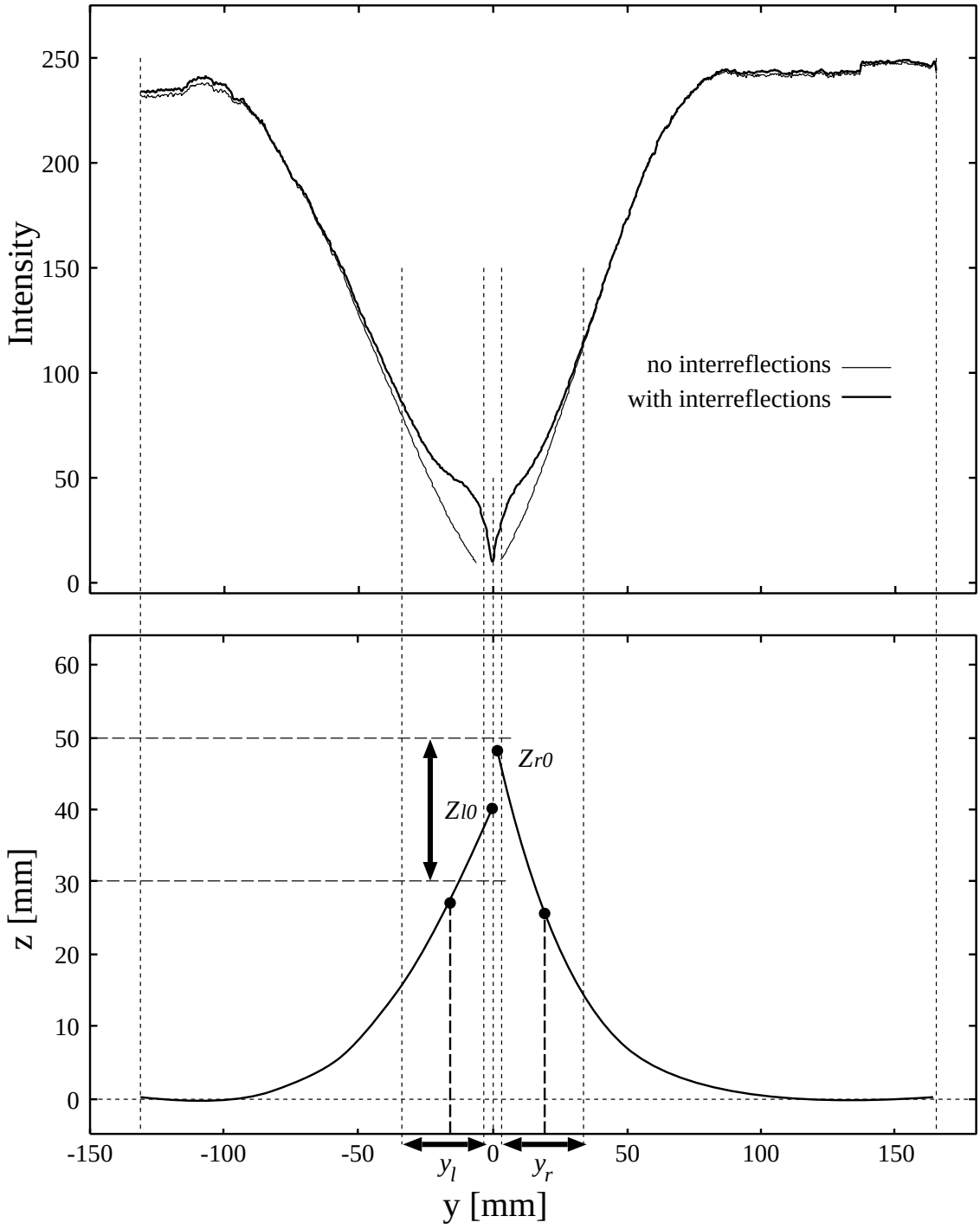

Figure 4.20: Shape models for convergence evaluation.

- At each combination of Z_{r0} and Z_{l0}, y_r are assigned from 3.387 to 33.87[mm] (interval: 3.387[mm]), and $y_l = y_r$. Hence, there are 10 cases for y_r and y_l.

The results of these experiments are:

- In case of $|\lambda_1|, |\lambda_2| < 1$: 231 cases,
- In case of $|\lambda_1|, |\lambda_2| \geq 1$, or λ_1 and λ_2 become the imaginary solutions: 19 cases.

From these results, we can see that the estimated shape can converge in the iterative shape reconstruction process.

Note that, in the following cases, λ_1 and λ_2 did not become appropriate values:

- The difference of Z_{r0} and Z_{l0} is large and y_r (y_l) is very close to the gutter position.
- The intensity of the interreflections is very weak at y_r and y_l. In this case, y_r and y_l are apart from the gutter position.

As similar to the results of Table 4.2, a_{rr}, a_{rl}, a_{lr}, and a_{ll} become $a_{rr}, a_{ll} > 0$, $a_{rl}, a_{lr} < 0$ in 173 cases. As described in Sect.4.3.3, $a_{rl}, a_{lr} < 0$ means that "when the height of the opposite side of the book surface is low, the intensity of the interreflections become strong, and when the height of the opposite side of the book surface is high, the intensity of the interreflections become weak." On the other hand, $a_{rr}, a_{ll} > 0$ means that "when the height of the estimated shape become low, the intensity of the interreflections become weak, and when the height of the estimated shape become high the intensity of the interreflections become strong." This is because of the following reason:

> When the right shape parameter Z_r is estimated by using the observed data at $y = y_r$, $\partial r I_{inter}(Z_{r0}, Z_{l0})/\partial Z_r$ of a_{rr} in Eq.(4.28) represents the gradient of the interreflections with respect to the change of the hight of the right shape. Since $rI_{inter}()$ is modeled as the reflected light intensity at $y = y_r$ of the reflected light on the left side of the book surface and the cross section shapes are modeled as the quadratic polynomial, the angle between the surface normal at $y = y_r$ and the direction of the left-to-right reflection become to be small when the hight of right shape become high. In result, the Lambertian component of the reflectance property become large, and $rI_{inter}()$ also become strong.

Therefore, in case of $a_{rr}, a_{ll} > 0$ and $a_{rl}, a_{lr} < 0$, since the conditions of Eq.(4.43) are not satisfied, the estimated shapes do not always repeat up and down regularly in the iterative process. The actual behavior of the transition of the shape height depends on the values of a_{rr}, a_{rl}, a_{lr}, a_{ll}, $\boldsymbol{Z}^{(i-1)}$, and $\boldsymbol{Z}^{(i-2)}$.

From the above results, we can show the convergence of the estimated shape under the following conditions:

- Each (left or right) cross section shape can be modeled as the single quadratic polynomial,
- The uniform and known albedo distribution,

- The photometric models can be approximated to the linear equations with respect to the shape parameters around the initial shape,

by using the proposed iterative shape reconstruction algorithm. And we also show that the estimated shapes do not always repeat up and down regularly in the iterative process.

4.6.5 Shape Reconstruction with Interreflections

Figure 4.21 shows the estimated cross section shape of Fig.4.18 under the interreflections. The dashed lines denote the initial shape, the bold lines the finally estimated shape and the dotted lines the true shape. In this experiment, the optimal numbers of the polynomials were 12 for $y < 0$ and 18 for $y > 0$ respectively by the MDL criterion. The tessellation is constructed by 20×20 same size rectangles per one side of the surface. The number of iteration for the shape estimation was 4 times. Figure 4.22 shows the error of the height at each y coordinate. The dashed lines are the difference between the initial shape and the true one, and the bold lines are the difference between the finally estimated shape and the true one. The initial shape is estimated lower than the actual one. But finally shape estimated with the interreflections is obtained accurately.

In Figure 4.21, the initial shape is estimated lower than the actual shape around $y = 0$ as described in Sect.4.3.2 because in the initial shape estimation, the photometric models takes no account of the interreflections. But, there is a difference of height between the left and right initial shapes at $y = 0$ (the gutter position). This reason is as follows: because the directional distribution of the light source is not isotropic as shown in Fig.4.17, the intensity of the interreflections near the gutter is different between the left and right book surface even if its shape is symmetrical. The initial shape is estimated by using the photometric models not taking account of the interreflections. Hence, due to the difference of the observed intensity including the interreflections intensity (Fig.4.19), there is a difference between the left and right initial shape heights.

Figure 4.23 shows estimated shapes at each iteration from 0 (initial shape) to 7. Figure 4.24 shows the transitions of the heights at the gutter ($y = 0$). The bold line is the right ($y > 0$) shape and the dashed line is the left ($y < 0$) one from 0 (initial) to 10 iterations. Figure 4.25 also shows the transitions of the heights where the tessellation is constructed by 40×40 same size rectangles per one side of the surface. In this case, the interreflections can be calculated more accurately. From these figures, we can see that estimated shapes at each iteration repeats low and high in turn in this case, and as shown in previous section, the finally estimated shape is converged. Especially, when the interreflections can be calculated accurately (Fig.4.25), the estimated shape become to be converged in a few iterations.

Figure 4.26 shows the shading and distortion restored image of Fig.4.18 using the estimated shape. The contrast emphasis method described in Sect.4.5.5 is applied to this image. On the surface of the artificial model, the letters are printed close to the gutter. Since this part is almost perpendicular to the scanning plane and the contrast between the white background and the printed black letter is very low, the restoration around this part (the hatching area in Fig.4.26) is not so clear in spite of applying the image enhancement method. But, the readability of the image is improved all over the book surface.

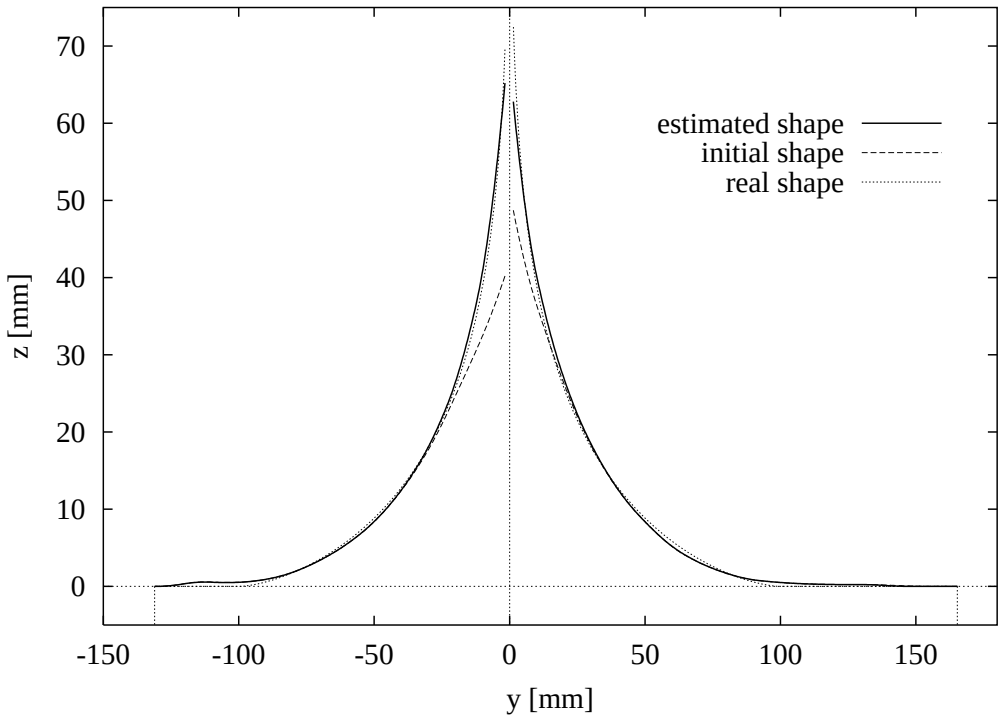

Figure 4.21: Estimated shapes and real shape.

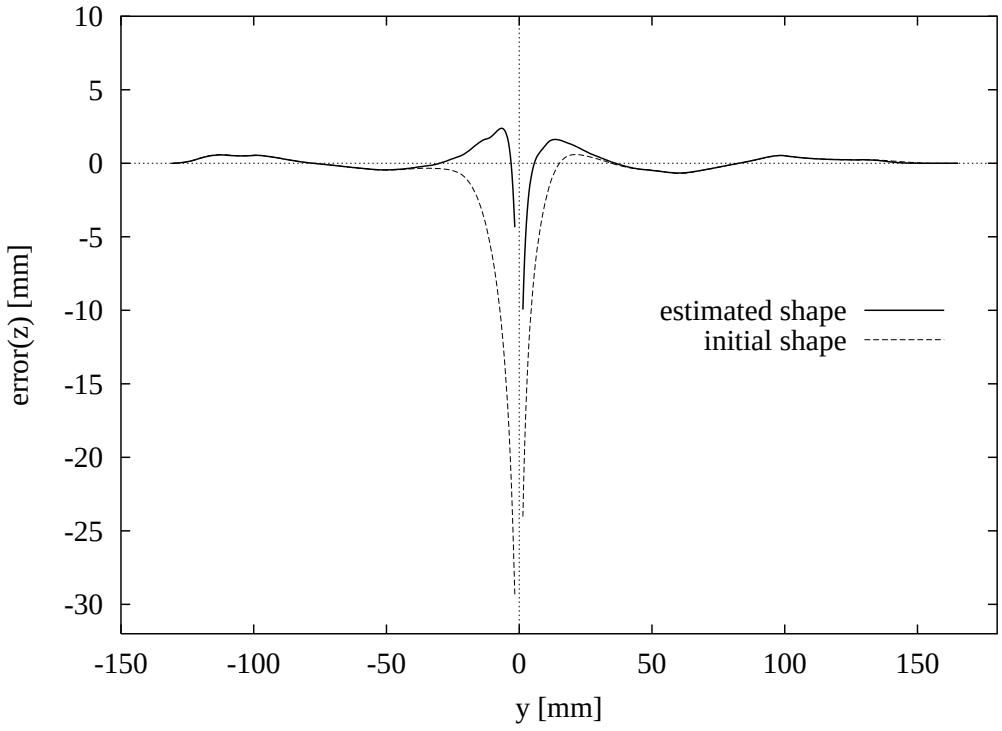

Figure 4.22: Error of initial shape and finally estimated shape.

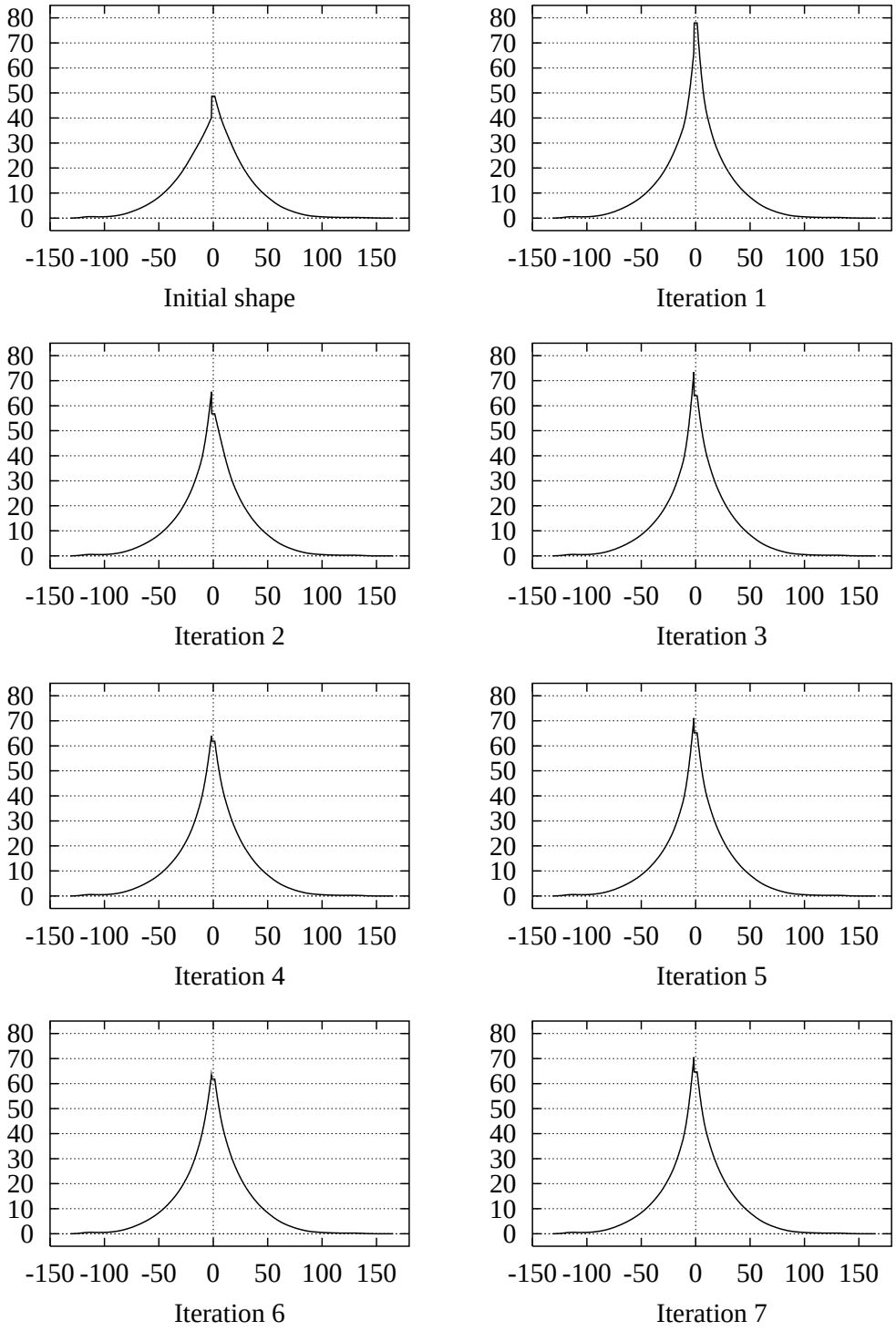

Figure 4.23: Estimated shape at each iteration.

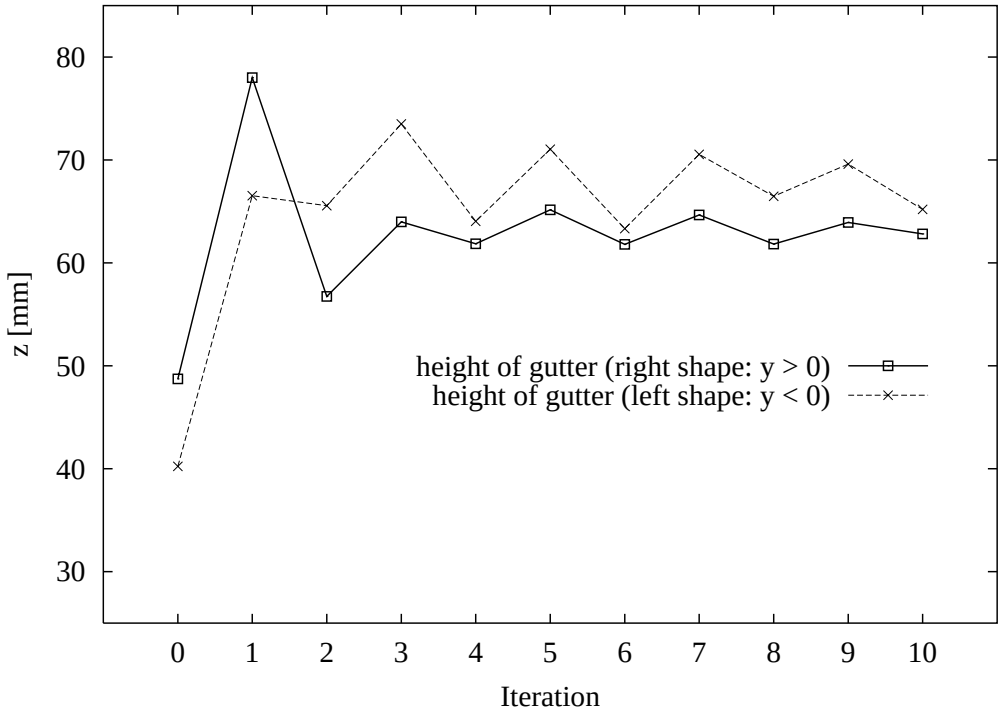

Figure 4.24: Transition of heights at $y = y_0$ (tessellation: 20×20).

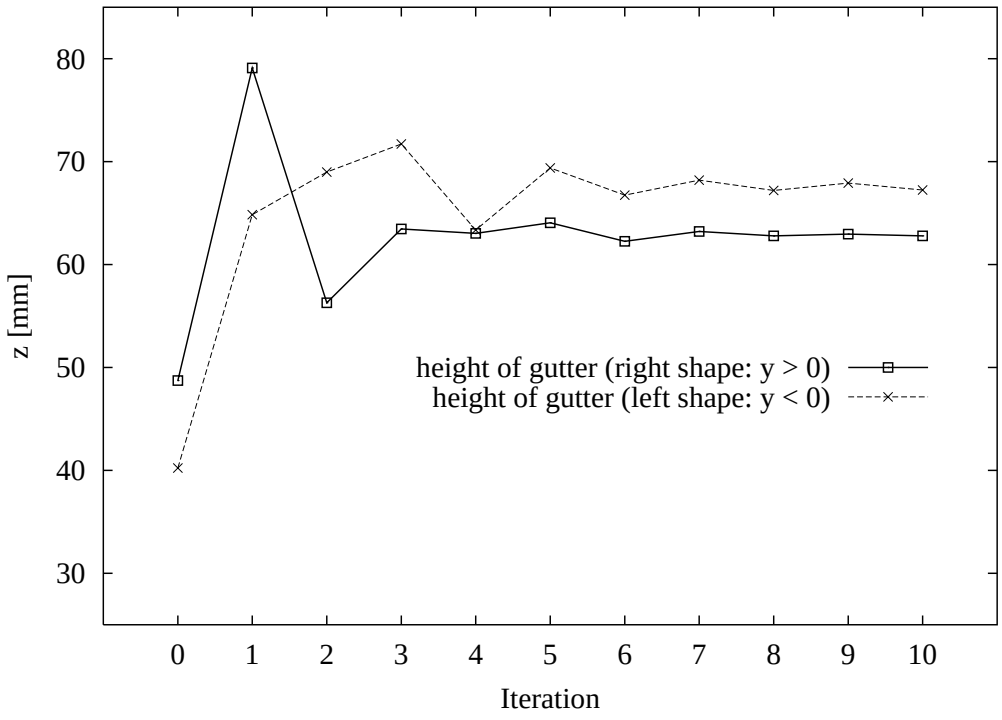

Figure 4.25: Transition of heights at $y = y_0$ (tessellation: 40×40).

Figure 4.26: Restored image (artificial model).

4.6.6 Comparison of Tessellation

Table 4.3 shows the computation times and the mean errors for $n \times n$ tessellations of the book surface[7]. The computation time is the average of the processing time from Step 3 to 5 in ten iterations. The lowest column in Table 4.3 shows the point-wise case.

From this results, we notice that the tessellation with an adequate number of rectangles, such as $n = 20$, greatly reduces the computation time while maintaining the accuracy of the result. In this case, the estimated shape is as accurate as the point-wise case.

We also examine the different configuration of the tessellation. It consists of the different size of rectangles (the size become small near the gutter). From this result, when the number of rectangles is equivalent to Table 4.3, the shape reconstruction error is also as good as Table 4.3 in spite of the configuration. Therefore, changing the configuration of the tessellation does not contribute the improvement of the shape estimation. In other word, the same size rectangle tessellation is effective to construct easily.

Table 4.3: Effectiveness of the tessellated book surface.

n	number of rectangles	time				error [mm]
		interreflections ([sec.])		reconstruction ([min.])		
1	2	0.0026	(0.07)	2.9	(1.3)	22.04
5	50	0.028	(0.76)	3.7	(1.7)	3.46
10	200	0.11	(2.90)	3.1	(1.5)	2.19
20	800	0.43	(11.8)	4.4	(2.1)	2.03
40	3,200	1.67	(46.2)	11.4	(5.4)	2.16
point-wise	628,145	100.0	(2735.5)	100.0	(47.1)	2.35

4.6.7 Recovering Real Book Surface

Next, we show the experimental results of the shape estimation and the image restoration of a real book surface. Figure 4.27 shows an image of a real book surface taken by the image scanner and Fig.4.28 intensity profile $P_w^*(y)$ of the white background. Note that due to the directional distribution of the illumination the profile is not symmetric. Figure 4.29 shows the estimated cross section shapes. The dashed lines denote the initial shape and the bold one the finally estimated shape. The optimal number of polynomials obtained by the MDL criterion was 13 for $y < 0$ and 6 for $y > 0$. The book surface was tessellated by 20×20 rectangles per one side. 7 iterations are required to obtain this shape.

In Fig.4.29, the initial shape has the difference of heights between the left and right shape at $y = 0$. This is because that the directional distribution of the illumination is not isotropic as we denoted in Sect.4.6.5. But, the finally estimated shape also has the difference of heights. It seems that this result is due to the following reasons:

[7]This tessellation divides $n \times n$ rectangles per one side of the book surface

- The difference of heights in the initial shape affects the later iterative process for the shape estimation, and then the height of the left and right finally estimated shape is different.

- The directional distribution of the illumination is not estimated accurately in the scanner calibration, because it is observed by the external camera which characteristics (such as the photo-electric transformation) are different from the image scanner.

To confirm these reasons, we estimate the book surface shape using another initial shapes which are forced into the symmetric shapes. In Fig.4.30, the dashed lines denote the symmetric initial shape which is constructed by the right ($y > 0$) initial shape in Fig.4.29, the bold lines denote the finally estimated shape using this initial shape, and the dotted lines denote the estimated shape of Fig.4.29. Figure 4.31 shows the result in case of that the left ($y < 0$) initial shape in Fig.4.29 is used as the symmetric initial shape. In Fig.4.30, the difference of heights of finally estimated shape is very smaller than that of in Fig.4.29. But in Fig.4.31, the finally shape cannot be estimated correctly. Since the initial shape is estimated more lower than the actual shape, the high symmetric initial shape of Fig.4.30 is more appropriate than that of Fig.4.31. Therefore, we can see that the initial shape influences the finally estimated shape, and if the height of actual left and right book surface shape is same, it is effective to use the high and symmetric book surface shape as the initial shape.

Next, we show the restored images using the estimated shapes. Here, we compare three restored images. Each image is restored by a different book surface shape. *Image-A*(Fig.4.32) shows the restored image using the initial shape in Fig.4.29. *Image-B*(Fig.4.33) is restored by using the finally estimated shape in Fig.4.29. *Image-C*(Fig.4.34) shows the restored image using the finally estimated shape from the symmetric initial shape in Fig.4.30. The contrast of these images are emphasized. In *Image-A*, the initial shape is lower than the actual one. Hence, the geometric distortions are still remained in the dashed box area of Fig.4.32. On the other hand, since the finally estimated shape of Fig.4.29 is higher than the actual one, *Image-B* is much expanded in the dashed box area of Fig.4.33 (especially the left side ($y < 0$) shape). Since the finally estimated shape of Fig.4.30 is most accurate in this experiment, we can confirm that the readability of *Image-C* is most improved among these images. These results demonstrate that the real book surface shape can be accurately estimated enough for the image restoration task by using the proposed method.

Figure 4.27: Observed image (real book).

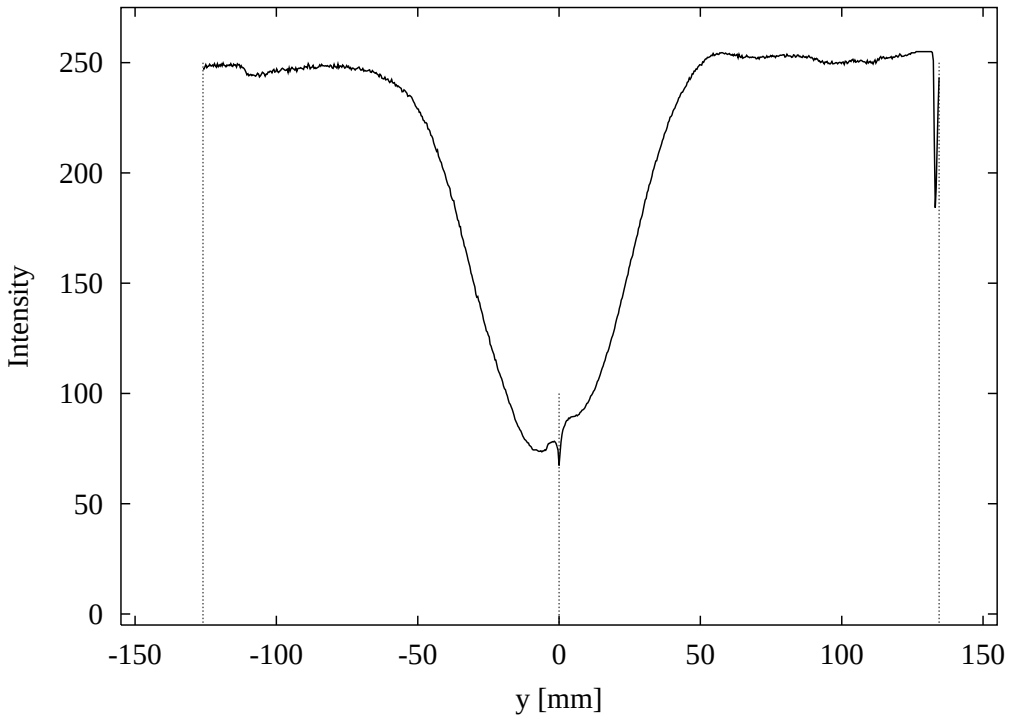

Figure 4.28: Image intensity of background paper.

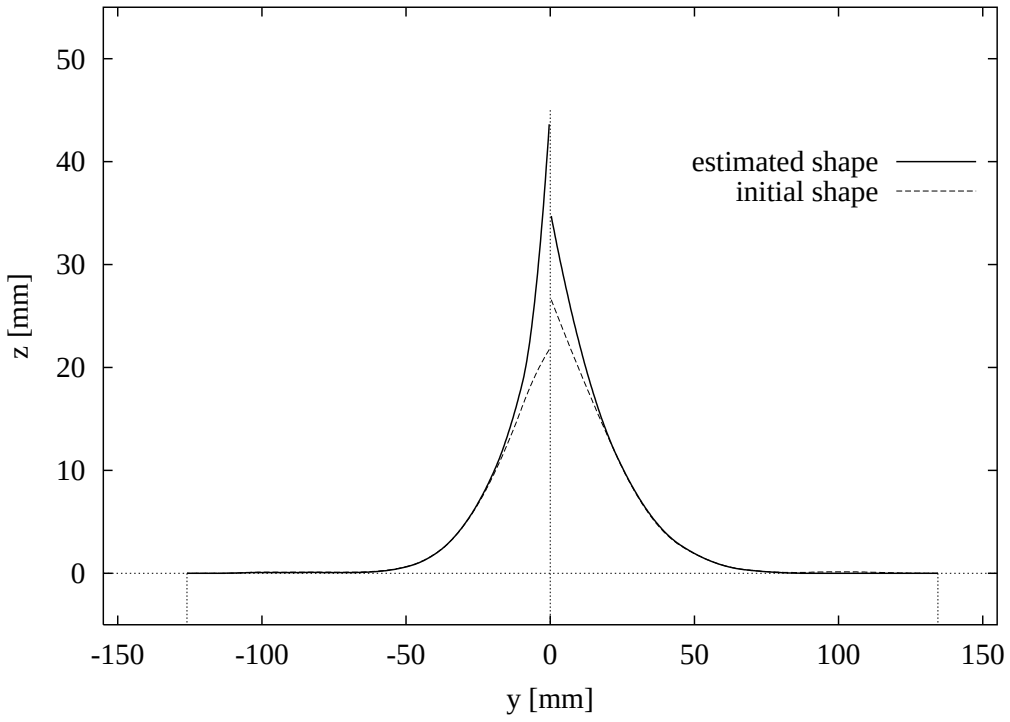

Figure 4.29: Estimated shapes.

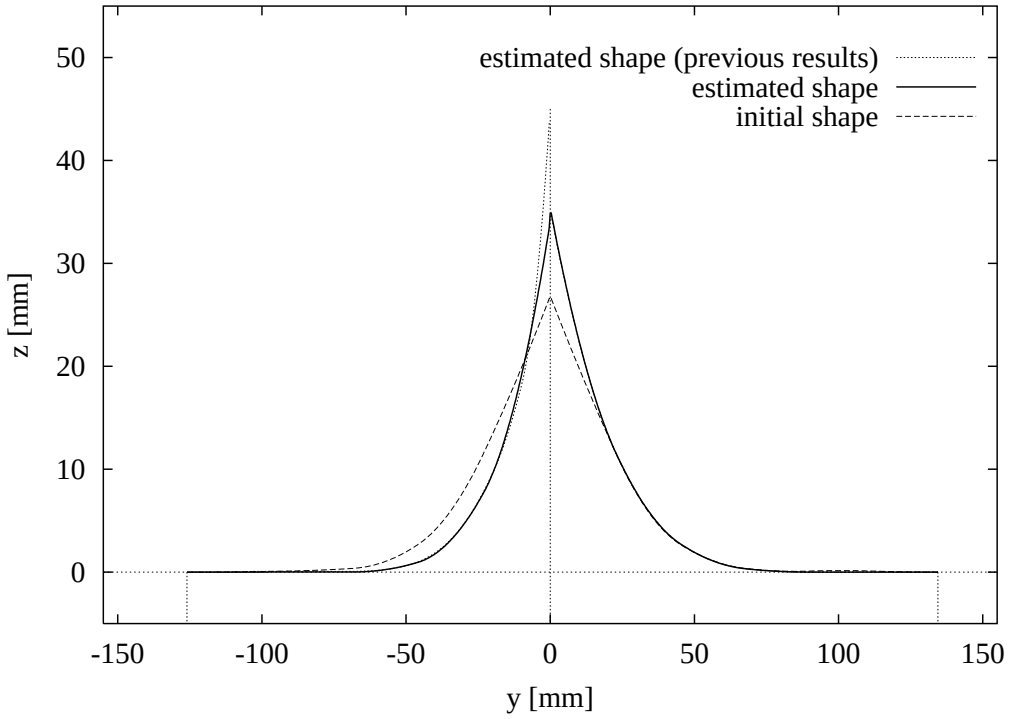

Figure 4.30: Estimated shape using symmetric initial shape constructed by right side of previous initial shape.

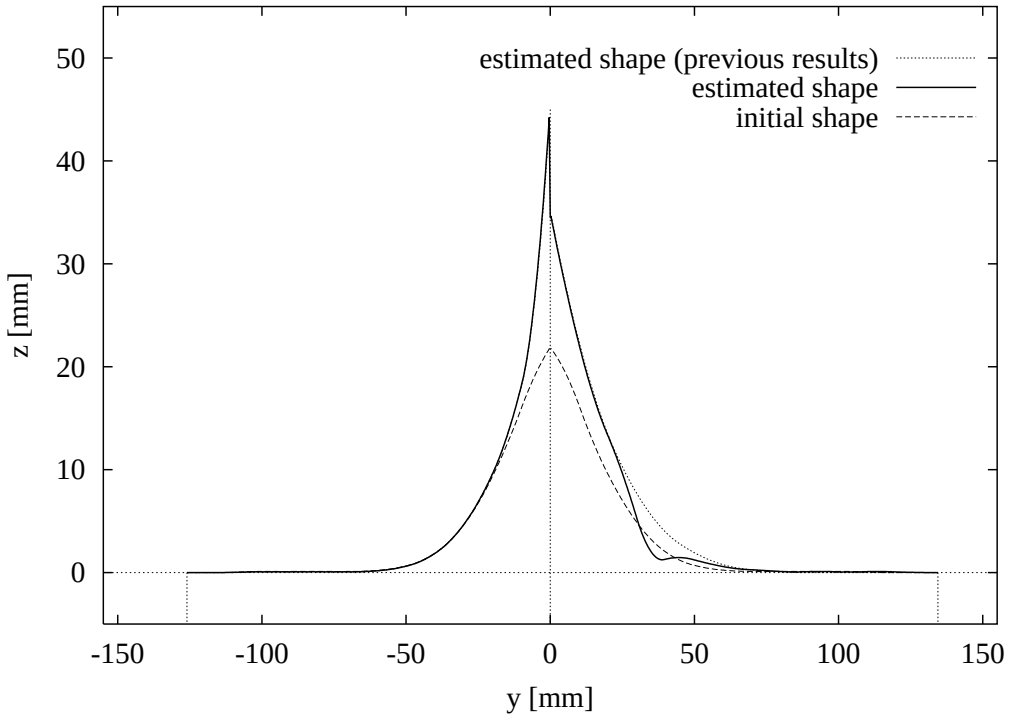

Figure 4.31: Estimated shape using symmetric initial shape constructed by left side of previous initial shape.

Figure 4.32: *Image-A*(restored image using initial shape).

Figure 4.33: *Image-B*(restored image using finally estimated shape started from anti-symmetric initial shape).

predominant land use in the nine cell area (Figure 8.5c), or the diversity of land use (Figure 8.5b) as indicated by the number of different categories found. After slope and soil conditions are simplified by recoding into just a handful of categories, each cell is given a weight based on the joint conditions of slope and soils, and then the worst case, the minimum value of the two numbers for a cell, is written out as the result.

The fourth category includes the creation of measures for spatial properties, like distance or narrowness of regions. It also includes determination of slope and aspect from elevation data by looking at the difference between a cell's value and that of immediate neighbours. Gradients may also be computed for other variables, like income level or percentage population with college degrees, that are scalar. Immediate and extended neighbourhoods or zones can be examined for spatial properties like length or area of objects, or gradients. Accumulations of properties with increasing distance from a focal point, line or area, can be determined by spreading outwards in distance increments and counting the numerical values for an attribute for the cells falling in different distance zones (Figure 8.4e).

Area and perimeter measures for homogeneous blocks of cells or other sets of contiguous units grouped into zones, perhaps via a special thematic overlay, are obtained, respectively, by cell counts and summing the exterior edges of cells in the zones. Distances, obtained by row and column coordinate differences and application of the Pythagoras' rule for right triangles, are quite easily obtained although, as pointed out in Chapter 6, subject to error. Distances for individual cells to a boundary of a zone or from a linear or point feature can be readily accomplished principally by cell counting operations. Shapes of blocks of cells can be measured crudely by comparing the perimeter of a zone to that length likely for a regular figure, usually a circle, of the same area, and basic spatial statistics like centroids are easily determined from row and column integer values for vertical and horizontal coordinate axes.

Thus, while the concept of the entity and spatial relationships are not natural for grid-cell systems, nonetheless, most spatial properties can be fairly effectively obtained via the attribute data. Polygons are identified by a common code, and a conceptual layer that consists of sets of cells coded for the different units, for example, counties. Or the counties may be shown by pixels coded for the boundaries of spatial units. Point features can have numerical codes referring to data in another table: for example, one containing city names. An overlay of county and city codes can produce the equivalent of a contained-within concept.

Grid-cell based map overlay modelling 319

8.3.2 Spatial modelling with grid-cell data

The grid-cell form of data encoding facilitates map analysis involving many data items or processing steps. Figure 8.6 serves to illustrate some of the arithmetic procedures commonly encountered in working with cell data for a **map overlay modelling task**. Preliminary planning has produced a flowchart of operations required to produce a single scale of numbers representing the potential for residential development in areas not yet built-up. The data processing consists of a mixture of operations drawn from the four categories noted above.

Proximity to services and highways is represented by incremental distance values, inverted to indicate declining desirability with distance, or based on a minimum distance as in the case of the highways. Original soil categories have been assigned code numbers suggesting their susceptibility to easy construction, especially the soil wetness. Slope gradients have been computed from elevation data. The variety of existing land cover in cells, computed by scanning the neighbourhood, is a measure of the likelihood of finding homogeneous conditions for building. The relative influence of slope and soil types is combined by assigning potential values after a cross-classification operation. New cell values are combined in various ways to obtain the composite final scale for the potential for residential development, as shown.

This procedure has used elementary logical operations in order to apply the renumbering. For example, the logical test logical OR has been applied to two attributes, looking for the existence of either D for the first variable, and 23 for the second, and then assigning a weight of 10 to the result of the selection. Cells with the joint condition of D and 23 are identified by the logical AND operation. A third situation of selecting the complement of the overlap can be undertaken using the logical XOR operation. Complex combinations can be created by suitable logical statements combining more than two attributes.

The ease of undertaking such logical processing (based on **set operations**) with cell data, arises from the use of identical spatial data units (the grid cells), and of simple binary or decimal arithmetic. In a comparison of two attributes, each of which can take on two states (presence or absence) denoted by 1 and 0 respectively, the intersection set operation (logical AND) of the two is the product of the two values 1. The other three possibilities each produce a zero product, when multiplying by zero. The union operation produces values of 0, 1 or 2 for the logical OR operation via addition, also identifying the complement of the union by the zero value.

Much use of grid-cell tessellations for spatial analysis arises from the

Figure 4.34: *Image-C* (restored image using finally estimated shape started from symmetric initial shape).

4.7 Conclusion

In this chapter, as the shape reconstruction problem from a scanned image in case of using the physically-based model between the shape and shading, we discuss the book surface shape reconstruction problem.

The photometric characteristics of this problem are 1.proximal and moving light source, 2.interreflections, 3.non-Lambertian surface, and 4.non-uniform albedo distributions. In this study, first, we showed the formulation of this problem taking account of these real world characteristics. And we denoted that the shape, depth and albedo are mutually dependent in this problem but they can be solved by an iterative non-linear optimization with the book surface shape constraints.

To improve the efficiency and stability, we employed piecewise approximations of the shape and the albedo distribution in the shape reconstruction algorithm. Experimental results demonstrated that the proposed algorithm can recover the 3D shape accurately and efficiently enough for the restoration of the distorted book image.

As the future work, to apply to practical applications, we must improve the computation time for the shape reconstruction. Moreover, to generalize our method, we must discuss the method to remove the limitations that the center line separating book pages must be aligned parallel to the x-axis, and the reflectance property of the book surface must be known.

Chapter 5

Shape Reconstruction of Book Surface Using Eigenspace Method

5.1 Introduction

In the previous chapter, the book surface shape was reconstructed by using the physically-based model of the reflection. In this method, since the interreflections could not be neglected, not only the book surface shape but also the albedo distribution should be estimated. Moreover, they are mutually dependent, so we employed the iterative non-linear optimization. But its computation costs became so much. To reduce computation costs, we used the piecewise approximation of the shape and albedo distribution. But, in order to recover the book surface shape in practical time, it is necessary to use more fast shape reconstruction method.

In this chapter, to recover the book surface rapidly, we discuss another shape reconstruction method with different approach to previous one. Here, the relationship between the shape and shading is constructed from the observed shape and shading information directly (not using the photometric models), and the book surface shape is reconstructed by using this relation. This method is one of the appearance-based model method, because it uses not the physical characteristics but the information of the shape and shading themselves, that is, appearances.

5.1.1 Eigen Image Analysis Methods

The appearance-based model has been developed in the study of the object recognition. Broadly speaking, the object recognition is a classification whether an input object image matches a preserved object model or not. But, especially, in case of the three dimensional object recognition, since the image of the object appearance varies with the object pose, the camera location and other factors, it is difficult to realize the object recognition by using a simple template matching method.

To attack this problem, as the frame work of the 3D object recognition, the feature-based method and the appearance-based method have been proposed. In the feature-based method, the two dimensional or three dimensional object features, ex. the edges, the corners and the end points of the object, are extracted from the image, and recognize by matching these features to the object model [2],[58]. But, in this method, it is difficult

to extract the features from an image stably, hence many researchers are now developing the improved methods.

In the object recognition using the appearance-based model, many images of object appearance is preserved beforehand, and the recognition is done by matching the input image to the appearance images. The difficulty of this method is to process a large number of image data. Toward this problem, the eigenspace method has been proposed. This method preserves the appearance images into the eigenspace, hence it can reduce image data size without losing main image features. In addition, as the performance of a computer become higher, this method can be realized easily.

The appearance-based object recognition using the eigenspace have been used in the character recognition system[59]. This method have been also used in the face recognition system[60]. To improve the face recognition, the method using Fourier transformation of a face image to remove a disparity of a face in the image[61], and the method extracting face parts (eye, nose, mouth, etc.) using the sub image eigenspace[62] were proposed.

5.1.2 Parametric Eigenspace Method

The eigenspace method has been developed to the parametric eigenspace method by Murase and Nayar[63]. This method estimates the parameters (the object pose, the illumination direction, etc.) with the object recognition for a given image by using the correspondence of the object image and its parameters. After this method was reported, it is applied to many studies[64].

The parameter estimation using the eigenspace method is divided into two methods as follows:

- *Nearest neighborhood method:*[65]-[70]
  Project the input image into the eigenspace constructed by sample image data, let the parameter of the nearest point of a sample image from the projected point of the input image be the estimated parameter.

- *Linear interpolation method:*[48],[71]
  From the relation of the location between the projected points of the input image and sample images in the eigenspace, the parameter is estimated by the linear interpolation.

The nearest neighborhood method is usually used because it can be performed easily. But when the input image is different from sample images, the parameters can be estimated more precisely by the linear interpolation method.

The shape reconstruction method using the appearance-based model is reported in [48]. In this study, the object shape is estimated as following algorithm:

1. By assuming that an object surface consists of a set of local quadric segments, the eigenspace is constructed from the shading information of the quadric segments with various parameters under the parallel light source.

2. Divide the input shading image into small segments which shape parameter regarded as constant, and estimate the shape parameters at each segment by the linear interpolation.

3. Reconstruct the whole shape by connecting shape segments smoothly.

This method can be used for general objects, but it is difficult to recover its shape accurately because the sum of the shape reconstruction error at each segments become very large in the integration process. In addition to this problem, since the image scanner has the linear light source, the illuminant intensity attenuates with respect to the distance from the light source. Hence, this problem should be treated as the depth[1] recovering problem. But, the reflectance intensity of the book surface varies with respect to the distance and slant of the surface, so, it is difficult to recover the depth and shape of the book surface from the shading information of the small segment on the surface.

5.1.3 Overview of Proposed Method

In this study, we use the cross section shape of the book surface (the distribution of heights from the scanning plane to the book surface) as the shape information and the white background intensity distribution along the cross section shape as the shading information. To recover the book surface shape accurately, we employ all over cross section shape reconstruction method as follows:

1. Extract the shape and shading information from multiple book surface images with known shape, and construct the eigenspaces respectively.

2. Project the shading information in the input image into the shading eigenspace, and estimate coefficients of the interpolation from the local linear interpolation using several sample points near the projected point.

3. In the shape eigenspace, apply coefficients of the interpolation to the shape sample points corresponding to the shading sample points for the local linear interpolation, and obtain the cross section shape.

This method is different from previous parametric eigenspace methods, because previous methods estimate parameters from the pattern (image) but the proposed method estimates the shape pattern from the shading pattern. Moreover, in spite of the pattern estimation, since the number of the data of the shape and shading information can be reduced drastically by using the eigenspace method, therefore, the whole cross section shape can be obtained in a little computation time.

In the proposed method, the relation between the shape and shading is regarded as the local linear relation between the shape and shading eigenspaces. But, the shape and shading relation is essentially the non-linear relation, hence this local linearity includes the approximation errors. To avoid the influence of such errors to the estimated shape, we improve the shape reconstruction method by using the SN ratio for the sample data in the shading eigenspace.

In the appearance-based model, we must consider the variation of the sample data. The freedoms of the book surface shape are the transformation of its shape and the position on the scanning plane. The more the number of freedom, the more the number of variation for the sample data. This means that the estimated shape become inaccurately. Hence, we

[1]The distance from the light source to the book surface (see Sect.4.2).

also propose the normalization method for the shape and shading information to remove the freedom of the position in the scanning plane by using Fourier transformation. More details are shown in the following sections.

5.2 Image Scanner and Observed Profiles

5.2.1 Image Scanner and Coordinate System

The structure of the image scanner used in this method (Fig.5.1) is basically same described in chapter 3[2], but the configuration of the coordinate system on the scanning plane is different from the previous method. In the previous chapter, the position of the gutter of the book surface is assumed to be known and aligned on x-axis (Fig.4.6). But, in this method, we assume that x-axis is located at the CCD scanning start position (Fig.5.2) and the position of the gutter in the input scanned image is unknown. In other word, the position of the book surface along y-axis on the scanning plane is free. The book surface (gutter) position is estimated with its shape.

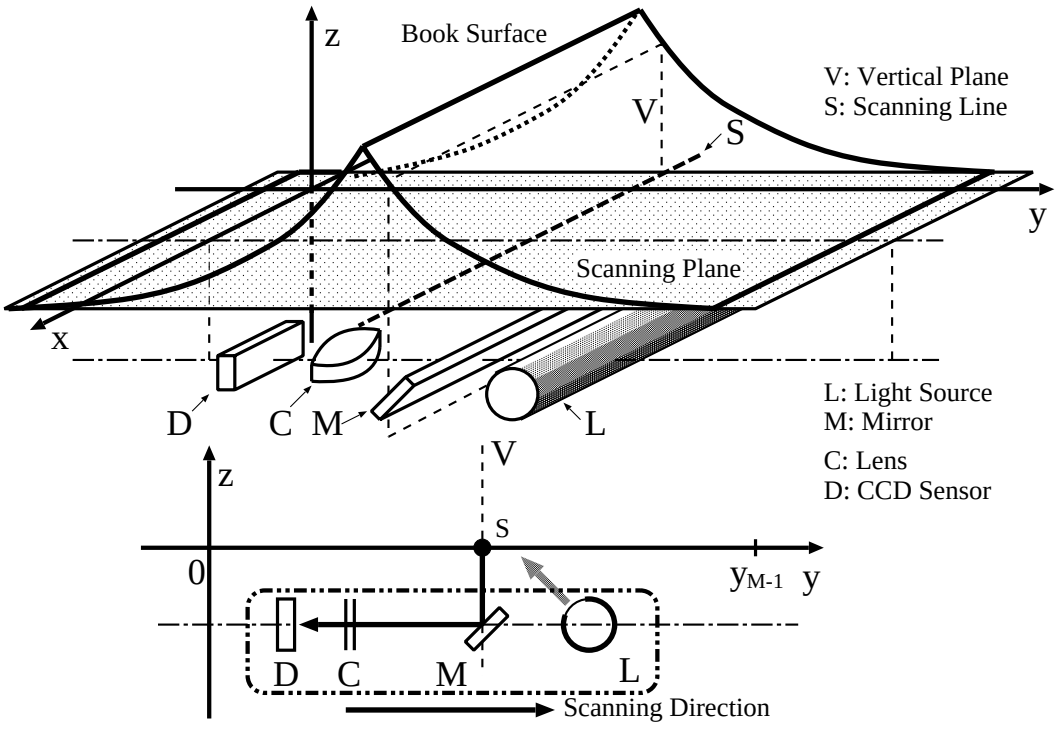

Figure 5.1: Structure of image scanner.

[2]In Fig.5.1, the arrangements of components in the scanner (the light source, the CCD sensor, etc.) are reversed for Fig.3.1, but there is no problem for the geometrical configuration.

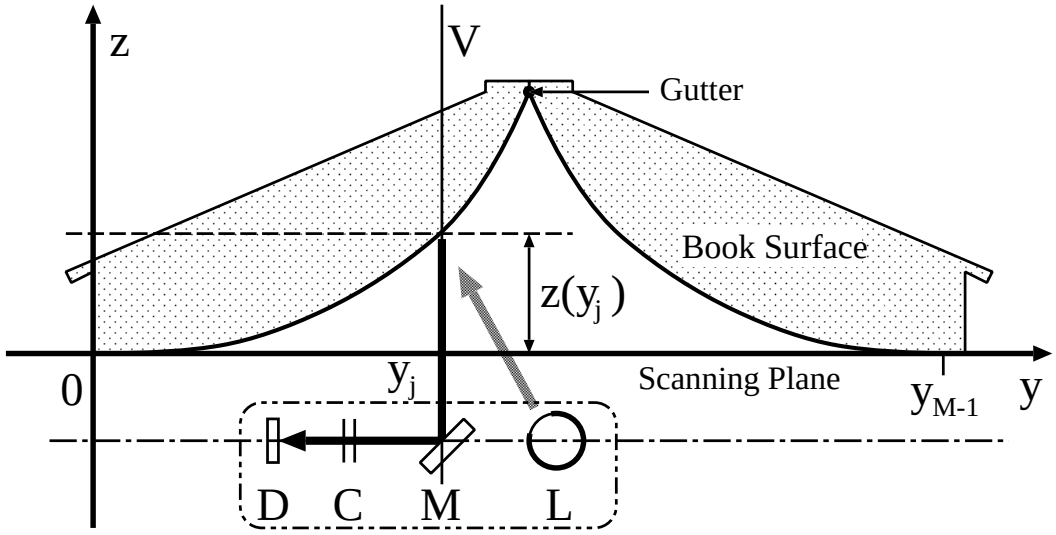

Figure 5.2: Cross section shape of book surface.

5.2.2 Observed Profiles

The unfolded book surface is arranged on the scanning plane as shown in Fig.5.2. Assumptions for the book surface shape is same in Sect.4.4.1. Hence, the target of the shape reconstruction is also the cross section shape of the book surface. In this study, the shape information is defined as a sequence of height data between the scanning plane and the book surface. It described as the vector $\boldsymbol{Z}$:

$$\boldsymbol{Z} = \left[\begin{array}{cccc} Z(y_0) & Z(y_1) & \cdots & Z(y_{M-1}) \end{array} \right]^T, \tag{5.1}$$

where M denotes the number of pixels along the y-axis in a scanned image, $Z(y_j)$ is the height. We call $\boldsymbol{Z}$ the shape profile.

The shading information is also defined as a sequence of the intensity data at the white background on the book surface. It described as the vector $\boldsymbol{P}$:

$$\boldsymbol{P} = \left[\begin{array}{cccc} P(y_0) & P(y_1) & \cdots & P(y_{M-1}) \end{array} \right]^T, \tag{5.2}$$

where $P(y_j)$ denotes the white background intensity. It is the same as $P^*_w(y_j)$ in Eq.(4.49). We call $\boldsymbol{P}$ the shading profile.

As shown in Sect.4.4.1, we assume that both end of the book surface touch the scanning plane. From this assumption, $Z(y_0)$ and $Z(y_{M-1})$ (and other components near them) are equal to 0, and $P(y_0)$ and $P(y_{M-1})$ (and other components near them) have the intensity of the reflection on the flat surface at height = 0.

By the parallel projection of the image scanner along y-axis, the form of a shading profile corresponding to a book surface shape is not changed wherever the book surface locates along y-axis. In addition, it is clear that the appearance of the shading profile is not changed under the perspective projection along x-axis because of the constant cross section shape assumption of the book surface.

5.2.3 Profile Normalization for Translation

As shown in later section, the book surface shape is reconstructed by using sample shape and shading profiles. But, the book surface is located freely along y-axis on the scanning plane described in Sect.5.2.1. Under such situation, sample shape and shading profiles should be prepared not only the shape variation but also each position along y-axis. But, it is not practical to obtain such an enormous amount of profile data. However, if the gutter positions of sample profiles are inconsistent, the book surface shape cannot be recovered correctly. To reduce the number of profiles and recover the book shape accuracy, we normalize sample profiles for the parallel translation along y-axis. This is the arrangement of the profile position. This normalization can be done by the characteristic of the parallel projection of the image scanner along y-axis. This normalization process is as follows:

Shape profile normalization

1. Obtain the position b_i of the gutter (binding position of book pages) in each sample shape profile $\boldsymbol{Z}_i$ ($1 \leq i \leq N$: N is the number of sample profiles), where b_i is defined as the y coordinate of the highest position in $\boldsymbol{Z}_i$.

2. Define $b_o = (M-1)/2$ as the common gutter position for all shape profiles. Shape profiles $\boldsymbol{Z}_i$ are translated along y-axis for $b_o - b_i$, hence the gutter position locates on b_o (Fig.5.3). The normalized shape profiles are represented as $\hat{\boldsymbol{Z}}_i$.

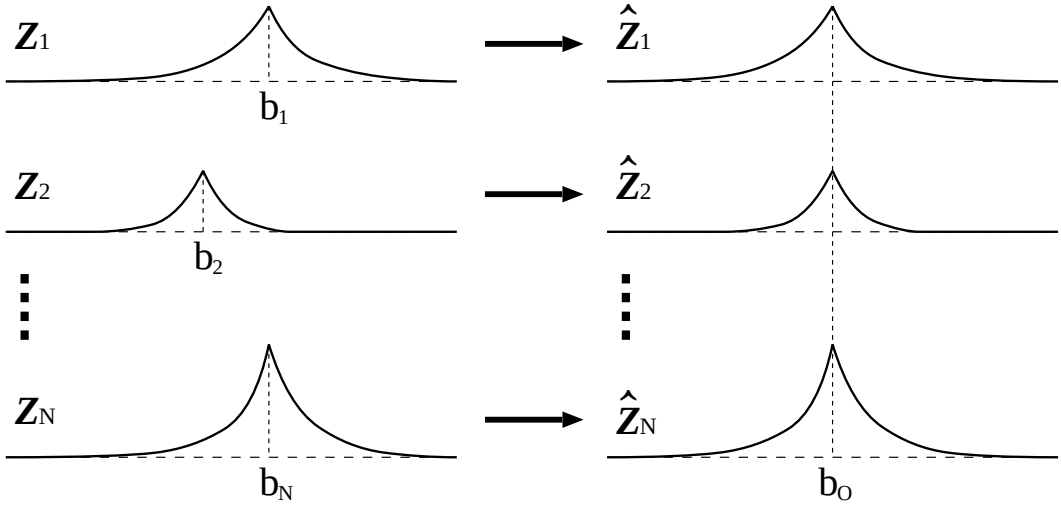

Figure 5.3: Shape profiles normalization.

Shading profile normalization

In the input shading profile for the shape reconstruction, the gutter position is not known. Hence a different parameter is used to normalize for the translation of the shading profile.

Since the shading profiles can be regarded as a periodic function, we use the phase of the first frequency component.

To normalize the shading profile $\boldsymbol{P}_i$, first, the discrete Fourier transform representation of $\boldsymbol{P}_i$ is obtained as follows:

$$P_i(y_j) = \sum_{k=0}^{M-1} A_k \cdot \cos(j \cdot w_k - \phi_{ik}) \quad (w_k = 2\pi k/M), \tag{5.3}$$

where

$$\phi_{ik} = \tan^{-1}\left\{\frac{\sum_{j=0}^{M-1} P_i(y_j)\sin(j \cdot w_k)}{\sum_{j=0}^{M-1} P_i(y_j)\cos(j \cdot w_k)}\right\}. \tag{5.4}$$

The phase τ_i of the cosine wave at $k = 1$ is calculated by:

$$\tau_i = \phi_{i1} \cdot M/2\pi. \tag{5.5}$$

Hence, the shading profile is normalized by translating to $-\tau_i$ along y-axis cyclically. Here, the normalized sample shading profiles are represented as $\hat{\boldsymbol{P}}_i$.

The gutter positions of the sample shading profiles are known because the correspondence of the shape and shading profiles is known. Hence, the gutter position of the *normalized* sample shading profiles $\hat{b}_i$ is

$$\hat{b}_i = b_i - \tau_i. \tag{5.6}$$

$\hat{b}_i$ is used to estimate the gutter position of the reconstructed shape.

Figure 5.4 and 5.5 show the examples of $\boldsymbol{P}_i$ and $\hat{\boldsymbol{P}}_i$. In these examples, Profile A, B and Profile C, D are obtained from same book surface shapes, respectively. In Fig.5.4 Profile B is translated to 50[mm] from Profile A, and Profile D is translated to 20[mm] from Profile C. Figure 5.5 shows $\hat{\boldsymbol{P}}_i$ of each profiles. Profile A,B and Profile C,D are aligned at same position, respectively. This result shows that the normalized shading profile is the shift-invariant profiles, and τ_i is unique with respect to the profile form.

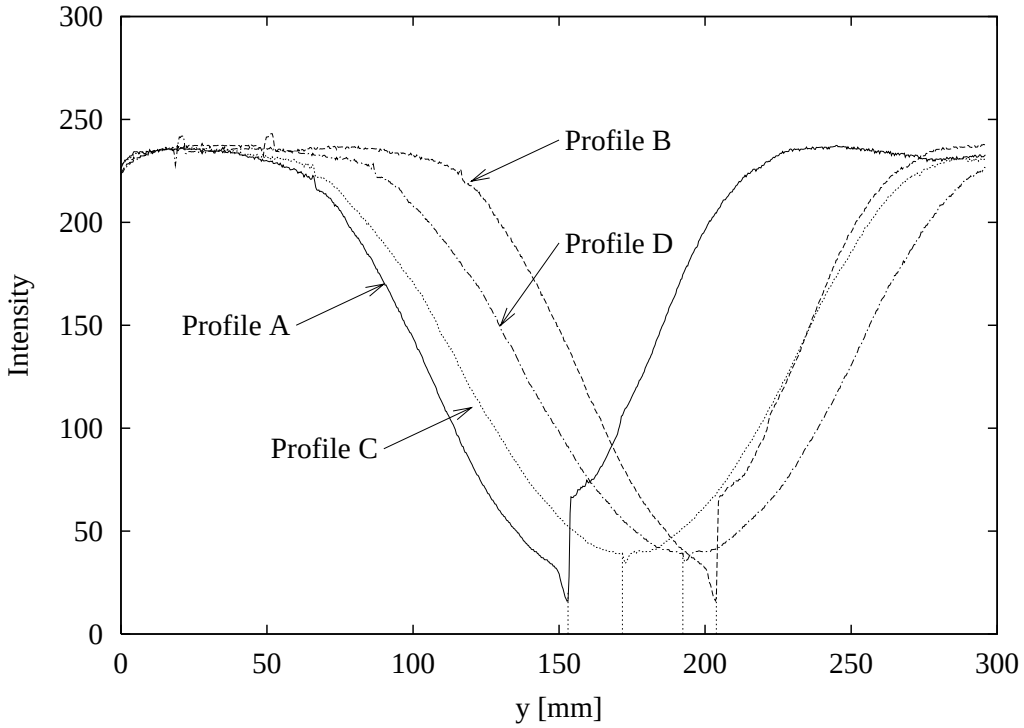

Figure 5.4: Observed shading profiles.

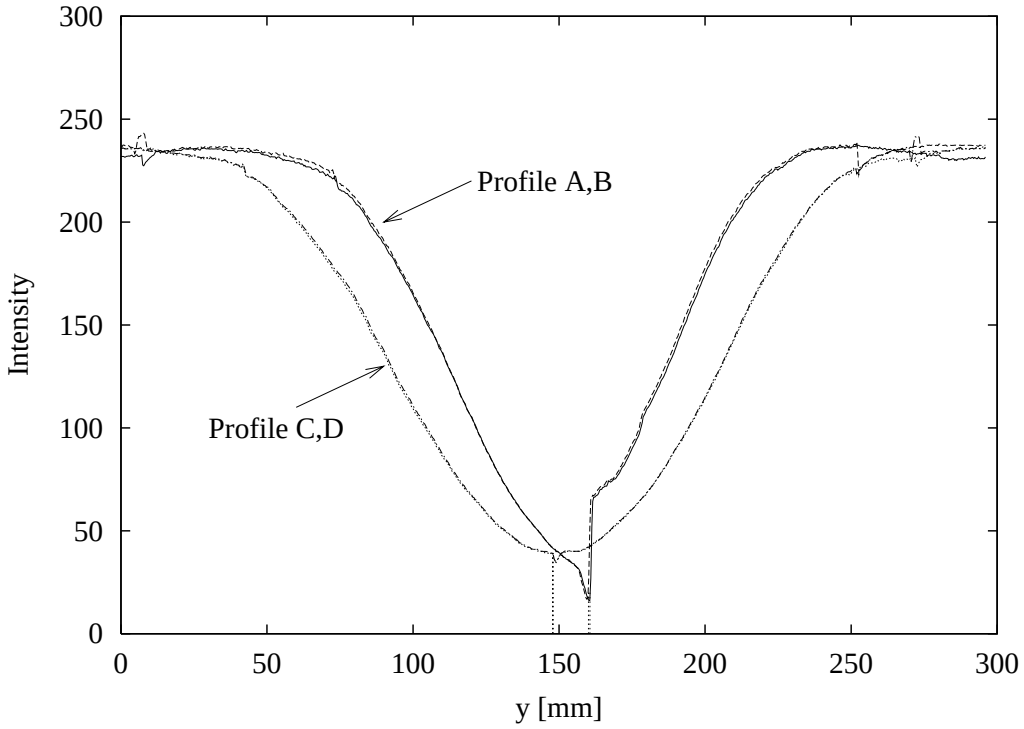

Figure 5.5: Normalized shading profiles.

5.3 Shape Reconstruction Using Eigen Space

5.3.1 Principle of Shape Reconstruction

First, we assume the functional relation between the normalized shading profile $\hat{\boldsymbol{P}}$ and shape profile $\hat{\boldsymbol{Z}}$ as follows:

$$\hat{\boldsymbol{P}} = f(\hat{\boldsymbol{Z}}). \tag{5.7}$$

The actual f is complex non-linear relation described in previous chapter. Let the set of the shading and shape sample profiles be

$$\left.\begin{array}{l} \boldsymbol{\Phi} = \left[\begin{array}{cccc} \hat{\boldsymbol{P}}_1 & \hat{\boldsymbol{P}}_2 & \cdots & \hat{\boldsymbol{P}}_N \end{array}\right], \\ \boldsymbol{\Psi} = \left[\begin{array}{cccc} \hat{\boldsymbol{Z}}_1 & \hat{\boldsymbol{Z}}_2 & \cdots & \hat{\boldsymbol{Z}}_N \end{array}\right], \end{array}\right\} \tag{5.8}$$

where N is the number of sample book surface, and $\hat{\boldsymbol{P}}_i$ corresponds to $\hat{\boldsymbol{Z}}_i$, that is, they are extracted from same book surface.

We represent an input shading profile for the shape reconstruction as $\boldsymbol{P}^*$, and its normalized profile as $\hat{\boldsymbol{P}}^*$. Let the subset of $\boldsymbol{\Phi}$ consist of L profiles near $\hat{\boldsymbol{P}}^*$ be $\boldsymbol{\Phi}_s$:

$$\boldsymbol{\Phi}_s = \left[\begin{array}{cccc} \hat{\boldsymbol{P}}_{\mathrm{s}1} & \hat{\boldsymbol{P}}_{\mathrm{s}2} & \cdots & \hat{\boldsymbol{P}}_{\mathrm{s}L} \end{array}\right], \tag{5.9}$$

and the subset of $\boldsymbol{\Psi}$ corresponding to $\boldsymbol{\Phi}_s$ be $\boldsymbol{\Psi}_s$:

$$\boldsymbol{\Psi}_s = \left[\begin{array}{cccc} \hat{\boldsymbol{Z}}_{\mathrm{s}1} & \hat{\boldsymbol{Z}}_{\mathrm{s}2} & \cdots & \hat{\boldsymbol{Z}}_{\mathrm{s}L} \end{array}\right]. \tag{5.10}$$

Let the mean of $\boldsymbol{\Psi}_s$ be $\boldsymbol{m}_{\mathrm{Zs}}$, the linear approximation of Eq.(5.7) around $\boldsymbol{m}_{\mathrm{Zs}}$ is derived as:

$$\hat{\boldsymbol{P}}_{\mathrm{s}i} - f(\boldsymbol{m}_{\mathrm{Zs}}) = F(\boldsymbol{m}_{\mathrm{Zs}}) \cdot (\hat{\boldsymbol{Z}}_{\mathrm{s}i} - \boldsymbol{m}_{\mathrm{Zs}}) + \boldsymbol{n}_{\mathrm{s}i}, \tag{5.11}$$

where

$$F(\boldsymbol{m}_{\mathrm{Zs}}) = \left[\partial f / \partial \hat{\boldsymbol{Z}}\right]_{\hat{\boldsymbol{Z}}=\boldsymbol{m}_{\mathrm{Zs}}}. \tag{5.12}$$

Equation (5.11) represents the linear transformation between the shading profile and the shape profile, and $\boldsymbol{n}_{\mathrm{s}i}$ denotes the sum of the error of the linear transformation and the noise error of the observed data. By summing Eq.(5.11) from $i = 1$ to L and dividing by L, Eq.(5.11) become

$$f(\boldsymbol{m}_{\mathrm{Zs}}) = \frac{1}{L}\sum_{i=1}^{L}\left(\hat{\boldsymbol{P}}_{\mathrm{s}i} - \boldsymbol{n}_{\mathrm{s}i}\right) \triangleq \boldsymbol{m}_{\mathrm{Ps}} - \bar{\boldsymbol{n}}_{\mathrm{s}}, \tag{5.13}$$

where $\bar{\boldsymbol{n}}_{\mathrm{s}}$ is the mean of $\boldsymbol{n}_{\mathrm{s}i}$. From Eq.(5.11) and Eq.(5.13), we can obtain

$$\Delta\hat{\boldsymbol{P}}_{\mathrm{s}i} = F(\boldsymbol{m}_{\mathrm{Zs}}) \cdot \Delta\hat{\boldsymbol{Z}}_{\mathrm{s}i} + \Delta\boldsymbol{n}_{\mathrm{s}i}, \tag{5.14}$$

where

$$\left.\begin{array}{l} \Delta\hat{\boldsymbol{P}}_{\mathrm{s}i} = \hat{\boldsymbol{P}}_{\mathrm{s}i} - \boldsymbol{m}_{\mathrm{Ps}}, \\ \Delta\hat{\boldsymbol{Z}}_{\mathrm{s}i} = \hat{\boldsymbol{Z}}_{\mathrm{s}i} - \boldsymbol{m}_{\mathrm{Zs}}, \\ \Delta\boldsymbol{n}_{\mathrm{s}i} = \boldsymbol{n}_{\mathrm{s}i} - \bar{\boldsymbol{n}}_{\mathrm{s}}. \end{array}\right\} \tag{5.15}$$

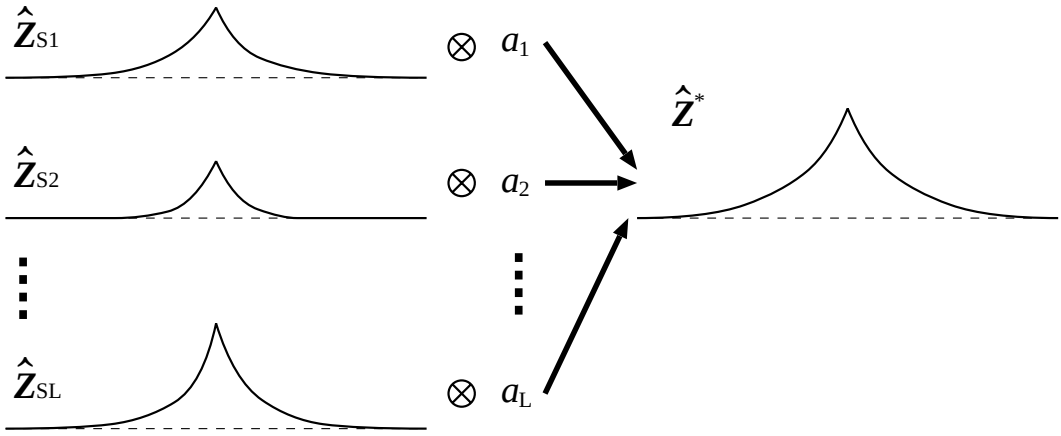

Figure 5.6: Constructing shape profile using weight vector.

By introducing the coefficient vector $\boldsymbol{A} = [a_1 a_2 \cdots a_L]^T$, we represent the reconstructed shape profile $\hat{\boldsymbol{Z}}^*$, which is the output normalized shape profile corresponding to the input normalized shading profile $\hat{\boldsymbol{P}}^*$, to be

$$\hat{\boldsymbol{Z}}^* = \Delta\hat{\boldsymbol{Z}}^* + \boldsymbol{m}_{Zs}, \tag{5.16}$$

$$\Delta\hat{\boldsymbol{Z}}^* = \sum_{i=1}^{L} a_i \cdot \Delta\hat{\boldsymbol{Z}}_{si}. \tag{5.17}$$

Broadly speaking, $\boldsymbol{A}$ in Eq.(5.17) is the weight vector to construct the shape profile $\hat{\boldsymbol{Z}}^*$ (Fig.5.6). Hence, if $\boldsymbol{A}$ can be obtained, $\hat{\boldsymbol{Z}}^*$ can be estimated.

In this method, we obtain $\boldsymbol{A}$ from the shading profiles $\boldsymbol{\Phi}_s$ and $\hat{\boldsymbol{P}}^*$. By multiplying Eq.(5.17) by $F(\boldsymbol{m}_{Zs})$ and assigning Eq.(5.14) to it, we can obtain:

$$\Delta\hat{\boldsymbol{P}}^* - \sum_{i=1}^{L} a_i \cdot \Delta\hat{\boldsymbol{P}}_{si} + \sum_{i=1}^{L} a_i \cdot \Delta\boldsymbol{n}_{si} = \boldsymbol{n}^*, \tag{5.18}$$

where $\boldsymbol{n}^*$ is the sum of the linear approximation errors in Eq.(5.14) and Eq.(5.17). Once the coefficient vector $\boldsymbol{A}$ can be computed from Eq.(5.18), $\hat{\boldsymbol{Z}}^*$ can be calculated from Eq.(5.17). Therefore, to obtain the reconstructed shape, the following processes are needed:

1. Obtain the subset $\boldsymbol{\Phi}_s$ near $\hat{\boldsymbol{P}}^*$,
2. Calculate $\boldsymbol{A}$ by using Eq.(5.18).

5.3.2 Estimation of Neighbor Points and Local Geometric Structure in Eigenspace

In order to compute above processes, it is necessary to measure the distance for the shading profiles. As the measure of this method, we use the Euclidean distance measurement in

the eigenspace constructed by the shading profiles. By using the eigenspace method, the number of dimension of the shading profiles (M) become extremely small to the number of dimension of projected points in the eigenspace (K).

To estimate the neighbor points in the eigenspace, first the shading eigenspace is constructed from the normalized sample shading profiles $\boldsymbol{\Phi}$. Let $\boldsymbol{m}_{\rm P}$ be the mean of all components in $\boldsymbol{\Phi}$ and obtain $\delta\hat{\boldsymbol{P}}_i$ as

$$\delta\hat{\boldsymbol{P}}_i = \hat{\boldsymbol{P}}_i - \boldsymbol{m}_{\rm P}, \tag{5.19}$$

where δ denotes the subtraction of the mean calculated by all components in $\boldsymbol{\Phi}$, on the other hand, Δ in Eq.(5.15) denotes the subtraction of the mean calculated by components in subset $\boldsymbol{\Phi}_s$, hence, $\boldsymbol{m}_{\rm P} \neq \boldsymbol{m}_{\rm Ps}$. Next, let the set of $\delta\hat{\boldsymbol{P}}_i$ be

$$\delta\boldsymbol{\Phi} = \left[\begin{array}{cccc} \delta\hat{\boldsymbol{P}}_1 & \delta\hat{\boldsymbol{P}}_2 & \cdots & \delta\hat{\boldsymbol{P}}_N \end{array}\right] : M \times N, \tag{5.20}$$

and after estimating the eigen values and the eigen vectors of $(1/N)\cdot\delta\boldsymbol{\Phi}\cdot\delta\boldsymbol{\Phi}^T$, let eigen vectors corresponding to K largest eigen values as

$$\boldsymbol{E}_{\rm P} = \left[\begin{array}{cccc} \boldsymbol{e}_{\rm P1} & \boldsymbol{e}_{\rm P2} & \cdots & \boldsymbol{e}_{{\rm P}K} \end{array}\right] : M \times K. \tag{5.21}$$

$\delta\boldsymbol{\Phi}$ is transformed into

$$\boldsymbol{G}_{\rm P} = \boldsymbol{E}_{\rm P}^T \cdot \delta\boldsymbol{\Phi} = \left[\begin{array}{cccc} \boldsymbol{g}_{\rm P1} & \boldsymbol{g}_{\rm P2} & \cdots & \boldsymbol{g}_{{\rm P}N} \end{array}\right] : K \times N \tag{5.22}$$

where $\boldsymbol{g}_{{\rm P}i}$ is the projected point of $\delta\hat{\boldsymbol{P}}_i$ in the K dimensional eigenspace spanned by $\boldsymbol{E}_{\rm P}$, and $\boldsymbol{G}_{\rm P}$ is the set of $\boldsymbol{g}_{{\rm P}i}$.

$\boldsymbol{\Phi}_s$, the subset near $\hat{\boldsymbol{P}}^*$, is constructed by $\boldsymbol{g}_{{\rm Ps}i}$ $(i = 1, 2, \cdots, L)$ which are L closest points to $\boldsymbol{g}_{\rm P}^*$ (the projected point of $\hat{\boldsymbol{P}}^*$) by calculating Euclidean distances:

$$d(\boldsymbol{g}_{\rm P}^*, \boldsymbol{g}_{{\rm P}i}) = ||\boldsymbol{g}_{\rm P}^* - \boldsymbol{g}_{{\rm P}i}||. \tag{5.23}$$

To calculate $\boldsymbol{A}$, by multiplying Eq.(5.18) by $\boldsymbol{E}_{\rm P}^T$, Equation (5.18) changes to

$$\boldsymbol{E}_{\rm P}^T \cdot \Delta\hat{\boldsymbol{P}}^* - \sum_{i=1}^{L} a_i \cdot \boldsymbol{E}_{\rm P}^T \cdot \Delta\hat{\boldsymbol{P}}_{{\rm s}i} + \sum_{i=1}^{L} a_i \cdot \boldsymbol{E}_{\rm P}^T \cdot \Delta\boldsymbol{n}_{{\rm s}i} = \boldsymbol{E}_{\rm P}^T \cdot \boldsymbol{n}^*, \tag{5.24}$$

where

$$\boldsymbol{E}_{\rm P}^T \cdot \Delta\hat{\boldsymbol{P}}^* = \boldsymbol{g}_{\rm P}^* + \boldsymbol{E}_{\rm P}^T(\boldsymbol{m}_{\rm P} - \boldsymbol{m}_{\rm Ps}), \tag{5.25}$$

$$\boldsymbol{E}_{\rm P}^T \cdot \Delta\hat{\boldsymbol{P}}_{{\rm s}i} = \boldsymbol{g}_{{\rm Ps}i} + \boldsymbol{E}_{\rm P}^T(\boldsymbol{m}_{\rm P} - \boldsymbol{m}_{\rm Ps}), \tag{5.26}$$

and, since $\sum_{i=1}^{L} \Delta\hat{\boldsymbol{P}}_{{\rm s}i} = 0$, we can obtain

$$\boldsymbol{E}_{\rm P}^T(\boldsymbol{m}_{\rm P} - \boldsymbol{m}_{\rm Ps}) = -\frac{1}{L}\sum_{i=1}^{L} \boldsymbol{g}_{{\rm Ps}i} \triangleq -\boldsymbol{m}_{\rm gPs}. \tag{5.27}$$

Hence,

$$\left.\begin{array}{l} \boldsymbol{E}_{\rm P}^T \cdot \Delta\hat{\boldsymbol{P}}^* = \boldsymbol{g}_{\rm P}^* - \boldsymbol{m}_{\rm gPs} \triangleq \Delta\boldsymbol{g}_{\rm P}^*, \\ \boldsymbol{E}_{\rm P}^T \cdot \Delta\hat{\boldsymbol{P}}_{{\rm s}i} = \boldsymbol{g}_{{\rm Ps}i} - \boldsymbol{m}_{\rm gPs} \triangleq \Delta\boldsymbol{g}_{{\rm Ps}i}. \end{array}\right\} \tag{5.28}$$

By assigning these equations to Eq.(5.24), we can get

$$\Delta \boldsymbol{g}^*_{\mathrm{P}} - \sum_{i=1}^{L} a_i \cdot \Delta \boldsymbol{g}_{\mathrm{Ps}i} + \sum_{i=1}^{L} a_i \cdot \boldsymbol{v}_{\mathrm{s}i} = \boldsymbol{v}^*, \tag{5.29}$$

where

$$\left.\begin{array}{l} \boldsymbol{v}_{\mathrm{s}i} = \boldsymbol{E}^T_{\mathrm{P}} \cdot \Delta \boldsymbol{n}_{\mathrm{s}i}, \\ \boldsymbol{v}^* = \boldsymbol{E}^T_{\mathrm{P}} \cdot \boldsymbol{n}^*. \end{array}\right\} \tag{5.30}$$

In order to estimate $\boldsymbol{A}$, we assume that $\boldsymbol{v}_{\mathrm{s}i}$ $(i = 1, 2, \cdots, L)$ is a Gaussian noise whose average is equal to 0 and covariance matrix is $\sigma^2 \boldsymbol{I}$. Under this assumption, the mean square of the left side of Eq.(5.29) is

$$\boldsymbol{J} = ||\Delta \boldsymbol{g}^*_{\mathrm{P}} - \Delta \boldsymbol{G}_{\mathrm{Ps}} \cdot \boldsymbol{A}||^2 + \sigma^2 K \boldsymbol{A}^T \boldsymbol{A}, \tag{5.31}$$

where

$$\Delta \boldsymbol{G}_{\mathrm{Ps}} = \left[\begin{array}{cccc} \Delta \boldsymbol{g}_{\mathrm{Ps}1} & \Delta \boldsymbol{g}_{\mathrm{Ps}2} & \cdots & \Delta \boldsymbol{g}_{\mathrm{Ps}L} \end{array} \right]. \tag{5.32}$$

$\boldsymbol{A}$ can be estimated by minimizing $\boldsymbol{J}$ in Eq.(5.31) as follows:

$$\boldsymbol{A} = \left(\Delta \boldsymbol{G}^T_{\mathrm{Ps}} \cdot \Delta \boldsymbol{G}_{\mathrm{Ps}} + \sigma^2 K \boldsymbol{I} \right)^{-1} \cdot \Delta \boldsymbol{G}^T_{\mathrm{Ps}} \cdot \Delta \boldsymbol{g}^*_{\mathrm{P}}. \tag{5.33}$$

Now, $\boldsymbol{A}$ can be regarded as a geometrical structure between $\Delta \boldsymbol{g}^*_{\mathrm{P}}$ and $\Delta \boldsymbol{g}_{\mathrm{Ps}i}$ in the shading eigenspace (Fig.5.7 in the next section). We apply this geometrical structure to the shape profile reconstruction.

In Eq.(5.33), the value of σ^2 is unknown but it can be assumed that

$$\sigma^2 = \nu \cdot \frac{\mathrm{tr}\left[\Delta \boldsymbol{G}^T_{\mathrm{Ps}} \cdot \Delta \boldsymbol{G}_{\mathrm{Ps}} \right]}{KL}, \tag{5.34}$$

where ν is assumed to be a small positive number and $\mathrm{tr}\,[\boldsymbol{X}]$ denotes the trace of matrix $\boldsymbol{X}$. The second term of the right side of Eq.(5.34) represents the mean square of elements in $\Delta \boldsymbol{g}_{\mathrm{Ps}i}$ $(i = 1, 2, \cdots L)$, hence $\sqrt{\nu}$ corresponds to the SN ratio of $\Delta \boldsymbol{g}_{\mathrm{Ps}i}$.

5.3.3 Shape Reconstruction

The reconstructed shape $\hat{\boldsymbol{Z}}^*$ can be estimated by using the coefficient vector $\boldsymbol{A}$. In this estimation, the eigenspace of the shape profiles is also used to reduce the data size. First,

$$\text{mean: } \boldsymbol{m}_{\mathrm{Z}}, \tag{5.35}$$

$$\text{eigen vectors: } \boldsymbol{E}_{\mathrm{Z}} = \left[\boldsymbol{e}_{\mathrm{Z}1}\ \boldsymbol{e}_{\mathrm{Z}2}\ \cdots\ \boldsymbol{e}_{\mathrm{Z}K'} \right], \tag{5.36}$$

$$\text{projected points in eigenspace: } \boldsymbol{G}_{\mathrm{Z}} = \left[\boldsymbol{g}_{\mathrm{Z}1}\ \boldsymbol{g}_{\mathrm{Z}2}\ \cdots\ \boldsymbol{g}_{\mathrm{Z}N} \right], \tag{5.37}$$

are obtained from $\boldsymbol{\Psi}$ in Eq.(5.8). Note that the number of dimension of the shape eigenspace K' is not related to K (the dimension of the shading eigenspace). $\hat{\boldsymbol{Z}}^*$ corresponding to $\hat{\boldsymbol{P}}^*$ is estimated as follows:

$$\left.\begin{array}{l} \boldsymbol{m}_{\mathrm{gZs}} = \dfrac{1}{L} \displaystyle\sum_{i=1}^{L} \boldsymbol{g}_{\mathrm{Zs}i}, \\ \boldsymbol{g}^*_{\mathrm{Z}} = \boldsymbol{m}_{\mathrm{gZs}} + \displaystyle\sum_{i=1}^{L} a_i \cdot (\boldsymbol{g}_{\mathrm{Zs}i} - \boldsymbol{m}_{\mathrm{gZs}}), \\ \hat{\boldsymbol{Z}}^* = \boldsymbol{E}_{\mathrm{Z}} \cdot \boldsymbol{g}^*_{\mathrm{Z}} + \boldsymbol{m}_{\mathrm{Z}}, \end{array}\right\} \tag{5.38}$$

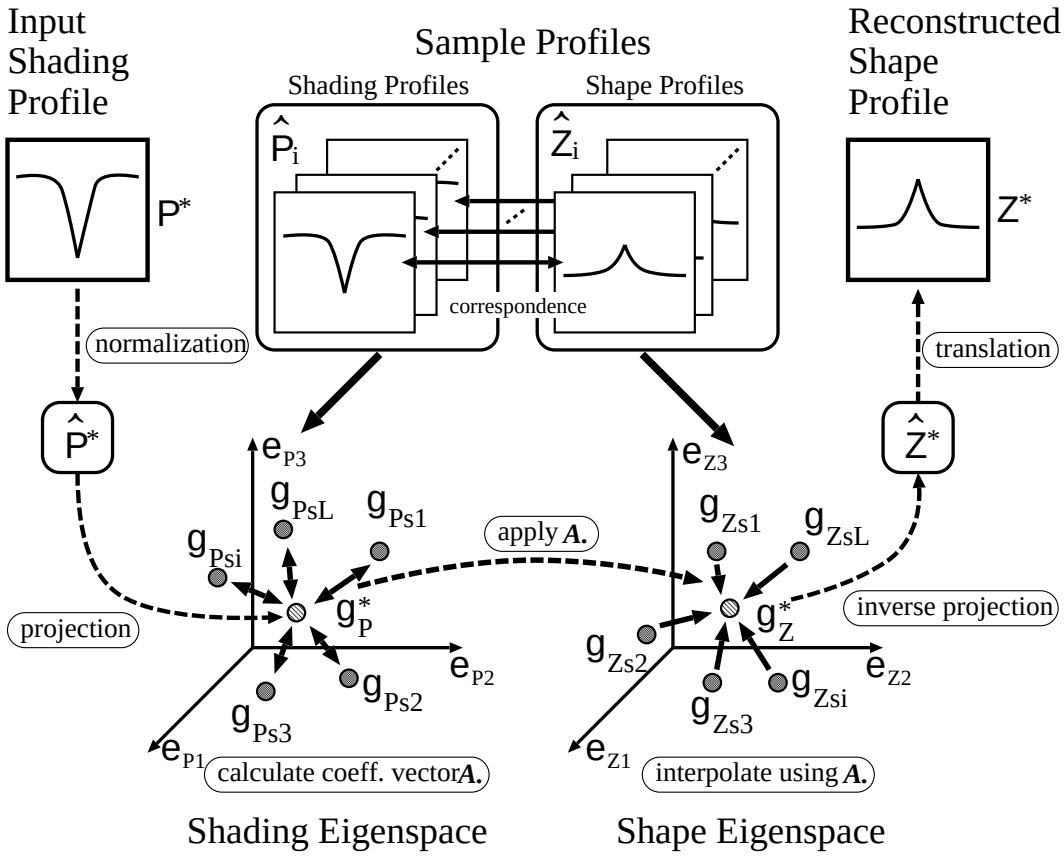

Figure 5.7: Flowchart of shape reconstruction.

where $\boldsymbol{g}_{\mathrm{Z}si}$ is components of $\boldsymbol{G}_{\mathrm{Z}}$ which are corresponding to $\boldsymbol{g}_{\mathrm{P}si}$.

The gutter position of estimated $\hat{\boldsymbol{Z}}^*$ is b_o. The finally reconstructed shape $\boldsymbol{Z}^*$ is obtained by translating $\hat{\boldsymbol{Z}}^*$ to $b^* - b_o$ where b^* is the estimated gutter position of input shading profile $\boldsymbol{P}^*$. b^* can be estimated by

$$b^* = \left[\begin{array}{ccc} (\hat{b}_{s1} - m_b) & \cdots & (\hat{b}_{sL} - m_b) \end{array} \right] \cdot \boldsymbol{A} + m_b + \tau^* \tag{5.39}$$

where $\hat{b}_{si}$ $(i = 1, 2, \cdots, L)$ is the gutter position of $\hat{\boldsymbol{P}}_{si}$, m_b the mean of $\hat{b}_{si}$, τ^* the phase of $\boldsymbol{P}^*$ in the normalization.

The following is the summary of the proposed shape reconstruction algorithm. The flowchart of this algorithm is shown in Fig.5.7.

[Off-line process]

Step 1. Obtain sample shape and shading information from various book surfaces, and extract shape and shading profiles as sample profiles.

Step 2. Normalize sample shape and shading profiles (Sect.5.2.3).

Step 3. Calculate the shape and shading eigenspaces and project points into them by using Eq.(5.20)–(5.22) and Eq.(5.35)–(5.37).

[On-line process]

Step 1. Extract the input shading profile ($\boldsymbol{P}^*$) and calculate the normalized profile $\hat{\boldsymbol{P}}^*$ and its phase τ^*. Project $\hat{\boldsymbol{P}}^*$ to $\boldsymbol{g}^*_{\rm P}$ in the shading eigenspace.

Step 2. Select L nearest projected points $\boldsymbol{g}_{{\rm Ps}i}$ evaluating the distance in Eq.(5.23).

Step 3. Calculate $\boldsymbol{A}$ by using Eq.(5.33).

Step 4. Apply $\boldsymbol{A}$ to $\boldsymbol{g}_{{\rm Zs}i}$ corresponding to $\boldsymbol{g}_{{\rm Ps}i}$ in the shape eigenspace, and calculate $\boldsymbol{g}^*_{\rm Z}$ and the inverse projection of it ($\hat{\boldsymbol{Z}}^*$) by using Eq.(5.38).

Step 5. Calculate the gutter position b^* of $\boldsymbol{P}^*$ (Eq.(5.39)), and by translating $\hat{\boldsymbol{Z}}^*$ to $b^* - b_o$, the reconstructed shape profile $\boldsymbol{Z}^*$ is obtained.

5.4 Image Restoration

By using the reconstructed shape profile, the geometric distortion in the input book surface image can be restored as described in Sect.4.5.3. But, in this chapter, since the physically-based model is not used, we cannot restore the shading (albedo distribution) by using Eq.(4.51) in Sect.4.5.2. Therefore, we restore the shading in the input image approximately by using the shape and shading profiles as follows:

1. Obtain a set of y_k which satisfies $Z(y_k) = 0.0$ among elements of the reconstructed shape profile $\boldsymbol{Z}^*$[3]. Here, let k be $1 \leq k \leq n$.

2. Calculate P_{wf}, which is the intensity of the white background at height $z = 0$ where this part is the flat plane in the book surface shape, by averaging the intensity at y_k of the input shading profile $\boldsymbol{P}^*$ as follows:

$$P_{wf} = \frac{1}{n} \sum_{k=1}^{n} P^*(y_k), \tag{5.40}$$

   where $P^*(y_k)$ denotes the element of $\boldsymbol{P}^*$.

3. Restore the intensity in the input image $P(x_i, y_j)$ by the following equation:

$$P'(x_i, y_j) = \frac{P(x_i, y_j)}{P^*(y_j)} P_{wf}, \tag{5.41}$$

   where $P'(x_i, y_j)$ denotes the restored intensity.

Note that, if we can assume the follows:

- The photometric parameter Δ in Eq.(4.46) is known,
- The intensity of the interreflections $I_{inter}(x_i, y_j)$ in Eq.(4.46) is almost unchanged about x coordinates,

[3]In the actual process, $Z(y_k) = 0.0$ is defines as $Z(y_k) < \varepsilon$ where ε is very small number.

the albedo distribution can be restored almost correctly by the following equation:

$$P'(x_i, y_j) = \frac{P(x_i, y_j) - \Delta}{P^*(y_j) - \Delta}(P_{wf} - \Delta) + \Delta \tag{5.42}$$

This reason is as follows: since P_{wf} is the intensity at the flat white background, it can be represented as follows:

$$P_{wf} = a\rho_w\{I_{dir}(z_0) + I_{inter}(z_0)\} + \Delta \tag{5.43}$$

where $I_{dir}(z_0)$ and $I_{inter}(z_0)$ are the intensity of the illumination and the interreflections at height $z = 0$ respectively[4]. Next, by using above assumptions and the following relations:

$$P(x_i, y_j) = a\rho(x_i, y_j)\{I_{dir}(x_i, y_j) + I_{inter}(x_i, y_j)\} + \Delta, \tag{5.44}$$

$$P^*(y_j) = a\rho_w\{I_{dir}(x(y_j), y_j) + I_{inter}(x(y_j), y_j)\} + \Delta, \tag{5.45}$$

the following relation can be derived from Eq.(5.42):

$$P'(x_i, y_j) = a\rho(x_i, y_j)\{I_{dir}(z_0) + I_{inter}(z_0)\} + \Delta. \tag{5.46}$$

This equation represents that the restored $P'(x_i, y_j)$ is the intensity where the height z of the book surface shape become 0 (flat plane). Therefore, if we can use the photometric parameter Δ, the albedo distribution can be restored correctly by using Eq.(5.42).

5.5 Experiments

5.5.1 Sample Shading and Shape Profiles

In this section, we show the experimental results of the shape reconstruction. The sample profiles of shape and shading are acquired by using the book surface models (Fig.5.8). As the texture of the surface, undistorted document papers are put on their surfaces, and since these models can change the length of w_1, h_1 and w_2, h_2, they can be form various shape. The shape profiles are measured by the arm-typed 3D digitizer, and the shading profiles are extracted from scanned images of model's surface. In this experiment, the image scanner and models are covered with a black box to avoid the outside illumination while scanning. The image resolution is 75 [dpi], the image size is 635 × 875 [dots] (hence $M = 875$). The specification of the computer we use is CPU:Alpha (500MHz), OS:RedHat Linux 4.2.

We use 64 pairs of the shape and shading profiles as the sample by using book surface models. Figure 5.9 shows a part of shape profiles (non-normalized). The 'height' in this figure denotes the height at the gutter position. After the normalization for sample profiles, the shading and shape eigenspaces are reconstructed respectively. Figure 5.10 and Fig.5.11 show eigen vectors of the shading and shape eigenspaces respectively. In these figures, eigen vectors are showed from first to fourth vectors. From Eq.(5.25) and Eq.(5.38), an eigen vector multiplied by a constant value represents the variation with respect to the average vector. Figure 5.12 and Fig.5.13 show the result of the sum of the

[4]Actually, $I_{inter}(z_0)$ is almost 0.

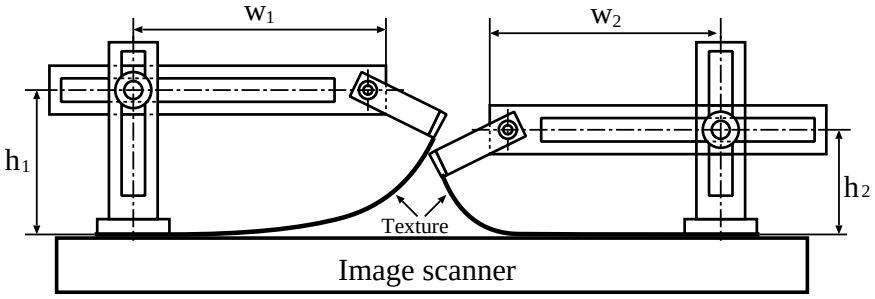

Figure 5.8: Book surface models.

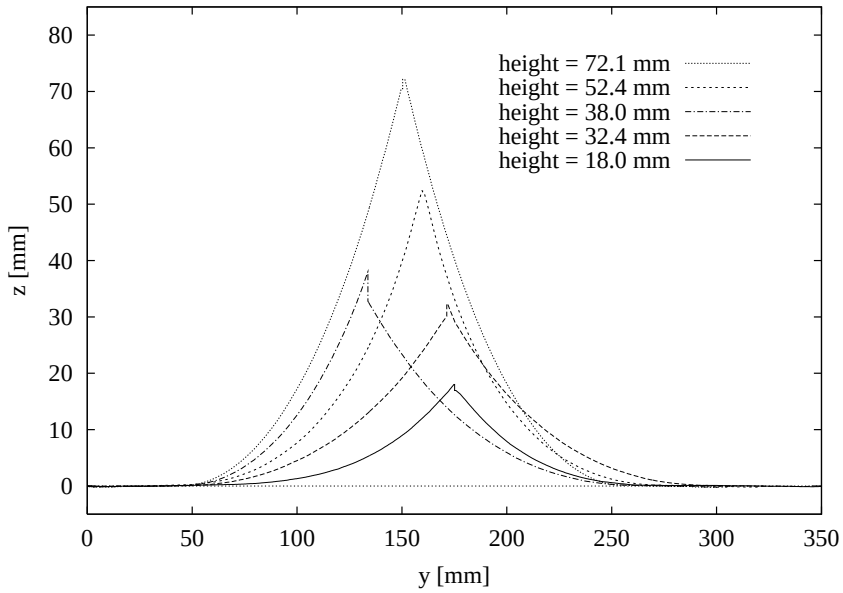

Figure 5.9: Observed cross section shape profiles using as referenced data.

average vector and the eigen vector multiplied by constant α. In these figures, the dashed line denotes the average vector, and the shading eigen vectors are multiplied by $\alpha = 300$, the shape eigen vectors by $\alpha = 150$. From Fig.5.11 and Fig.5.13, each shape eigen vector represents the following partial shape features of the book surface:

- *First eigen vector:* the height of the shape,
- *Second eigen vector:* the discontinuity at the gutter position,
- *Third eigen vector:* the anti-symmetrical shape at curved surface,
- *Fourth eigen vector:* the distortion at curved surface.

The feature of shading eigen vectors are not so clear than the shape eigen vectors but it seems that they represent the variation of the shading profiles corresponding to the shape eigen vectors.

The validity of the sample shape profiles is examined by approximating the observed real 20 book surface shape by using shape eigen vectors from first to tenth. The shape reconstruction errors (Eq.(5.47)) between the observed shape and approximating shape are very small (the mean error is 0.35[mm]), hence the sample profiles are valid for the shape reconstruction.

5.5.2 Error Analysis Using Book Surface Models

For the evaluation of the shape reconstruction, we use 150 scanned images using book surface models which are different from the sample profiles. The shape profiles for the evaluation are also measured to use them as the true shape profiles. To evaluate the accuracy of the reconstructed shape, we use the shape reconstruction error (err) calculated from the following equation:

$$err = \sqrt{\frac{1}{E_n} \sum_{i=0}^{M-1} \left(Z^*(y_i) - Z_t(y_i)\right)^2}, \tag{5.47}$$

where $Z^*(y_i)$ denotes the reconstructed shape profile, $Z_t(y_i)$ the true shape profile, E_n the number of y_i in which $Z^*(y_i)$ or $Z_t(y_i)$ is not equal to 0[5]. This mean that in Eq.(5.47) we ignore the error calculation in case of $Z^*(y_i) = Z_t(y_i) = 0$, because the error value become 0.

First, we compare the accuracy of the shape reconstruction whether the approximation error term ($\sigma^2 K \boldsymbol{I}$ in Eq.(5.33)) is included or not in the calculation of $\boldsymbol{A}$. Figure 5.14 shows the mean of 150 shape reconstruction errors where the number of nearest points L varies from 2 to 30 and the dimension of eigenspaces K, K' are fixed to 10. The thick line denotes the case of including the approximation error term and the dots lines denotes the case of not including it. In the case of not including the approximation error term, the shape reconstruction error become extremely large where L is close to K. But, by including the approximation error term, the shape reconstruction error become small. In case of changing the values of K, K', the results are similar to Fig.5.14.

The shape reconstruction error become large in case of not including the approximation error term. This reason is explained as follows: in this case, $\sigma = 0$ in Eq.(5.33), hence $\boldsymbol{A}$ is calculated by using the pseudo inverted matrix[72] which elements are inverse numbers of non-zero eigen values calculated from $\Delta \boldsymbol{G}_{\mathrm{Ps}}$. When $L \approx K$, extremely small eigen value is often estimated and it causes $\boldsymbol{A}$ to have very large elements. In this situation, the linear interpolation of the shading profiles by Eq.(5.18) is valid, but the interpolation of the shape profiles using $\boldsymbol{A}$ is not accurate because various errors are enlarged.

Figure 5.15 shows the histogram of 150 reconstruction errors where the number of nearest points L fixed to 11. In this figure, we show the results in case of including the approximation error term, not including it and the nearest neighborhood method. The nearest neighborhood method obtains the sample shape profile itself corresponding to the shading profile which is the nearest to the input shading profile in the shading eigenspace by estimating d of Eq.(5.23) as the reconstructed shape profile. In Fig.5.15, in case of not including the approximation error term (the dots line), the shape reconstruction errors are

[5]Strictly speaking, we define the height 0 as $|Z^*(y_i)|$, $|Z_t(y_i)|$ smaller than 0.3387[mm](width of a pixel under 75[dpi]).

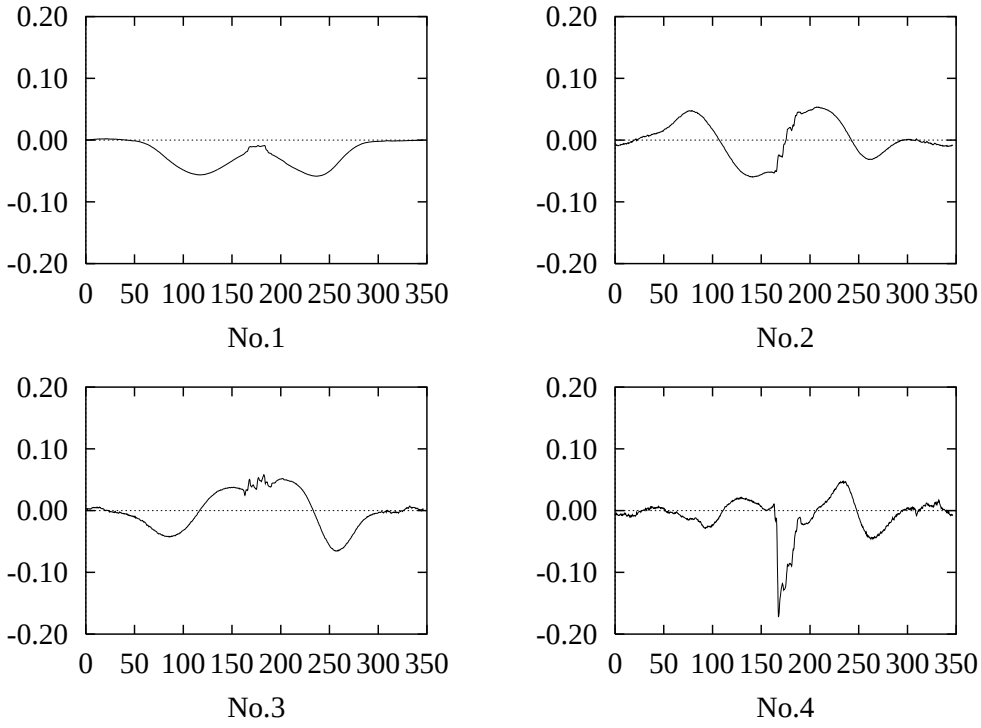

Figure 5.10: Eigen vectors of intensity profile data (No.1∼4).

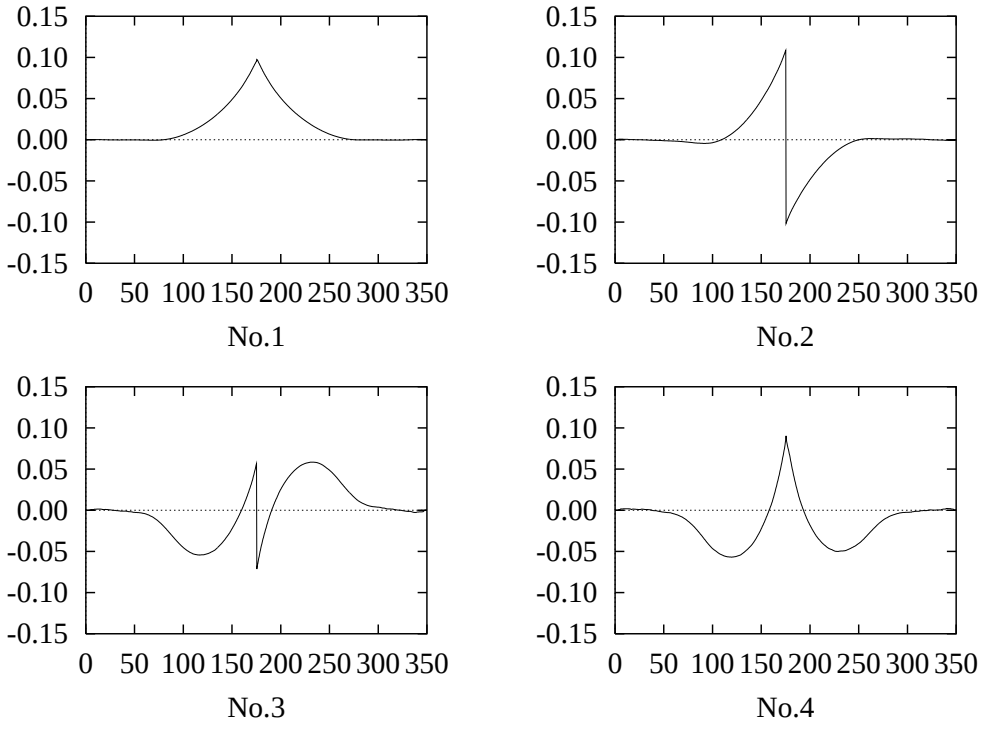

Figure 5.11: Eigen vectors of shape profile data (No.1∼4).

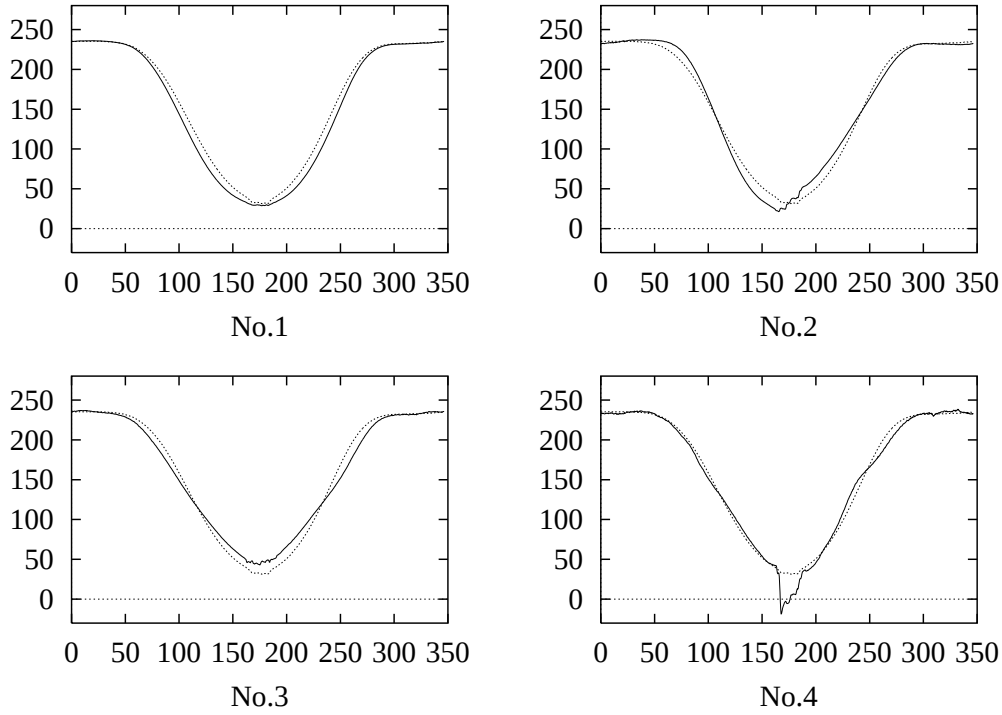

Figure 5.12: Eigen vectors with average vector (intensity profile data No.1∼4).

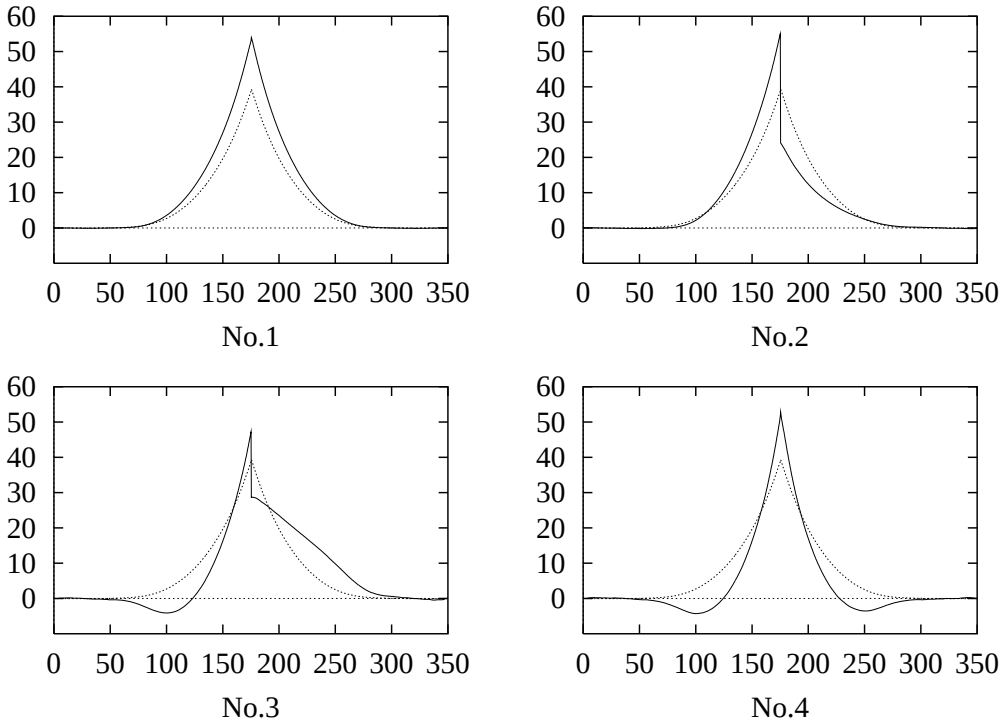

Figure 5.13: Eigen vectors with average vector (shape profile data No.1∼4).

large and shape profiles are not estimated stably. The result of the nearest neighborhood method (the dash line) also has large shape reconstruction error. On the other hand, the result of including the approximation error term (the thick line), all shape reconstruction errors are smaller than 3.0[mm], hence this method can be estimated the reconstruction shape accurately to various input images.

Figure 5.16 shows the comparison of the shape reconstruction error under various SN ratio ($\sqrt{\nu}$) as 1, 5, 10, 20, 50% where L varies from 2 to 30 and $K, K' = 10$. From this results, in case of $10 \sim 20\%$ SN ratio, the shape reconstruction error become very small. In case of changing the values of K, K', the results are similar to Fig.5.16.

Figure 5.17 shows the shape reconstruction error under various K as 5, 10, 15, 20, 25, 30 where $K' = K$ and SN ratio is 10%. The shape reconstruction error tend to decrease with increment of K, but the results of $K \geq 20$ are not changed. Hence the adequate number of $K(K')$ is 20 in this experiment.

Next, we show the effectiveness of the profile normalization. Figure 5.18 shows the histogram of shape reconstruction errors by two methods. The dotted line shows the result by using the eigenspaces constructed from non-normalized sample profiles, and the thick line shows the result of proposed method where $L = 13$,$K = K' = 20$, SN ratio is 10%. The means of all shape reconstruction errors are 0.73[mm] (with normalization) and 1.93[mm] (without normalization). From this result, the shape profiles can be reconstructed accurately by using the profile normalization.

Figure 5.20 shows one of the input book surface images used for the shape reconstruction. Figure 5.19 shows estimated shape profiles. The thick line is estimated by the proposed method, the dotted line is estimated by non-normalized method and the thin line is the real shape. The restored images are shown in Fig.5.21 and Fig.5.22. The shading in the input image is restored by Eq.(5.41) in Sect.5.4. The estimated shape by non-normalized method is misshapen and the gutter position is not located on the right position. Hence, the geometric distortions are still remained around the gutter (the hatching area in Fig.5.21). On the other hand, the estimated shape by using the proposed method is reconstructed accurately, so the geometric and photometric distortion can be removed in the restored image.

The computation time of the off-line process for the construction of the shape and shading eigenspaces is 146 seconds. And the shape reconstruction for one input image (on-line process) costs about 2 seconds. On the other hand, when we execute the shape reconstruction using the physically-based model described in chapter 4 on same computer (CPU:Alpha,500MHz), the total computation time to obtain the reconstruction shape as shown in Fig.4.21 is 325 seconds. Even if we consider that this computer can calculate 3$\sim$4 times faster than the computer used in experiments of chapter 4, this result shows that the appearance-based method proposed in this chapter can recover the book surface shape extremely faster than the physically-based method. Moreover, we evaluate the accuracy of the reconstructed shape for each method from scanned images used in this experiment. For some scanned images, the physically-based method can recover the book shape more accurately than the appearance-based method, but as the whole result, the appearance-based method can recover more accurately than the physically-based method.

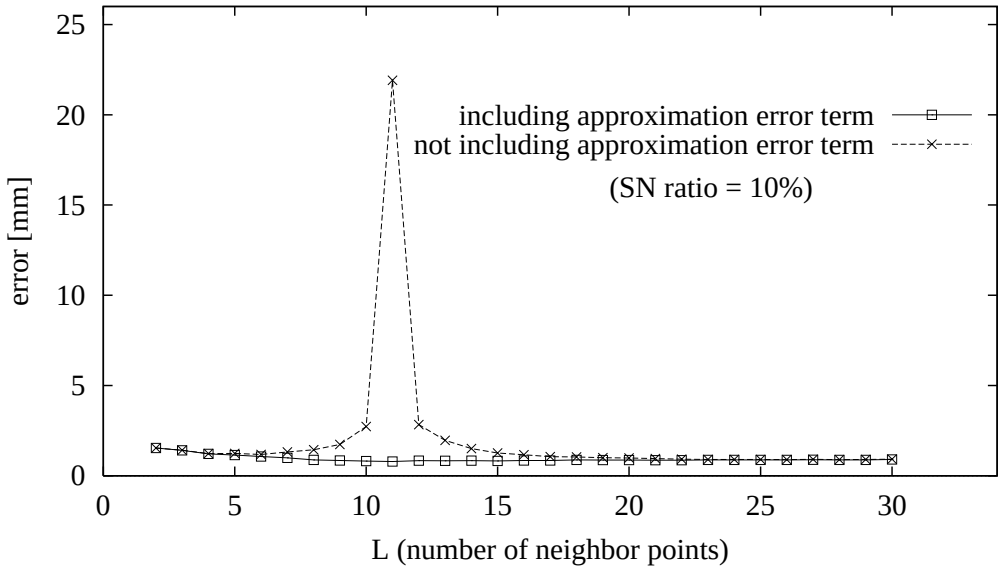

Figure 5.14: Reconstructed shape error (including or not including linear approximation error term.)

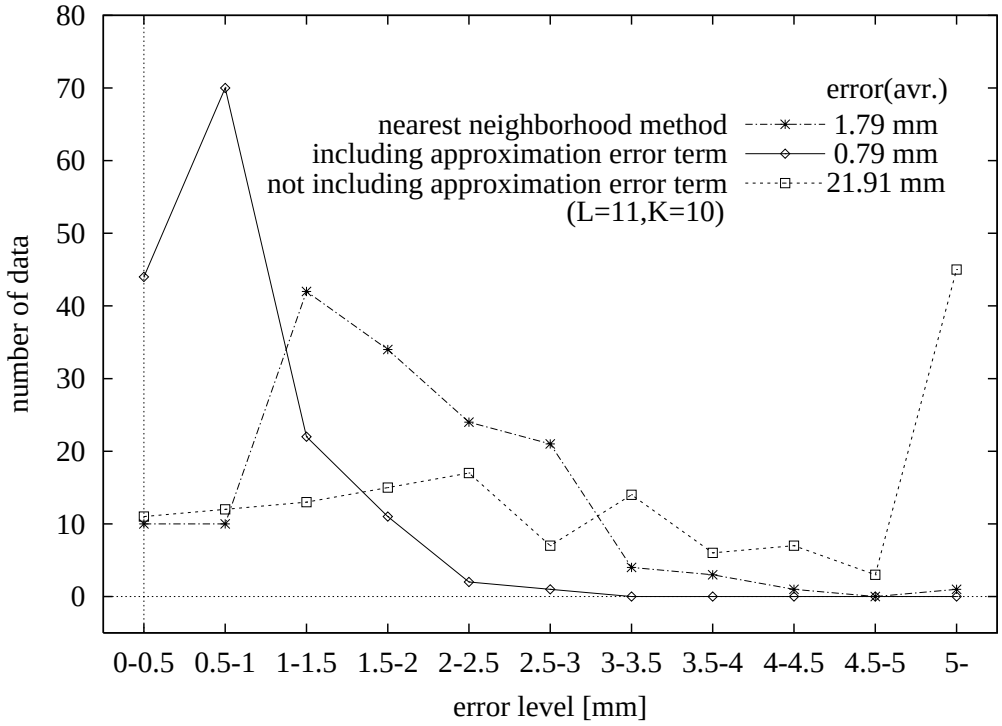

Figure 5.15: Histogram of shape error (including or not including linear approximation error term, and nearest neighborhood method.)

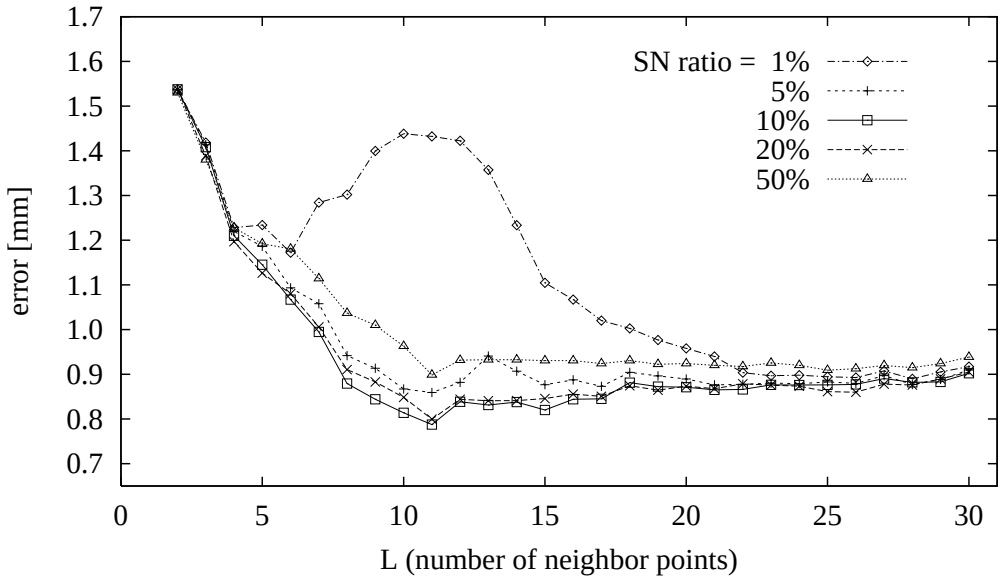

Figure 5.16: Reconstructed shape error varying with signal-to-noise ratio.

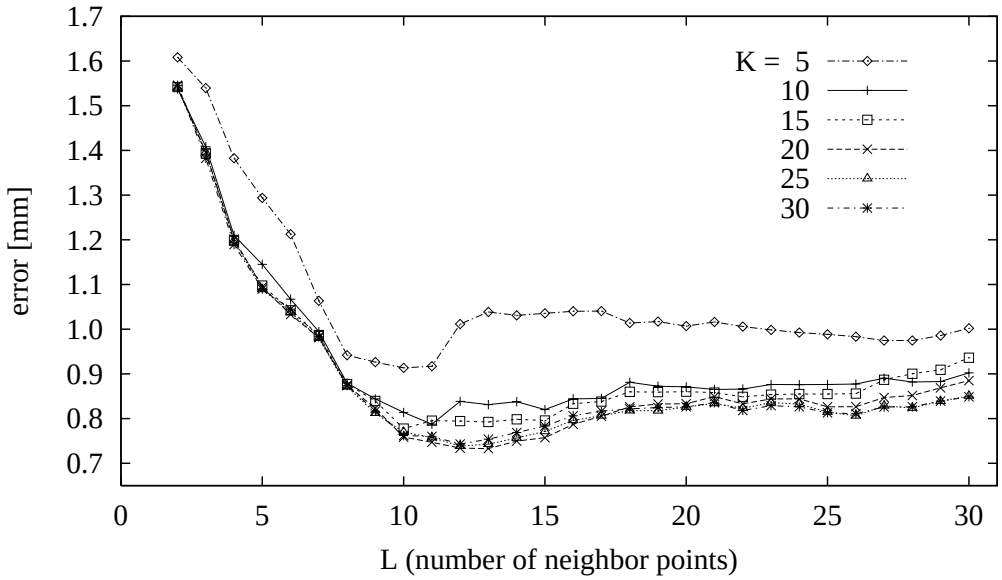

Figure 5.17: Reconstructed shape error varying with eigen space dimension.

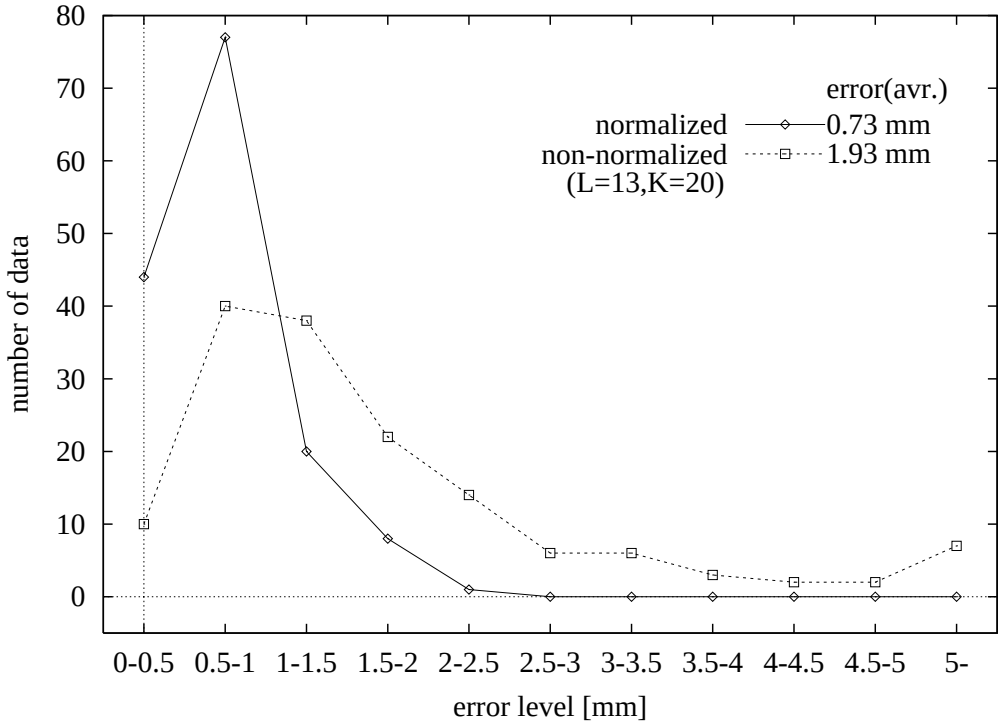

Figure 5.18: Histogram of shape error (normalized or non-normalized profiles.)

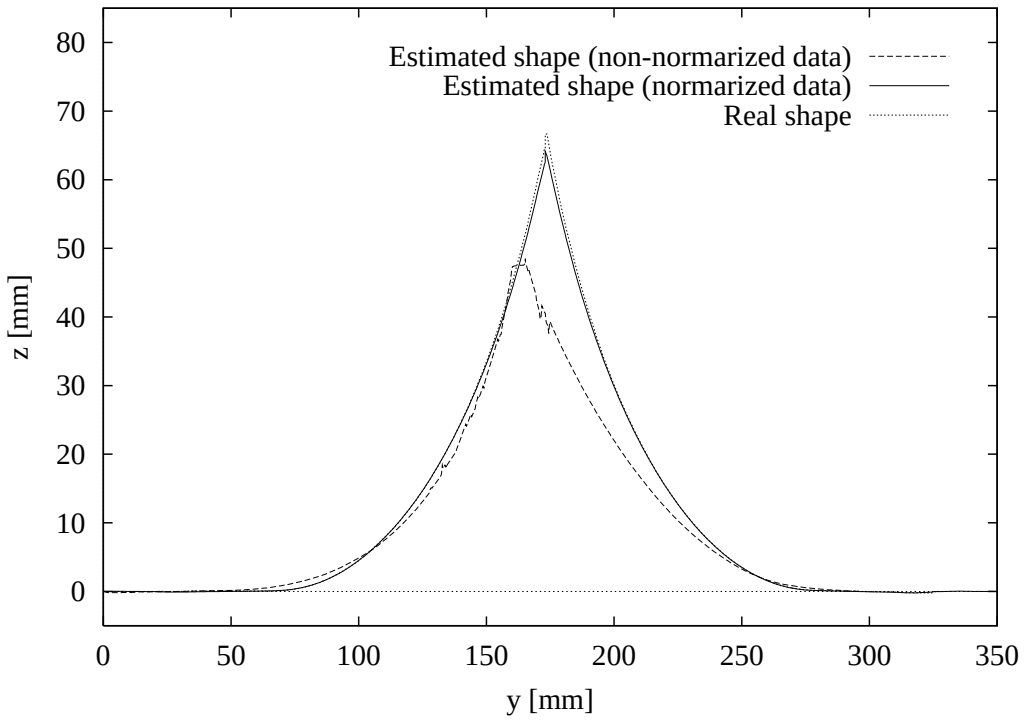

Figure 5.19: Estimated shapes.

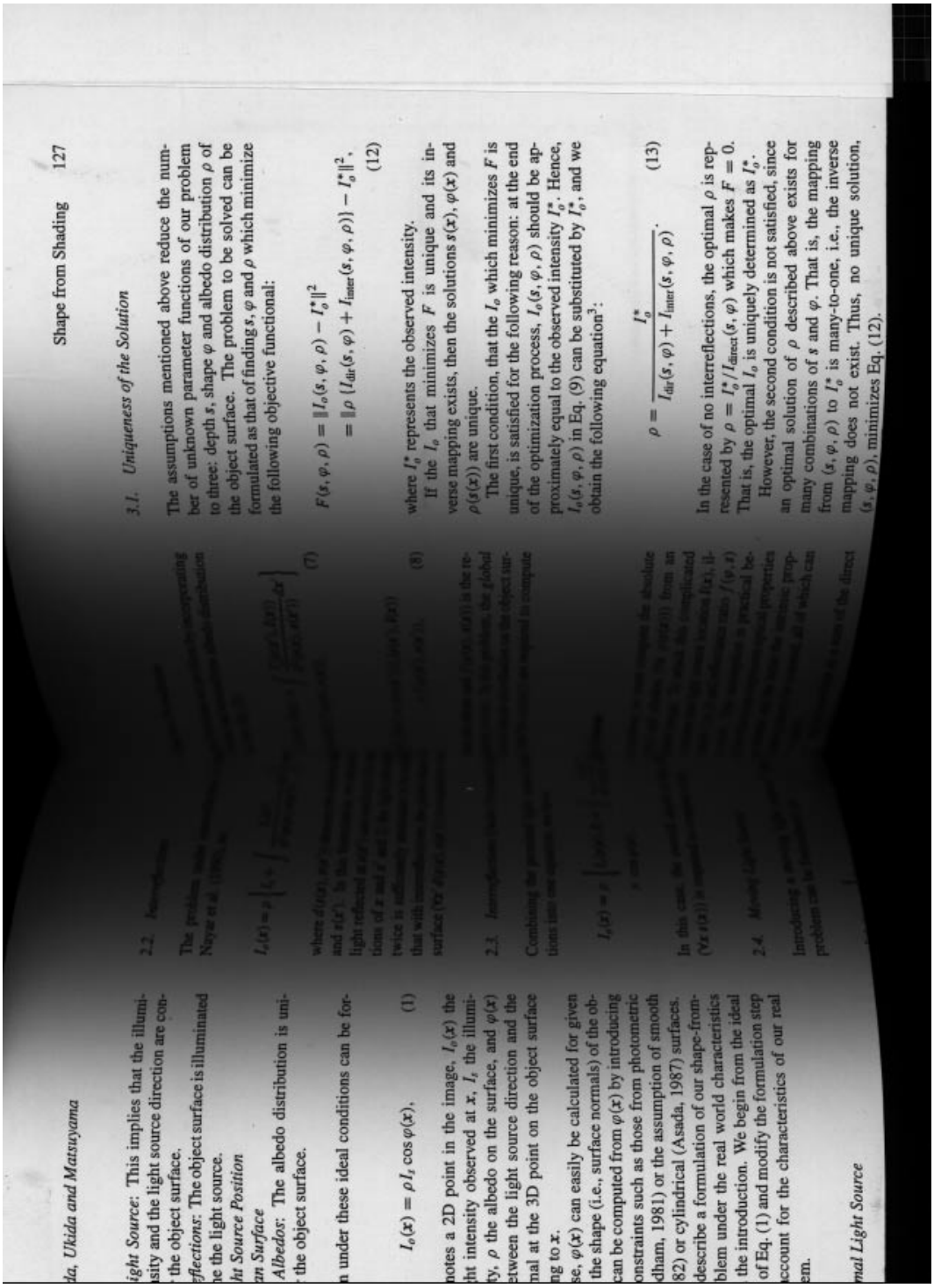

Figure 5.20: Observed image.

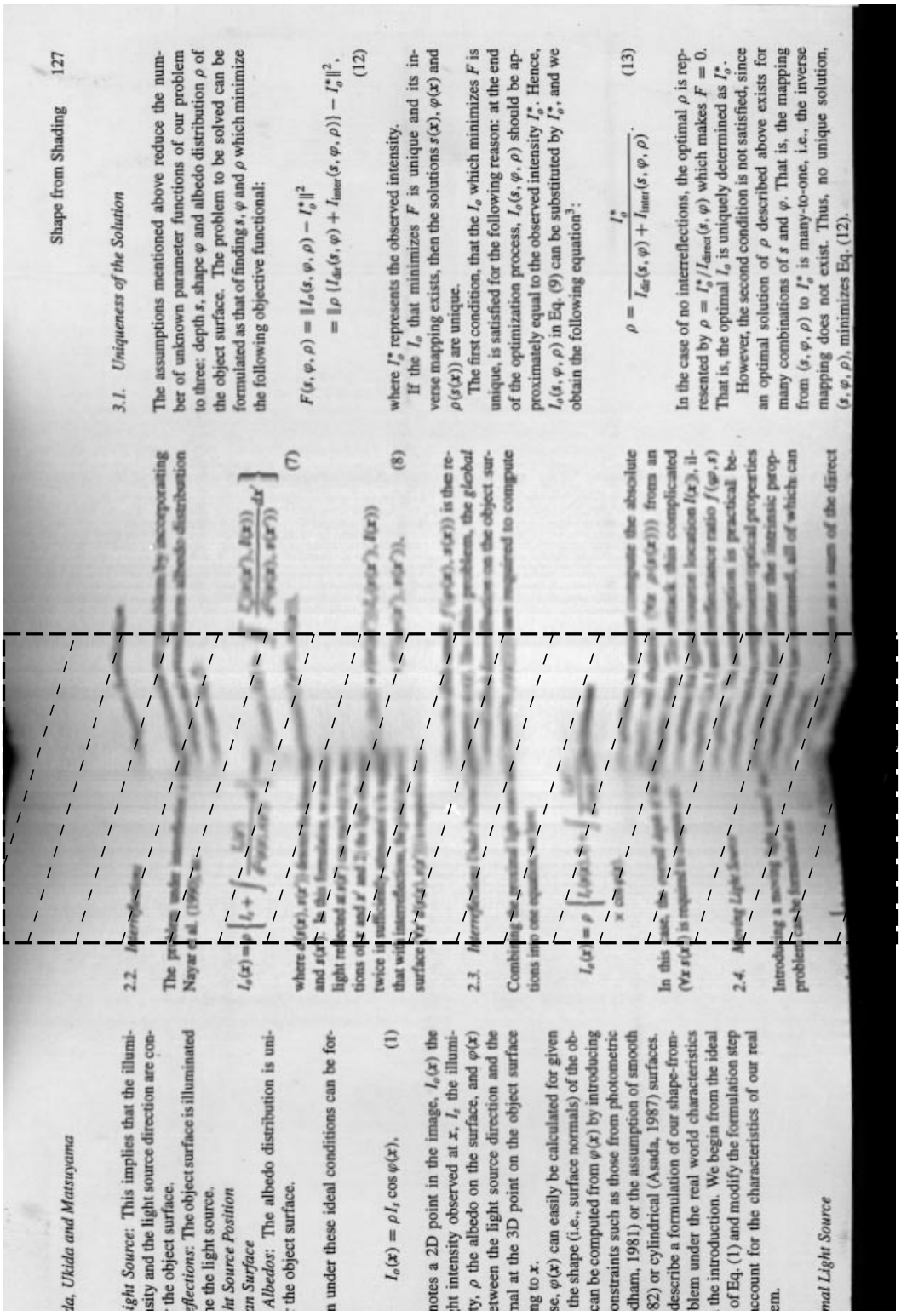

Figure 5.21: Restored image using non-normalized profiles.

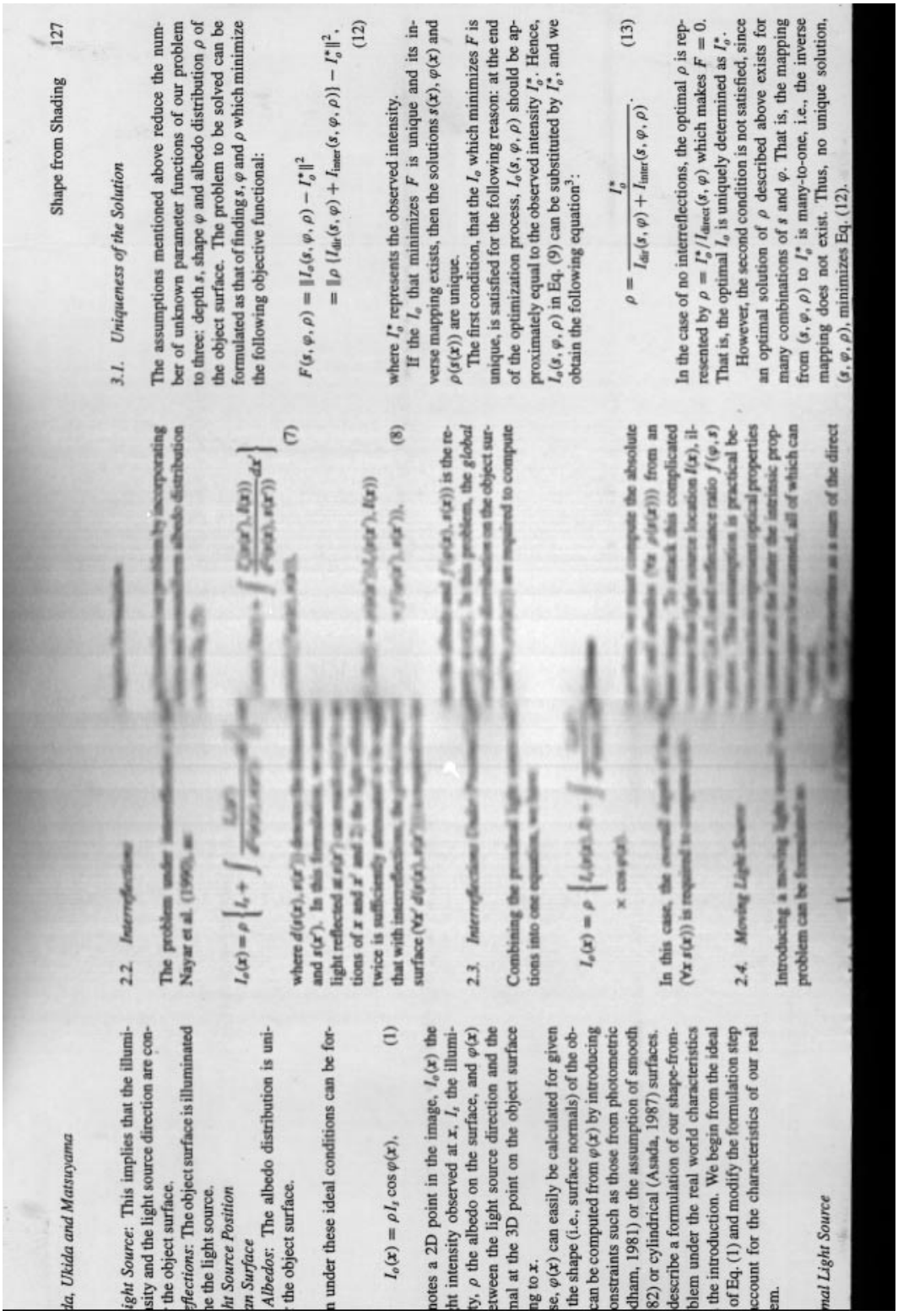

Figure 5.22: Restored image using normalized profiles.

5.5.3 Shape Reconstruction Using Real Book Surface

Here, we show the results of the shape reconstruction using the real book. In this experiment, we use the book which reflectance property on the surface is similar to the book surface models. The sample profiles to construct the shape and shading eigenspaces are same to the previous section. The cross section shape is reconstructed under $L = 13$, $K, K' = 20$ and SN ratio is 10%.

Figure 5.23 shows the input scanned image of the real book surface. Figure 5.24 is the shading profile of Fig.5.23. Figure 5.25 is the estimated shape and Fig.5.26 shows the restored image. The input image can be restored as well as the result of the previous section. In Fig.5.26, the geometric distortion is still remained around the gutter. This means that the estimated shape is lower than the actual one. This reason is explained as follows: on the book surface model using for the sample profiles, the texture is printed close to the gutter, but on the real book surface, the texture is not printed near the gutter. Because of this effect, the intensity of the interreflections near the gutter of the real book is brighter than the book surface model. The brighter intensity usually means the lower shape, hence, the estimated shape was lower than the actual[6].

From these results, the proposed method is effective when the reflectance property of the book surface is similar to the sample profile data. But, in general, to apply the proposed method for real book surfaces, we must consider the influence of the interreflections. The interreflections depend on the albedo distribution, the reflectance property, and the opposite side shape of the book surface. Theoretically, if the sample profiles taking account of these factors are prepared, the book surface shape could be estimated accurately for various books. But, this method has some problems such as 1.enormous sample profiles are required, 2.one shape profile corresponds to multiple shading profiles. Hence, to improve the proposed method, we must discuss these problems.

[6]This influence is examined by using the book surface model. When the width of the white background around the gutter varies from 10[mm] to 50[mm], the estimated shape is changed from 1.4[mm] to 4.7[mm] lower than the true shape.

Figure 5.23: Observed image of real book surface.

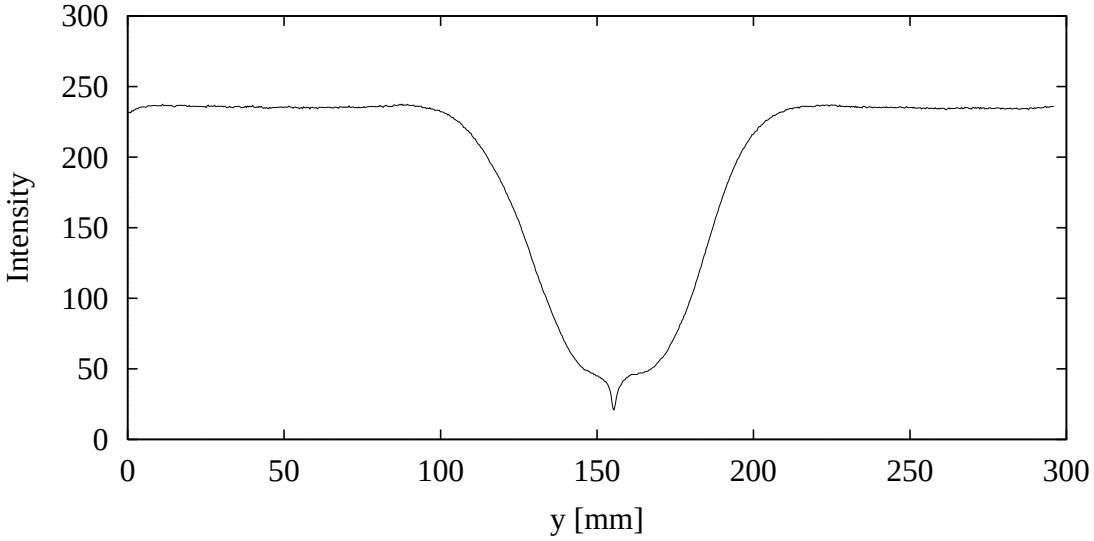

Figure 5.24: Shading profile of observed image.

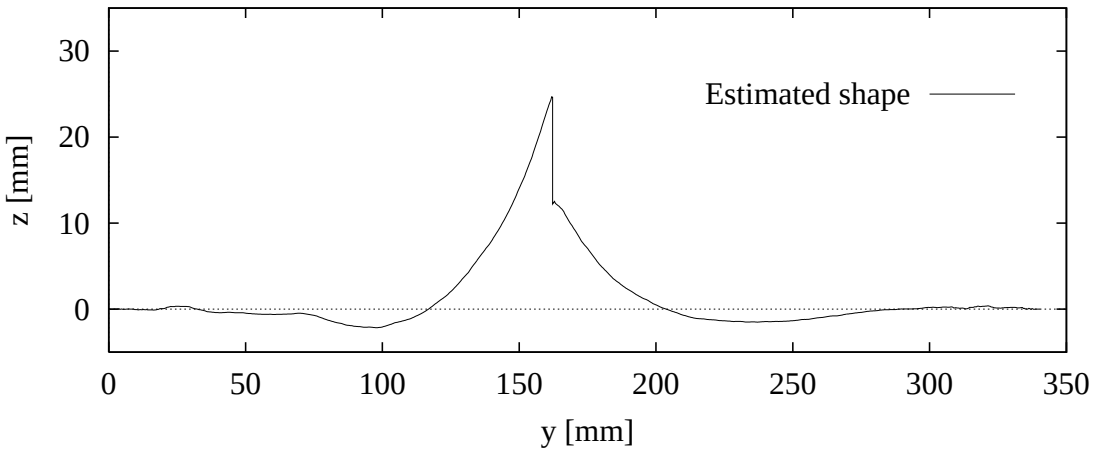

Figure 5.25: Estimated shape.

Figure 5.26: Restored image of real book surface.

5.6 Conclusion

In this chapter, we discussed the book surface shape reconstruction method using the appearance-based model from the scanned image. In this method, the relation between the shape and shading is approximated to the local linear transformation by using the directly measured shape and shading profiles, and the book surface shape can be estimated by this relation from the input shading profile.

To apply this method to the actual shape reconstruction problem, since the number of the sample shape and shading profiles become enormous, these profiles are preserved into eigenspaces, and the relation between the shape and shading are reconstructed as the relation between two eigenspaces. Moreover, to recover the book surface shape accurately, we propose that 1. the normalization of the shape and shading profiles with respect to the translation on the scanning plane using Fourier transformation, 2. the shape reconstruction including the approximation error caused by the local linear interpolation in the shading eigenspace and the linear transformation from the shading eigenspace to the shape eigenspace.

We examined the effectiveness of the proposed method by the shape reconstruction experiments using many input scanned images, and confirm that the real book surface also can be estimated fast and accurately. These results showed that the shape reconstruction using the appearance-based model is effective for the book surface shapes which are limited for the form variation.

As the future work, to recover the various book surface shape, we must consider the difference of the reflectance property in the input image to the sample data. In this case, the number of the sample data become very large, hence more effective methods are required. And to deal with more general situation for the book copying, we should discuss the shape reconstruction method in case of that the cross section shape of the book surface can not be assumed to be constant.

Chapter 6

3D Shape Reconstruction Using a Color Image Scanner

6.1 Introduction

In previous chapters, we used the book surface shape as the target for the shape reconstruction. The book surface shape has simple characteristics because it can be assumed that the cross section shape is constant, and it is approximated by polynomials, hence it was enough to recover 2D cross section shape of the book surface. But if these constraints are not assumed, for example, the direction of the gutter in the book surface is not parallel to the CCD sensor and the light source on the scanning plane, or the book surface shape is distorted three dimensionally when the unfolded book surface cannot be held down with uniform pressure, actual 3D shape of whole book surface should be recovered to restore the scanned image. In this chapter, we discuss the method to reconstruct not only the book surface but also the arbitrary shape from a scanned image.

In the arbitrary shape reconstruction, since geometric constraints of the object shape cannot be assumed, we cannot employ the shape models for whole shape of the object such as polynomials for the book surface. Hence, we must obtain the local shape parameters which are the surface normal vector (slants) and the distance between the light source and the surface (depth) for over all object surface. The reason why we must estimate the depth and slants on the surface simultaneously is that the reflectance intensity varies with respect to not only the incident angle on the surface but also the distance from the light source because of the linear light source in the image scanner. In other word, the brightness on the object surface depends on slants and depth of the surface.

As shown in the previous chapter, [48] proposes the arbitrary shape reconstruction method using the quadric segments with the eigenspace. In this method, the parallel light source is assumed. But, the illuminant intensity of the image scanner varies with the distance. Hence it is difficult to apply this method to the scanned image, because the number of the shading information for the sample data become extremely large. Therefore, we employ the physically-based models for the arbitrary shape reconstruction.

To reconstruct the arbitrary shape, the following assumptions are used, that is, no inter-reflections, a Lambertian surface, and an uniform albedo distribution. These assumptions make the photometric characteristics more simpler than the problem of chapter 4. But, even if we use these assumptions, we cannot estimate multiple shape parameters (slants

and depth) from single observed intensity because the light source in the image scanner is the proximal linear light source. In order to supply the lack of conditions, we propose another shape reconstruction method using a color scanned image taken by a color image scanner which has three light sources, red, green, and blue.

As the 3D shape reconstruction method using multiple light sources, the photometric stereo method has been studied [29], [30], [31]. As shown in Sect.2.2, the photometric stereo method often assumes the parallel light source in order to simplify the photometric formulation. In this case, the reflections depend on the surface slants, hence the object slants can be estimated but the absolute depths can not. On the other hand, under the proximal linear light source of the image scanner, the reflections depend on both the slants and depth. Therefore, if we can use complex characteristics of multiple linear light sources well, we can estimate both the slants and depth from the scanned image.

Some photometric stereo studies have proposed the method to estimate the depth of the object surface under the point light source [42], [43], [44]. These methods simplified the photometric models by using three and more light sources or assuming the surface smoothness. But, the shape reconstruction method under the linear light sources have not been studied. Moreover, each linear light source has different color in this study. Hence, our shape reconstruction problem is more complex photometric situation than previous studies.

Under complex photometric models, in order to estimate mutually dependent shape parameters, slants and depth, efficiently and accurately, we propose the following two step algorithm. The first step is the rough estimation of the shape parameters by the iteration; estimate one parameter under fixed other parameters; and the second step is the optimal estimation of all parameters simultaneously by the non-linear optimization. In the following sections, we describe more details to recover the arbitrary shape from a color scanned image by the proposed method.

6.2 Color Image Scanner with Three Light Sources

6.2.1 Structure of Color Image Scanner

Figure 6.1 shows the structure of the color image scanner (EPSON GT–9000) and the coordinate system. This scanner has one monochrome linear CCD sensor D, mirror M, lens C as same as shown in Sect.3.1. But, the light source is different. This scanner has three light sources which are red (R), green (G)[1], and blue (B).

As shown in Sect.3.1, the sensor D takes a 1D image $P^*(x_i)$ along the scanning line S and moves with M, C, and light sources. The sequence $P^*(x_i)$ forms a 2D image $P^*(x_i, y_j)$. $P^*(x_i)$ is obtained by the perspective projection, but the projection along the y-axis is equivalent to the orthogonal projection.

Each light source in this image scanner can illuminate an object on the scanning plane independently. By scanning three times using each light source, we can obtain the red $P_r^*(x_i, y_j)$, green $P_g^*(x_i, y_j)$, and blue $P_b^*(x_i, y_j)$ images. A color image consists of these three images.

[1]This scanner actually has two green light sources. However, they locates very close to each other, so we assume them to be one light source.

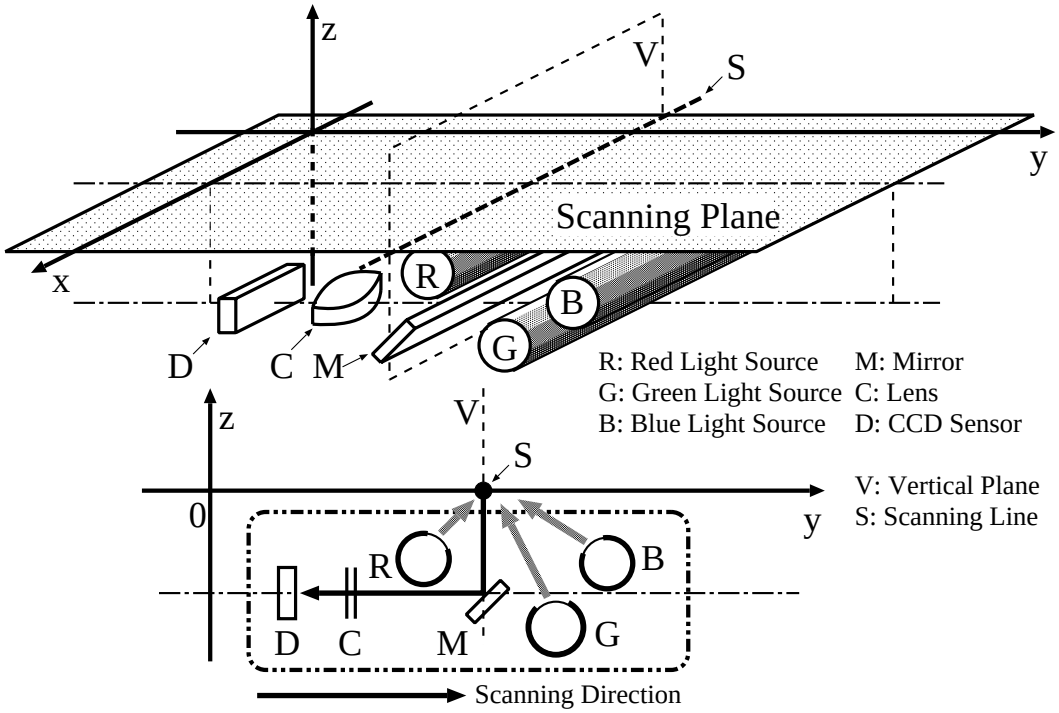

Figure 6.1: Structure of color image scanner.

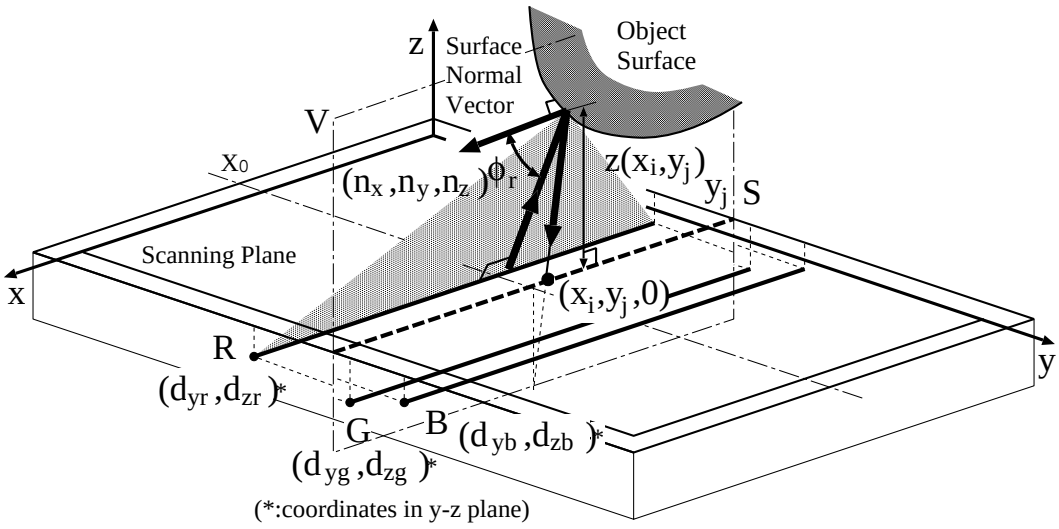

Figure 6.2: Direction and location of three light sources.

6.2.2 Light Source Models

Three light sources of this scanner can be modeled as the linear light sources, because they are long and narrow fluorescent tubes and they can be treated as sequences of point light sources. In this study, we assume that the length of the light source is much longer than objects.

When the scanning line S locates at $y = y_j$ as shown in Fig.6.2, the illuminant intensity of the red light source $Is_r(x_i, y_j)$ is formulated as follows:

$$Is_r(x_i, y_j) = \frac{\alpha_r}{\sqrt{d_{yr}^2 + (z(x_i, y_j) - d_{zr})^2}} + Ie_r, \tag{6.1}$$

where $z(x_i, y_j)$ denotes the height from the point (x_i, y_j) on the scanning plane to the object surface, (d_{yr}, d_{zr}) $(d_{zr} < 0)$ the locations of the light source relative to the scanning line S in $y-z$ plane, α_r the parameters of the illuminant intensity, and Ie_r the environment light intensity caused by the irregular reflection of the illumination inside of the scanner[2]. The green and blue light sources are also modeled similarly. These models are expressed by substituting the index 'r' in Eq.(6.1) to 'g' or 'b'.

6.3 Photometric Models

First, to formulate photometric models, we assume the following conditions:

1. The object surface is Lambertian,
2. The albedo on the surface is uniform (constant),
3. There are no interreflections and self-shadowing on the object surface.

Let $(n_x(x_i, y_j), n_y(x_i, y_j), n_z(x_i, y_j))$ be the surface normal vector at the point on the object surface projected to $(x_i, y_j, 0)$ where $n_x^2(x_i, y_j) + n_y^2(x_i, y_j) + n_z^2(x_i, y_j) = 1$. In case of the red light source, the image intensity $P_r(x_i, y_j)$ in the observed image is formulated as:

$$P_r(x_i, y_j) = a_r \cdot \rho_r \cdot Is_r(x_i, y_j) \cdot \cos(\phi_r(x_i, y_j)) + \Delta_r, \tag{6.2}$$

where a_r and Δ_r denote the gain and the bias of the photo-electric transformation in the image scanner respectively. ρ_r is the albedo on the surface for the red light source. $\phi_r(x_i, y_j)$ is the angle between $(n_x(x_i, y_j), n_y(x_i, y_j), n_z(x_i, y_j))$ and the direction from the surface to the red light source (Fig.6.2) represented as:

$$\cos(\phi_r(x_i, y_j)) = \frac{d_{yr} \cdot n_y(x_i, y_j) - n_z(x_i, y_j) \cdot (z(x_i, y_j) - d_{zr})}{\sqrt{d_{yr}^2 + (z(x_i, y_j) - d_{zr})^2}}. \tag{6.3}$$

[2]As the another property of the scanner light source, the directional distribution of the illumination in the $y - z$ plane is included in the light source model in Sect.3.2. This property is caused by the cover surrounding the light source, and because of interreflections, it is necessary to consider this property in Sect.3.2. But, in this chapter, because we can take account of only the illuminant intensity existing in the vertical plane V above S, the directional distribution is not so effective. Hence, this property is not considered in light source models.

In this study, we assume that the photometric parameters (α_r, d_{yr}, d_{zr}, a_r, ρ_r, Δ_r) are known. They are estimated by using the white surface object before the shape reconstruction process (Section 6.4.1). But a_r, ρ_r and α_r can not be estimated separately, so we introduce 'the albedo ratio', ρ'_r, as follows:

$$\rho'_r = \rho_r / \rho_{wr}, \tag{6.4}$$

where ρ_{wr} is the albedo on the white surface. The albedo ratios can be regarded as the color of the object surface. When $(\rho'_r, \rho'_g, \rho'_b) = (1.0, 1.0, 1.0)$, the object surface is white. $(\rho'_r, \rho'_g, \rho'_b) = (1.0, 0.0, 0.0)$ means red, $(\rho'_r, \rho'_g, \rho'_b) = (1.0, 1.0, 0.0)$ means yellow, and so on. The albedo ratios are also assumed to be known in the shape reconstruction process. They are estimated from the intensities of the input image at a point where the object surface contacts with the scanning plane, that is, the height $z = 0$ and the surface normal $(n_x, n_y, n_z) = (0, 0, -1)$.

By using albedo ratios, all photometric models are written as follows:

$$\begin{aligned}
P_r(x_i, y_j) &= \rho'_r \cdot a_r \cdot \rho_{wr} \cdot Is_r(x_i, y_j) \cos(\phi_r(x_i, y_j)) + \Delta_r \\
&= \rho'_r \cdot a_r \cdot \rho_{wr} \left\{ \frac{\alpha_r}{\sqrt{d_{yr}^2 + (z(x_i, y_j) - d_{zr})^2}} + Ie_r \right\} \\
&\quad \cdot \left\{ \frac{d_{yr} \cdot n_y(x_i, y_j) - n_z(x_i, y_j) \cdot (z(x_i, y_j) - d_{zr})}{\sqrt{d_{yr}^2 + (z(x_i, y_j) - d_{zr})^2}} \right\} + \Delta_r, \qquad (6.5) \\
P_g(x_i, y_j) &= \rho'_g \cdot a_g \cdot \rho_{wg} \cdot Is_g(x_i, y_j) \cos(\phi_g(x_i, y_j)) + \Delta_g \\
&= \rho'_g \cdot a_g \cdot \rho_{wg} \left\{ \frac{\alpha_g}{\sqrt{d_{yg}^2 + (z(x_i, y_j) - d_{zg})^2}} + Ie_g \right\} \\
&\quad \cdot \left\{ \frac{d_{yg} \cdot n_y(x_i, y_j) - n_z(x_i, y_j) \cdot (z(x_i, y_j) - d_{zg})}{\sqrt{d_{yg}^2 + (z(x_i, y_j) - d_{zg})^2}} \right\} + \Delta_g, \qquad (6.6) \\
P_b(x_i, y_j) &= \rho'_b \cdot a_b \cdot \rho_{wb} \cdot Is_b(x_i, y_j) \cos(\phi_b(x_i, y_j)) + \Delta_b \\
&= \rho'_b \cdot a_b \cdot \rho_{wb} \left\{ \frac{\alpha_b}{\sqrt{d_{yb}^2 + (z(x_i, y_j) - d_{zb})^2}} + Ie_b \right\} \\
&\quad \cdot \left\{ \frac{d_{yb} \cdot n_y(x_i, y_j) - n_z(x_i, y_j) \cdot (z(x_i, y_j) - d_{zb})}{\sqrt{d_{yb}^2 + (z(x_i, y_j) - d_{zb})^2}} \right\} + \Delta_b. \qquad (6.7)
\end{aligned}$$

We estimate $z(x_i, y_j)$ and $(n_x(x_i, y_j), n_y(x_i, y_j), n_z(x_i, y_j))$ at each point (x_i, y_j) from the observed intensities in the input image by using above photometric models.

6.4 Shape Reconstruction

6.4.1 Photometric Calibration for 3D Shape Reconstruction

In this section, we show the method to obtain the photometric parameters. In order to estimate parameters, we use some scanned images of the slope model as shown in Fig.6.3.

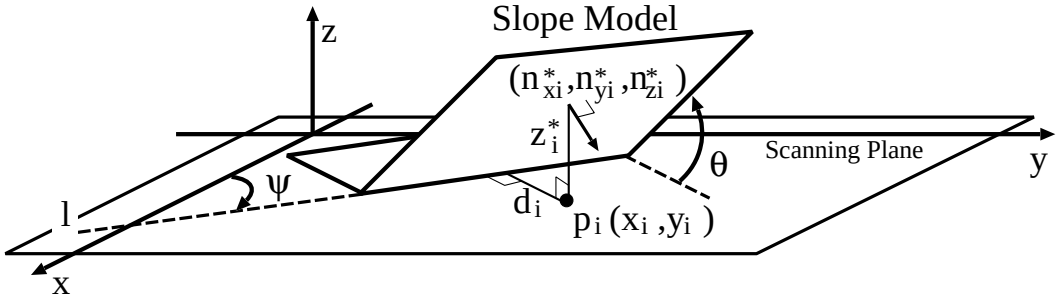

Figure 6.3: Slope model on scanning plane.

The surface of this model is put to the white paper approximated to a Lambertian surface, and the slant angle θ and the rotation angle ψ ($\theta, \psi > 0$) can be changed.

Let $p_i(x_i, y_i)$ be a point at the slope region in a scanned image, d_i the distance between p_i and line l, and $(P^*_{ri}, P^*_{gi}, P^*_{bi})$ image intensities at (x_i, y_i). The height z^*_i and the surface normal vector $(n^*_{xi}, n^*_{yi}, n^*_{zi})$ of the slope surface at (x_i, y_i) is calculated as follows:

$$\left.\begin{array}{ll} z^*_i = d_i \cdot \tan\theta, & n^*_{xi} = \sin\psi \cdot \sin\theta, \\ n^*_{yi} = \cos\psi \cdot \sin\theta, & n^*_{zi} = -\cos\theta. \end{array}\right\} \tag{6.8}$$

Here, we assume that N observed data (P^*_{ri}, P^*_{gi}, P^*_{bi}, z^*_i, n^*_{xi}, n^*_{yi}, n^*_{zi}) ($1 \le i \le N$) can be extracted from slope images.

The photometric parameters are estimated by using the observed data. In case of the red light source, by assigning the observed data to Eq.(6.5) and assuming Ie_r and Δ_r to be 0, we construct the following linear equations:

$$P^*_{ri}A + z^*_i n^*_{zi} B - n^*_{yi} C + n^*_{zi} D + 2P^*_{ri} n^*_{zi} E = -P^*_{ri} z^{*2}_i \quad (1 \le i \le N) \tag{6.9}$$

where

$$\begin{aligned} A &= d^2_{yr} + d^2_{zr}, && (6.10)\\ B &= \rho_{wr} \cdot a_r \cdot \alpha_r, && (6.11)\\ C &= \rho_{wr} \cdot a_r \cdot \alpha_r \cdot d_{yr}, && (6.12)\\ D &= \rho_{wr} \cdot a_r \cdot \alpha_r \cdot d_{zr}, && (6.13)\\ E &= d_{zr}. && (6.14) \end{aligned}$$

Parameters from A to E are solved by linear least squares from Eq.(6.9), and d_{yr}, d_{zr} and $\alpha'_r (= \rho_{wr} \cdot a_r \cdot \alpha_r)$ are obtained from Eq.(6.10) to Eq.(6.14). Finally, by using these results as initial values, all photometric parameters are estimated by non-linear least squares to minimize the following function F_r:

$$F_r = \sum_{i=1}^{N} \left\{ P^*_{ri} - P_r(x_i, y_i; z^*_i, n^*_{xi}, n^*_{yi}, n^*_{zi}) \right\}^2 \tag{6.15}$$

In case of green and blue light sources, photometric parameters are also estimated by this method.

The albedo ratios ρ'_r, ρ'_g, and ρ'_b are also estimated at each objects before the shape reconstruction. They are estimated by using the intensity at $z = 0$ and $(n_x, n_y, n_z) = (0, 0, -1)$[3] such as:

$$\rho'_r = (P^*_{r0} - \Delta_r)/(Is_{r0} \cdot \cos(\phi_{r0})) \tag{6.16}$$

where P^*_{r0} is the intensity, Is_{r0} is the illuminant intensity and ϕ_{r0} is the angle for the direction of the red light source at $z = 0$ and $(n_x, n_y, n_z) = (0, 0, -1)$. ρ'_g and ρ'_b are also estimated similarly.

6.4.2 Shape Reconstruction Algorithm

Here, we describe the method to estimate the shape parameters; z, n_x, n_y and n_z at (x_i, y_j) from observed three image intensities; $P^*_r(x_i, y_j)$, $P^*_g(x_i, y_j)$, and $P^*_b(x_i, y_j)$; by using three photometric models; $P_r(x_i, y_j)$, $P_g(x_i, y_j)$, and $P_b(x_i, y_j)$.

In the basic photometric stereo method under the parallel light source [29], one quadratic curve corresponding to one observed intensity is plotted on the parameter (gradient) plane[4] spanned by two surface slants parameters for the estimation. If we can use three observed intensities obtained from different light positions, two surface slants parameters can be estimated as a closed-form solution.

But, in our method, since we must estimate three parameters[5], one observed intensity draws a curve line in 3D parameter space. Moreover, since our photometric models includes the linear light source model, it is difficult to estimate three parameters as a closed-form solution. Therefore, we employ a minimization solution. The basic idea to estimate z, n_x, n_y and n_z is to minimize the following objective functional F by non-linear least squares:

$$F = \{P^*_r(x_i, y_j) - P_r(x_i, y_j)\}^2 + \left\{P^*_g(x_i, y_j) - P_g(x_i, y_j)\right\}^2 + \{P^*_b(x_i, y_j) - P_b(x_i, y_j)\}^2, \tag{6.17}$$

But in this problem, observed image intensities depend on the height z and the surface normal vector (n_x, n_y, n_z), hence it is necessary to estimate appropriate initial values. If initial values are not appropriate, then:

1. Finally estimated shape parameters are not optimal estimations,
2. It costs much computation time to minimize F.

To avoid such problems, we use the following iterative algorithm to obtain the initial estimation which is based on the alternating minimization algorithm[73] and then optimal parameters are estimated by non-linear least squares. We show the shape reconstruction algorithm as follows (Fig.6.4 shows this flowchart):

Step 0. Approximate initial directions of light sources.

Calculate $\cos(\phi_r)$, $\cos(\phi_g)$, and $\cos(\phi_b)$ from Eq.(6.3) under $(n_x, n_y, n_z) = (0, 0, -1)$ and $z = 0$.

[3]The intensity at this position is selected manually in the observed image.

[4]This plane is also called the reflectance map.

[5]One of surface normal parameters n_x, n_y, n_z can be estimated from $n_x^2 + n_y^2 + n_z^2 = 1$.

Step 1. Estimate heights under fixed surface normal vector.

Calculate heights z_r, z_g, and z_b which are parameter z in each photometric model Eq.(6.5), (6.6), and (6.7) by using $\cos(\phi_r)$, $\cos(\phi_g)$, and $\cos(\phi_b)$.

Step 2. Estimate surface normal vector under fixed heights.

Formulate three linear equations for n_y and n_z by substituting z_r, z_g, and z_b for Eq.(6.5), (6.6), and (6.7) again. Estimate n_y and n_z by linear least squares, and then obtain n_x^2.

Step 3. Estimate height and check convergence.

Ideally, values of z_r, z_g, and z_b will be equal to each other. But due to the influence of the noise and the approximated calculation from Step 0 to Step 2, they do not become same values. Therefore, we assign z to $(z_r + z_g + z_b)/3$ as the estimated height.

Calculate $\cos(\phi_r)$, $\cos(\phi_g)$, and $\cos(\phi_b)$ from Eq.(6.3) using z, n_y, and n_z and iterate from Step 1.

In the loop of this iteration, if z is converged or the number of iteration exceeds a preset value, then go to Step 4.

Step 4. Optimal estimation.

Let values of z, n_x^2, n_y, and n_z obtained until Step 3 be initial estimations, estimate optimal z, n_x^2, n_y, and n_z from Eq.(6.17) by non-linear least squares. In this study, we use the Levenberg-Marquardt method[74] for the non-linear least-squares method.

Step 5. Determine sign of n_x and restore distortions by perspective projection.

After Step 4, $n_x(x_i, y_j)$ is calculated from $n_x^2(x_i, y_j)$, and its sign is determined by heights around $z(x_i, y_j)$.

As we explained in the Sect.6.2.1, the object surface is taken by the perspective projection along the x-axis, so it is necessary to correct the distortion of the estimated shape. The corrected coordinate x_i' corresponding to x_i is described as follows:

$$x_i' = \frac{z(x_i, y_j) + f}{f}(x_i - X_0) + X_0, \tag{6.18}$$

where $z(x_i, y_j)$ is the estimated height at (x_i, y_j), f is the focal length, and X_0 is the focal position in the image scanner.

6.5 Experiments

In experiments, we use the cylindrical model shown in Fig.6.5 to evaluate the photometric parameters estimations and shape reconstructions. This model's width (w) is 210[mm], the length of the curved surface (l) is 180[mm] and the maximum height ($h_{\max}$) is 57.0[mm].

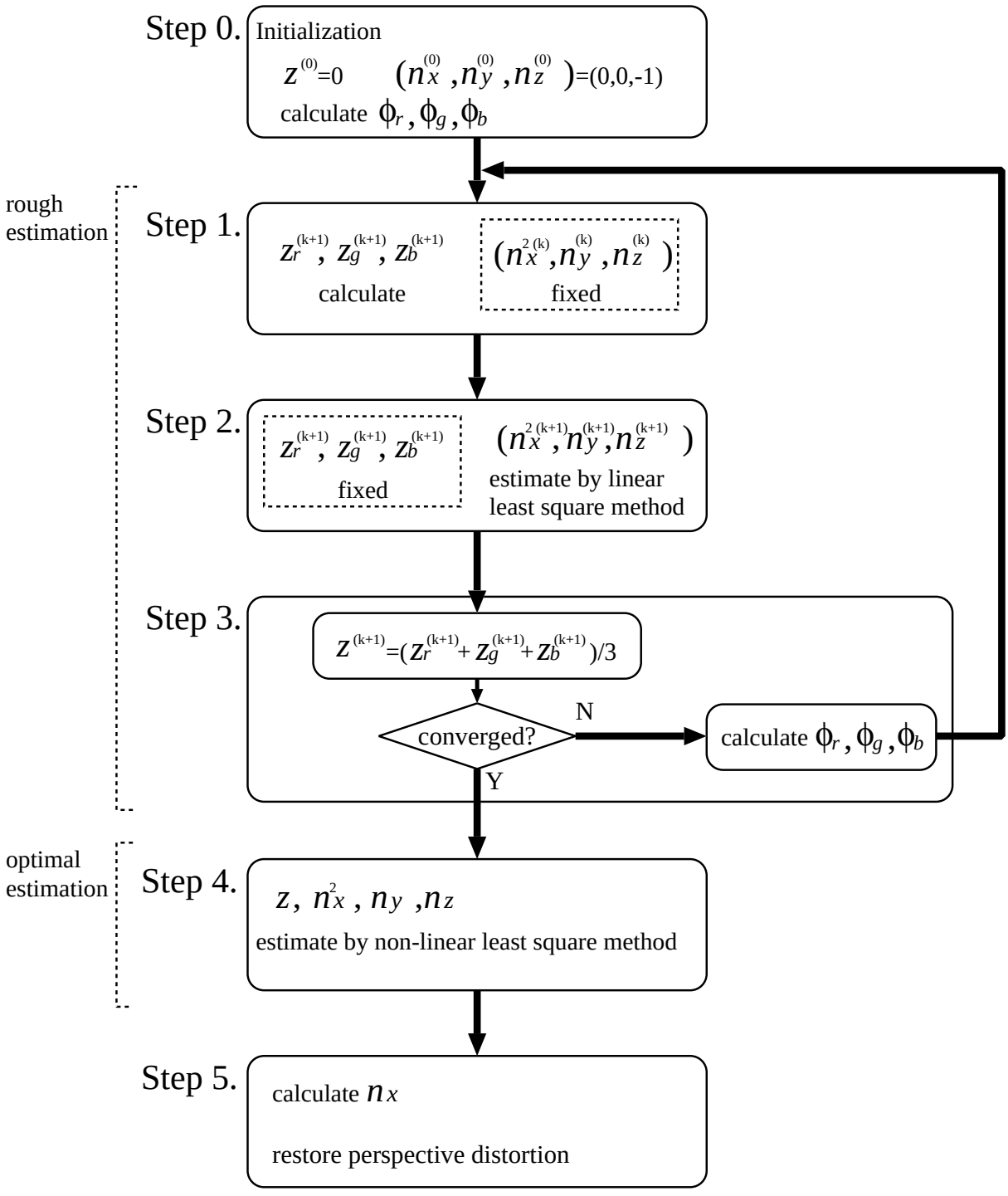

Figure 6.4: Flowchart of shape reconstruction algorithm.

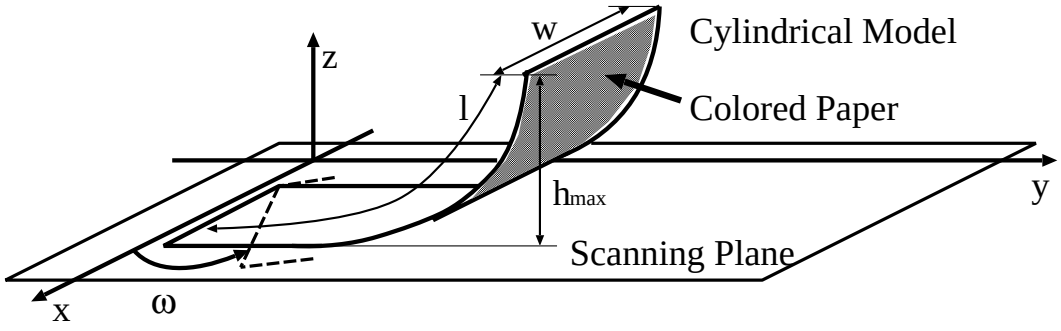

Figure 6.5: Cylindrical model on scanning plane.

This model can be rotated (ω) around the z-axis on the scanning plane, and the white or colored paper can be put on this surface.

To evaluate the accuracy of the shape reconstruction, we use the root-mean-square (RMS) errors of the height (z_{err}) and the angle (ϕ_{err}) between the true and estimated shapes:

$$z_{err} = \sqrt{\frac{1}{M}\sum_{i=1}^{M}(z_i^* - z_{ti})^2} \tag{6.19}$$

$$\phi_{err} = \sqrt{\frac{1}{M}\sum_{i=1}^{M}\arccos^2\left(\frac{\boldsymbol{n}_i^* \cdot \boldsymbol{n}_{ti}}{||\boldsymbol{n}_i^*|| \cdot ||\boldsymbol{n}_{ti}||}\right)} \tag{6.20}$$

where M is the number of points which can be estimated the shape parameters, z_i^* and $\boldsymbol{n}_i^*$ are the estimated shape parameters and z_{ti} and $\boldsymbol{n}_{ti}$ are the true shape parameters which are measured by the arm-typed 3D digitizer.

In experiments, the resolution of the scanned image is 75[dpi] and the intensity levels are 256 at each light source. To reduce the noise, intensities are averaged 3×3 pixels and shape parameters are estimated at 5 pixels intervals of (x_i, y_j) when observed intensities $P_r^*, P_g^*, P_b^* \geq 5$. Note that, to avoid the influence of the external illumination, the image scanner and objects are covered with a black box.

6.5.1 Evaluation of Photometric Parameters

In this section, we examine the stability of photometric parameters. This examination is done by the evaluation of the shape reconstruction error estimated from various photometric parameters which are obtained by various slope scanned images.

Table 6.1 shows values of θ and ψ of the slope model. Labels named T_i and P_i denote the set of θ and ψ. In this experiment, a set of photometric parameters is estimated by a set of slope scanned images which are combination of T_i and P_j. Table 6.2 shows the number of slope scanned images and observed data at each set. Hence, we estimate 24 sets of photometric parameters. Figure 6.6 shows distributions of the image intensities in case of $\theta = 30$[deg.] and ψ is the set of P_6.

The cylindrical model which surface is put a white paper is used as the object for the shape reconstruction. The rotation angle is set at $\omega = 0, 30, 45, 60, 90, 120, 135, 150, 180$[deg.]. Hence, we use nine scanned images of the cylindrical model.

Figure 6.7 shows the average of z_{err} of nine reconstructed shapes estimated by each set of the photometric parameters in Table 6.2. Note that, the case of $T_1\&P_1$, $T_1\&P_2$, and $T_1\&P_3$ are omitted in this figure because the average of z_{err} become extremely large. From these results, when the total number of data is increased, the average of z_{err} tend to be small, so photometric parameters can be estimated accuracy. Especially, when the number of θ is increased, photometric parameters become stable.

From these results, we use photometric parameters in case of $T_4\&P_6$ in the following experiments, because the more the number of the slope image data, the more parameters become stable. Table 6.3 shows all values of estimated photometric parameters we use.

Table 6.1: Setting angles of slant model.

Label	θ [deg.]	Label	ψ [deg.]
T_1	15, 30	P_1	0, 180
T_2	15, 45	P_2	0, 90, 180, 270
T_3	15, 30, 45	P_3	0, 60, 120, 180, 240, 300
T_4	15, 30, 45, 60	P_4	30, 90, 150, 210, 270, 330
		P_5	30, 60, 120, 150, 210, 240, 300, 330
		P_6	0, 30, 60, 90, 120, 150, 180, 210, 240, 270, 300, 330

Table 6.2: Number of images and observed data for photometric parameter estimation.

	P_1	P_2	P_3	P_4	P_5	P_6
T_1	$\frac{4}{1378}$	$\frac{8}{2652}$	$\frac{12}{3821}$	$\frac{12}{3848}$	$\frac{16}{5017}$	$\frac{24}{7669}$
T_2	$\frac{4}{1259}$	$\frac{8}{2410}$	$\frac{12}{3466}$	$\frac{12}{3469}$	$\frac{16}{4525}$	$\frac{24}{6935}$
T_3	$\frac{6}{1909}$	$\frac{12}{3653}$	$\frac{18}{5239}$	$\frac{18}{5242}$	$\frac{24}{6828}$	$\frac{36}{10481}$
T_4	$\frac{8}{2269}$	$\frac{16}{4343}$	$\frac{24}{6106}$	$\frac{24}{6110}$	$\frac{32}{7873}$	$\frac{48}{12216}$

upper: the number of images,
lower: the number of observed data

6.5.2 Shape Reconstruction and Error Analysis

This section shows results of the shape reconstruction and its evaluation. The cylindrical model is used as the object. As a variety of the albedo ratio, the colored paper is put on its surface. We use seven colors (including white), and estimated albedo

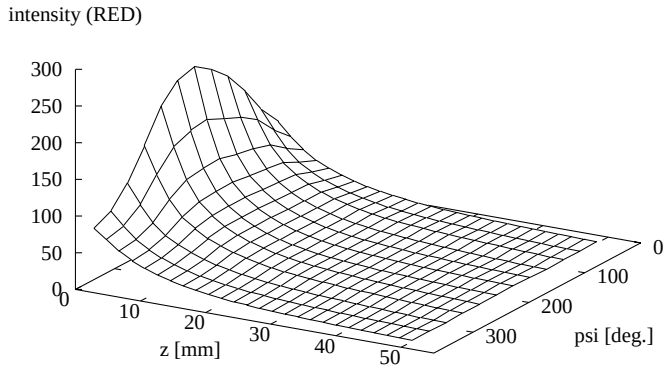

(a) Red light source.

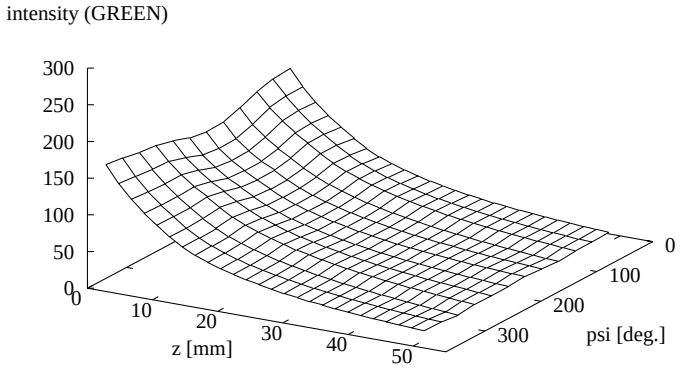

(b) Green light source.

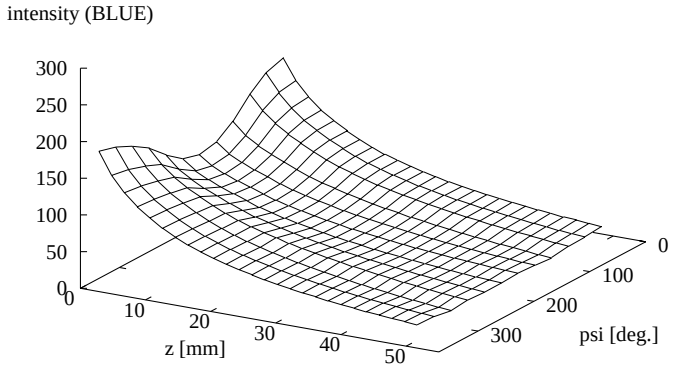

(c) Blue light source.

Figure 6.6: Distribution of slope image intensities ($\theta = 30$ [deg.]).

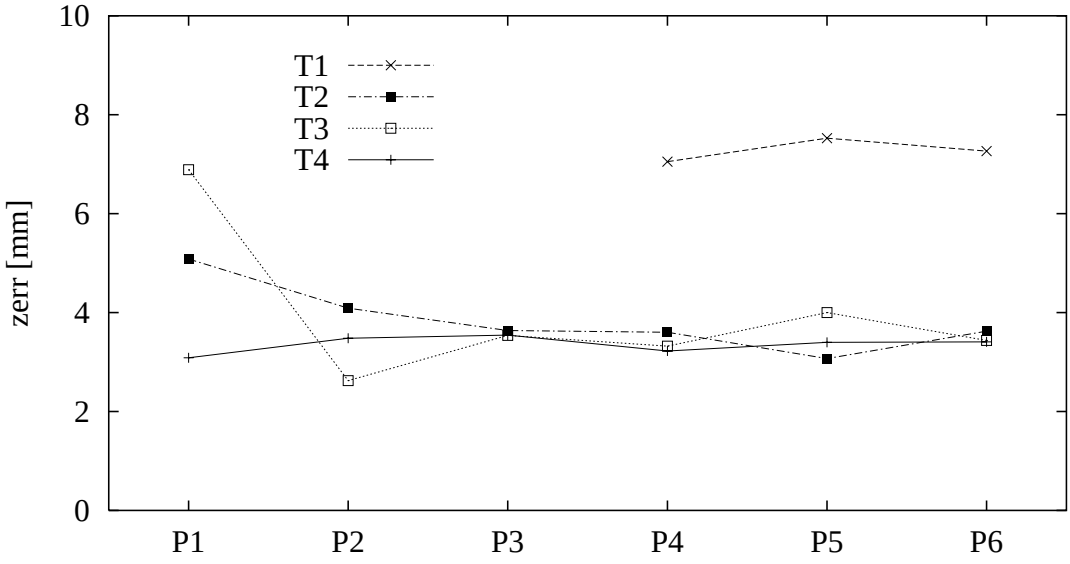

Figure 6.7: Average of z_{err} at each estimated parameters.

Table 6.3: Estimated photometric parameters.

Parameters	Red	Green	Blue
$\alpha'(=\rho_w \cdot a \cdot \alpha)$	1013.32	2923.21	2539.89
$d_y[mm]$	-2.19	1.58	4.26
$d_z[mm]$	-2.01	-11.41	-9.54
$I'_e(=\rho_w \cdot a \cdot I_e)$	-19.82	-28.93	-6.47
Δ	3.89	0.48	-5.78

ratios of each color are shown in Table 6.4. Because of the fluctuation of the illuminant intensity, the white albedo ratios exceed 1.0. The rotaion angle ω is set to $0, 30, 45, 60, 90, 120, 135, 150, 180$[deg.] to each of color papers.

Figure 6.8 shows input images of colored paper where $\omega = 0$[deg.], and Fig.6.9 also shows input images of the white surface where $\omega = 0, 45, 150$[deg.]. Because of the difference of the light source location, image intensities are different at the same point on the surface, so the white surface is colored. Figure 6.10 is the estimated shape of Fig.6.9(b), and Fig.6.11 is the needle map of the surface normal. In these results, shape parameters at edge parts cannot be estimated accurately, because the image intensity can not be observed correctly. In addition, because the light source length is finite, the illuminant intensity is decreasing near the ends of the light source. Hence, the estimated shape is not accurate near these parts.

Table 6.5 shows z_{err} and ϕ_{err} of estimated shapes (in case of $\omega = 0$[deg.]) for each color paper. In this result, the range for the error evaluation is same in each input images. When albedo ratios are higher, the variance of the image intensity can be observed sensitively, hence, not only the white but the colored surface shape can be recovered.

Figure 6.12 shows z_{err} at each rotate angle ω of all colored papers, and Table 6.6 shows averages of estimated point numbers and RMS errors from $\omega = 0$ to 180[deg.] at each colors. When albedo ratios are small, the reflectance intensity at the high part of the model is very small. Hence, it become a few number of points which can estimate shape parameters. On the other hand, when albedo ratios are large, the range which can be estimate shape parameters is expanded. In this case, RMS errors are increasing, but z_{err} is small to the model size (about 6 % of the maximum height), so the model shape can be estimated accurately about z.

But in Table 6.5 and Table 6.6, ϕ_{err} is seemed to be larger than z_{err}. This reason is as follows: the function F in Eq.(6.17) has a sharp valley with respect to the height z, while it has a flat valley to the n_x, n_y, and n_z. Therefore, it is not easy to find optimal n_x, n_y, and n_z. As a result, ϕ_{err} become large. We confirm this property to plot F using actual observed data. Hence, we need more discussions to improve this problem.

Table 6.4: Albedo ratios of colored papers.

Color	ρ'_r	ρ'_g	ρ'_b
blue	0.071	0.100	0.321
red	1.031	0.130	0.147
magenta	1.053	0.143	0.377
green	0.188	0.496	0.227
cyan	0.185	0.666	0.783
yellow	1.135	0.804	0.240
white	1.135	1.061	1.137

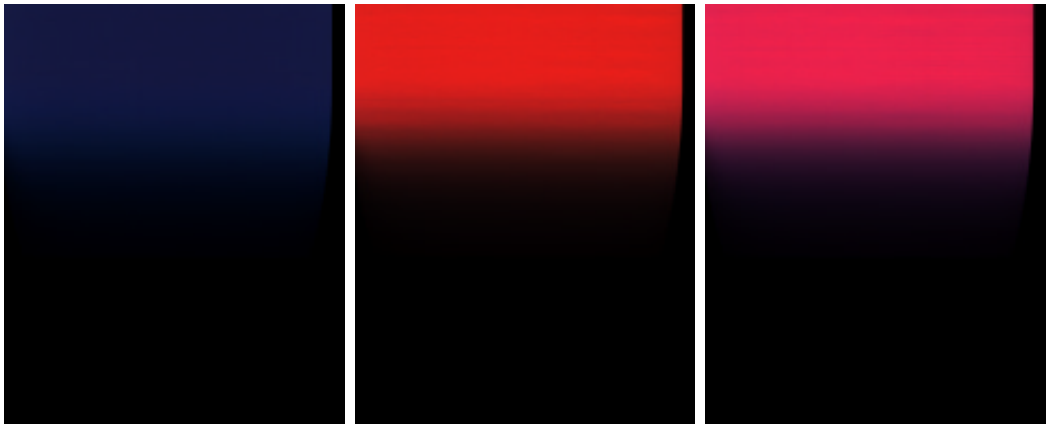

(a) blue (b) red (c) magenta

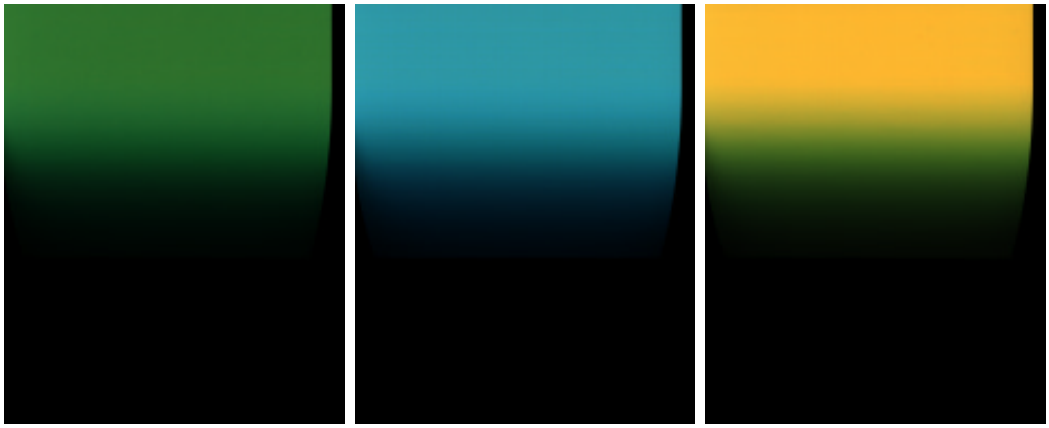

(d) green (e) cyan (f) yellow

Figure 6.8: Input images of cylindrical model ($\omega = 0$[deg.]).

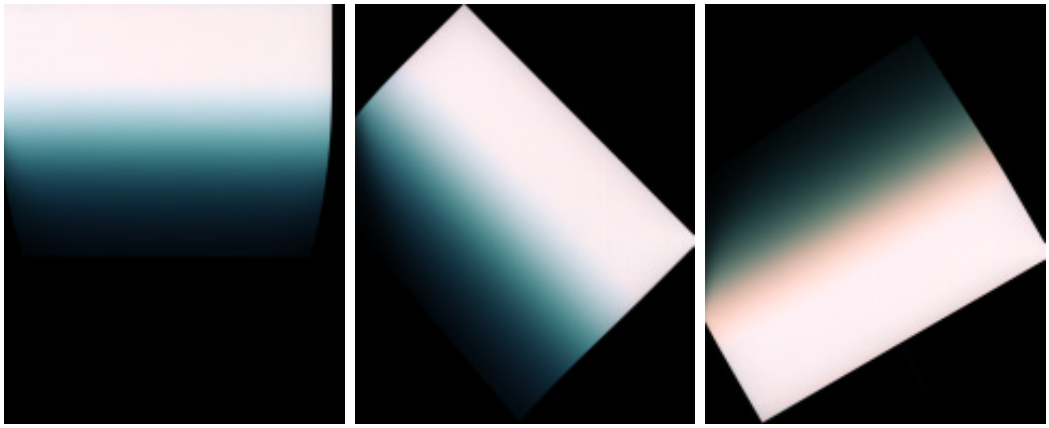

(a) $\omega = 0$. (b) $\omega = 45$. (c) $\omega = 150$.

Figure 6.9: Input images of cylindrical model (white).

Table 6.5: RMS errors of reconstructed shape ($\omega = 0$[deg.]).

Color	z_{err}[mm]	ϕ_{err}[deg.]
blue	1.600	35.46
red	1.253	14.12
magenta	1.066	15.78
green	0.683	18.38
cyan	1.184	29.98
yellow	1.067	11.41
white	0.480	12.13

Table 6.6: Number of shape reconstructed points and RMS errors (average from $\omega = 0$ to 180[deg.]).

Color	Number of points	z_{err}[mm]	ϕ_{err}[deg.]
blue	7350.9	1.384	24.86
red	8861.1	1.886	23.28
magenta	9083.9	1.673	23.81
green	8324.1	1.393	25.78
cyan	8308.6	1.421	27.16
yellow	9727.4	3.024	26.60
white	10365.4	3.407	29.55

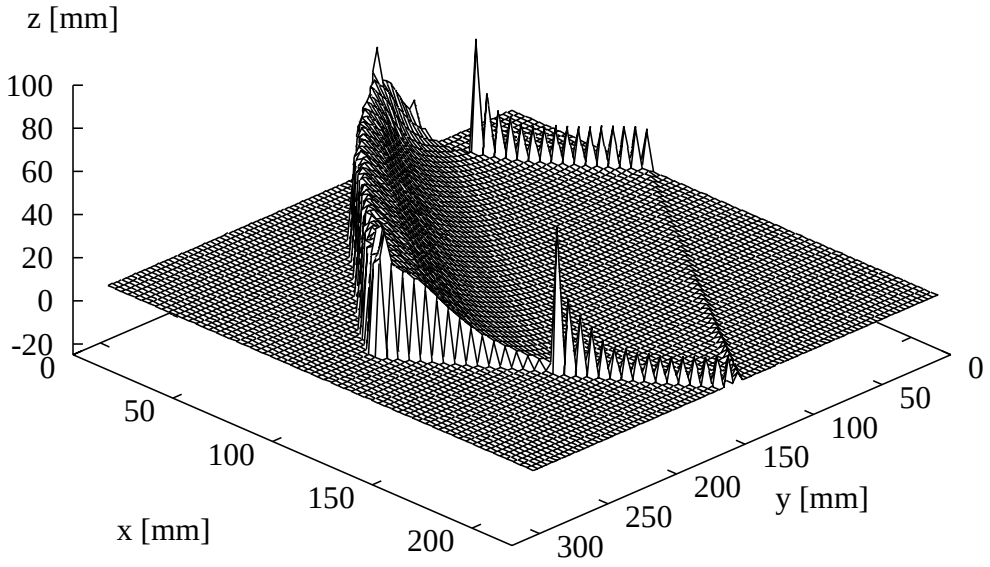

Figure 6.10: Estimated shape of cylindrical model (white, $\omega = 45$[deg.]).

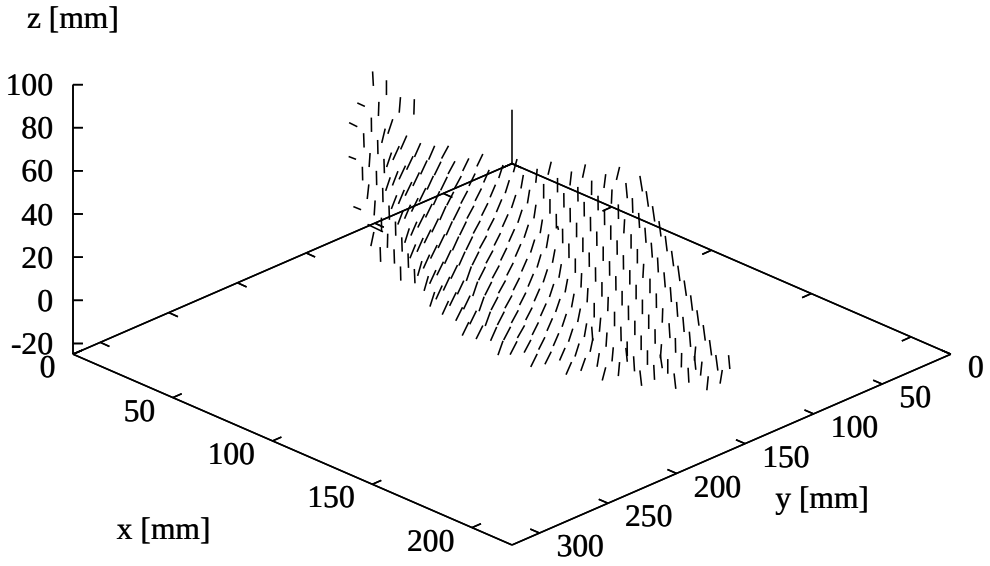

Figure 6.11: Estimated surface normal vectors of cylindrical model.

To compare the proposed method, we examine the another method which uses only non-linear least-squares method. In this method, the initial values are fixed as $(n_x, n_y, n_z) = (0, 0, -1)$ and $z = 0$. This result is shown in Table 6.7. From this result, z_{err} are larger than the proposed method. On the other hand, ϕ_{err} are slightly small, but because the estimated n_x, n_y and n_z tend to include large errors, ϕ_{err} are not so different. Therefore, we can see the proposed algorithm is effective to the shape reconstruction.

We also examine the shape reconstruction of the object with the interreflections. Figure 6.13 (a) is the scanned image of the unfolded book-like shape using two cylindrical models, and (b) is only the upper side model for comparison. In this case, the maximum height $h_{\max} = 23.0$[mm](Figure 6.5). Table 6.8 shows z_{err} of both reconstructed shapes evaluating in the same region affected by the interreflections for (a). Figure 6.14 shows the cross section shapes at $x = x_c$ for (a), (b) and the true shape. Because of the interreflections, the image intensity of (a) is brighter than (b) in the curved surface, so the lower shape is recovered. To recover the general objects, it is necessary to consider the interreflections. However, the interreflections depend on the object shape (Sect.4.2). Hence, it is necessary to discuss the effective method to estimate the interreflections of the arbitrary shape, such as the piecewise shape and albedo approximation in Sect.4.5.2.

Table 6.7: RMS errors in case of using only non-linear least-squares method.

Color	z_{err}[mm]	ϕ_{err}[deg.]
blue	3.340	15.72
red	7.494	21.39
magenta	8.272	22.71
green	5.751	20.05
cyan	5.722	19.93
yellow	11.461	24.88
white	14.729	28.05

Table 6.8: z_{err} of estimated shapes using Fig.4.12.

	z_{err}[mm]
(a) interreflections	3.045
(b) no interreflections	1.374

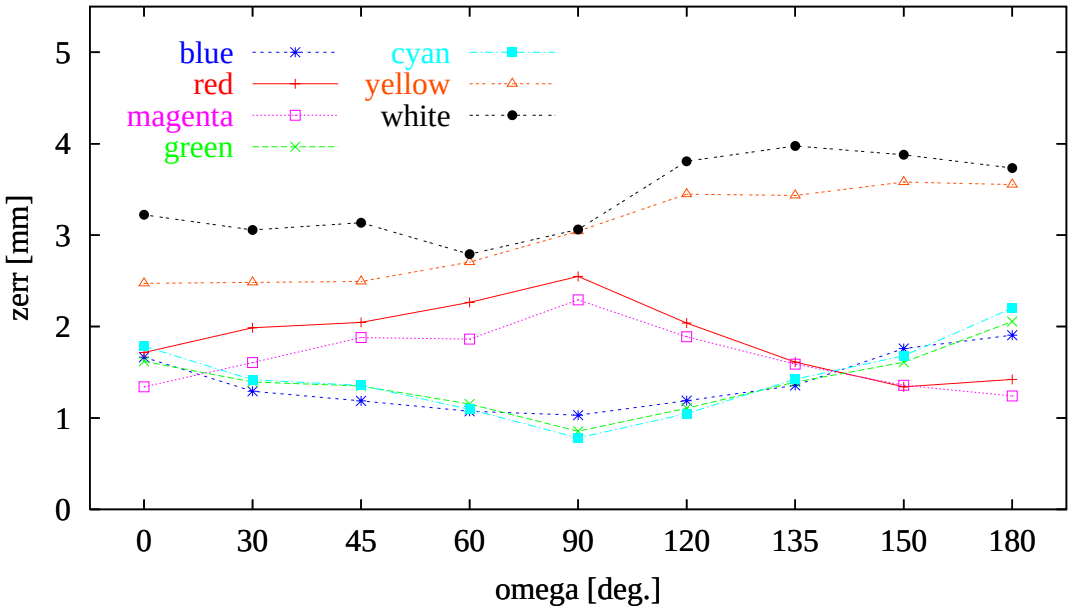

Figure 6.12: z_{err} of cylindrical models.

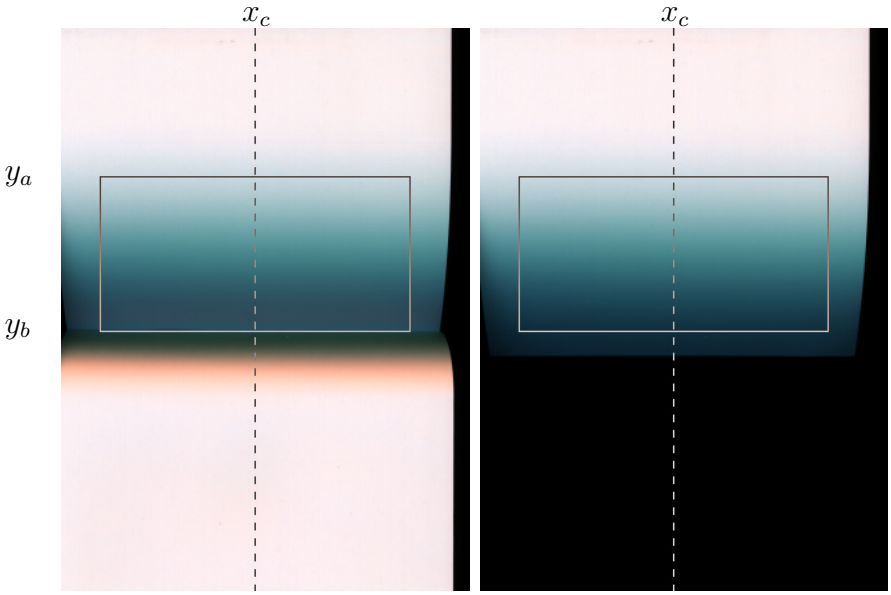

(a) interreflections (b) no interreflections

Figure 6.13: Input images affected/no affected by interreflections.

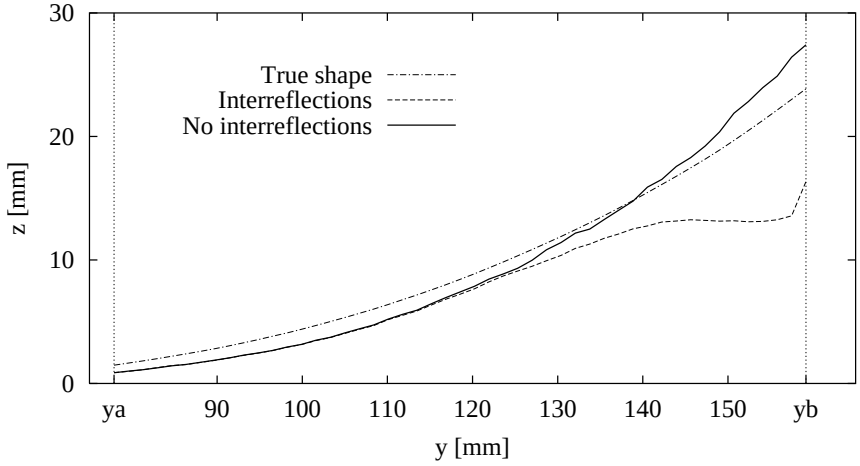

Figure 6.14: Estimated shapes with/without interreflections.

6.5.3 Shape Reconstruction of Real Objects

Next, we show shape reconstruction results of real objects. Figure 6.15 shows the input image of the torus of the toy block as the example of the simple shape. The observed albedo ratios are $\rho'_r = 0.843$, $\rho'_g = 0.310$ and $\rho'_b = 0.505$. Figure 6.16 shows the reconstructed shape and Fig.6.17 is the texture mapped image using re-estimated albedos calculated from the observed intensity, photometric models and the estimated shape. Note that, in Fig.6.16 and the following results, the height z is reversed, and the texture mapping image is painted by using the synthesized illumination.

In Fig.6.17, the part of the surface which albedo is different from other parts means that shape parameters can not be estimated precisely, because if the shape is reconstructed precisely, the albedo on the surface should be constant. In Fig.6.17, because of specular components, some parts of the torus shape can not be estimated precisely, but the whole shape is almost recovered.

As the example of the complex shape, Fig.6.18 shows the input scanned image of the animal puppet, Fig.6.19 is the reconstructed shape and Fig.6.20 is the texture mapped image. Observed albedo ratios are $\rho'_r = 0.909$, $\rho'_g = 0.445$ and $\rho'_b = 0.116$. Because of the interreflections, a part of shape around the puppet's neck is not recovered correctly, but other parts can be recovered accurately.

Figure 6.21 shows the scanned image of the surface of the mouse device which reflectance property is approximated to white Lambertian surface but there are some parts of different albedos. In this case, we use albedo ratios as $\rho'_r = \rho'_g = \rho'_b = 1.0$. Figure 6.22 shows the reconstructed shape and Fig.6.23 is its texture mapped image. The shape can be recovered all over the object but a part of the surface at the wheel button and the printed letters are not recovered because of the difference of the albedo and the reflectance property.

From these experimental results, to recover real objects, we can see that we must consider characteristics in the real world such as the interreflections, lengths of the light sources, specular components, various albedos, and so on. These characteristics make photometric models more complex, so we need more discussion about these problems.

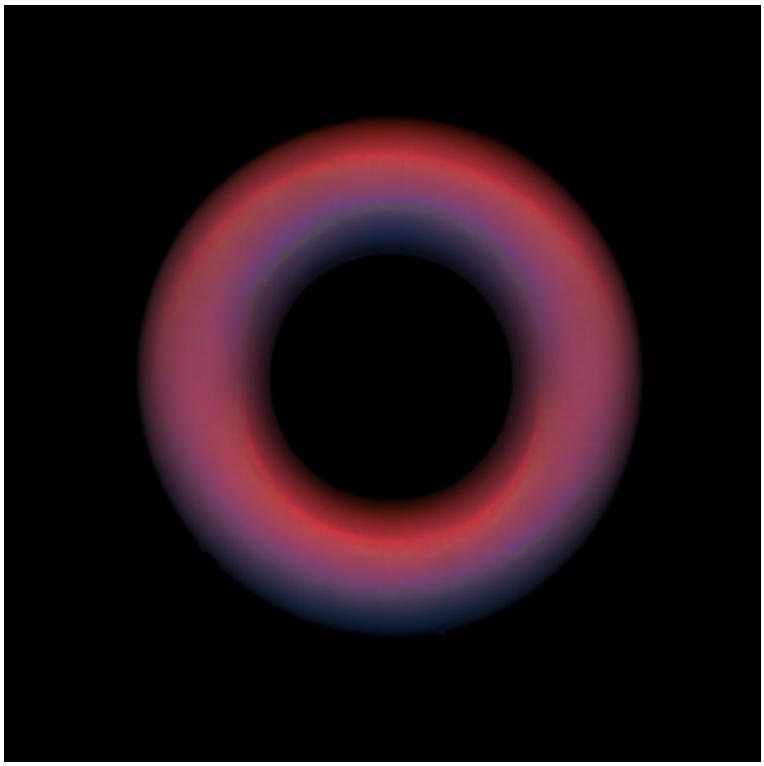

Figure 6.15: Input image of torus (toy block).

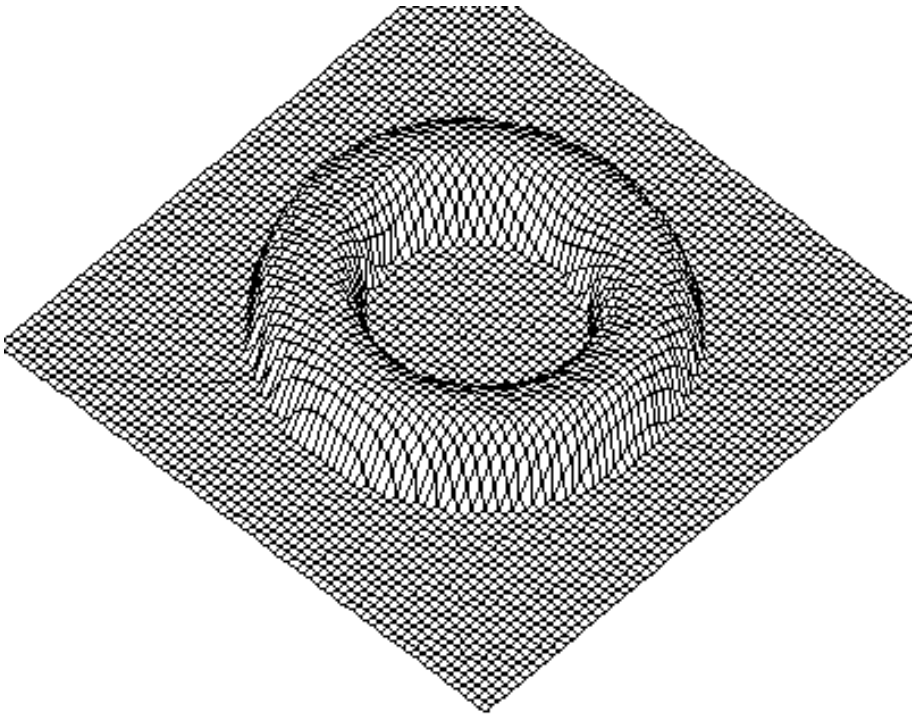

Figure 6.16: Reconstructed shape of torus.

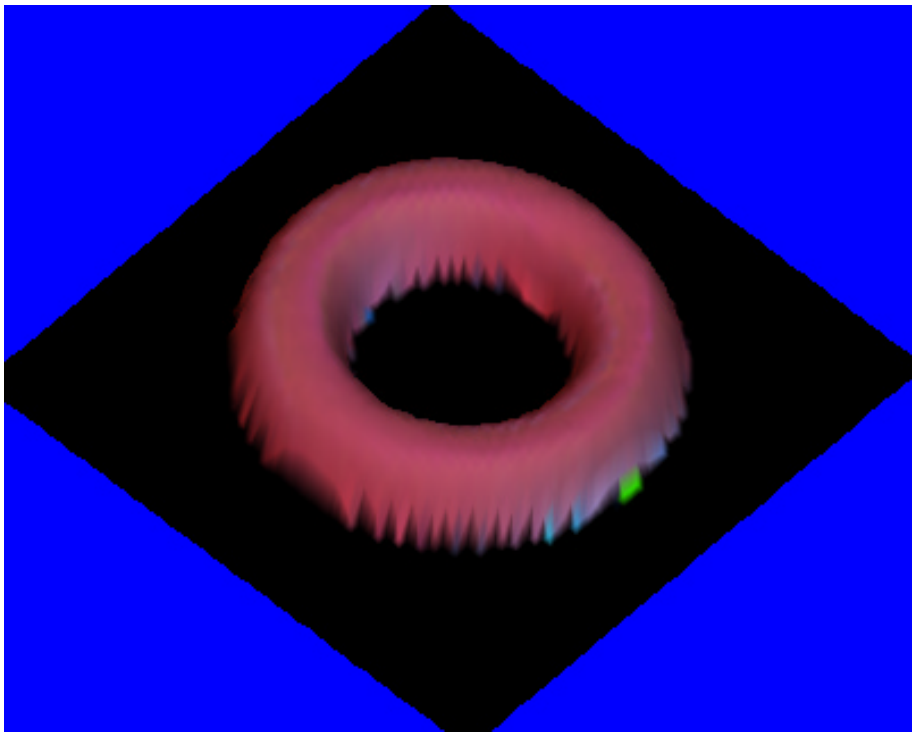

Figure 6.17: Restored texture mapped image of torus.

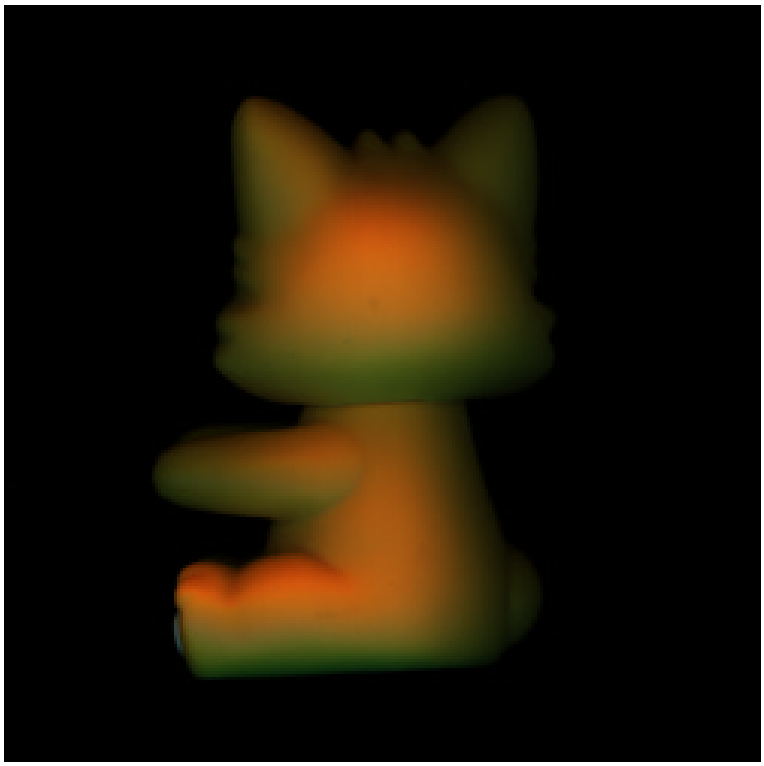

Figure 6.18: Input image of animal puppet.

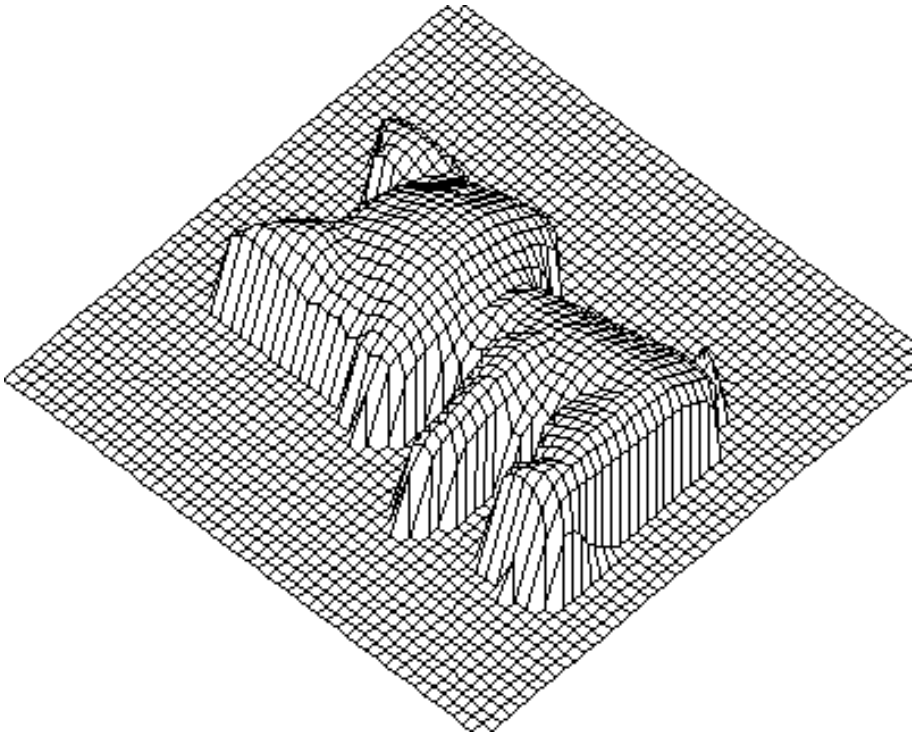

Figure 6.19: Reconstructed shape of animal puppet.

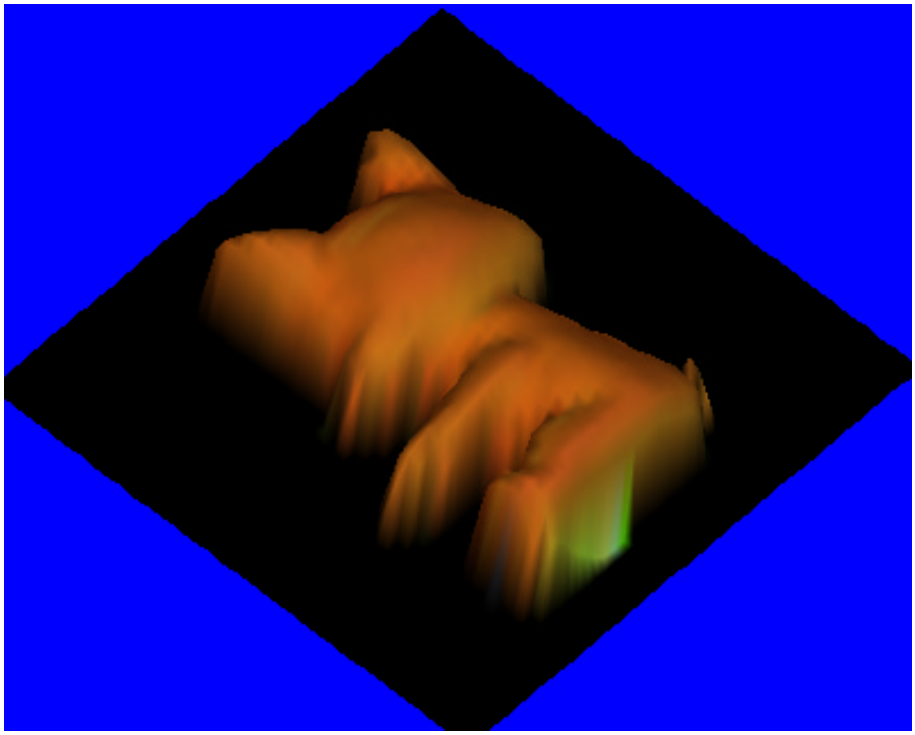

Figure 6.20: Restored texture mapped image of animal puppet.

Figure 6.21: Input image of mouse.

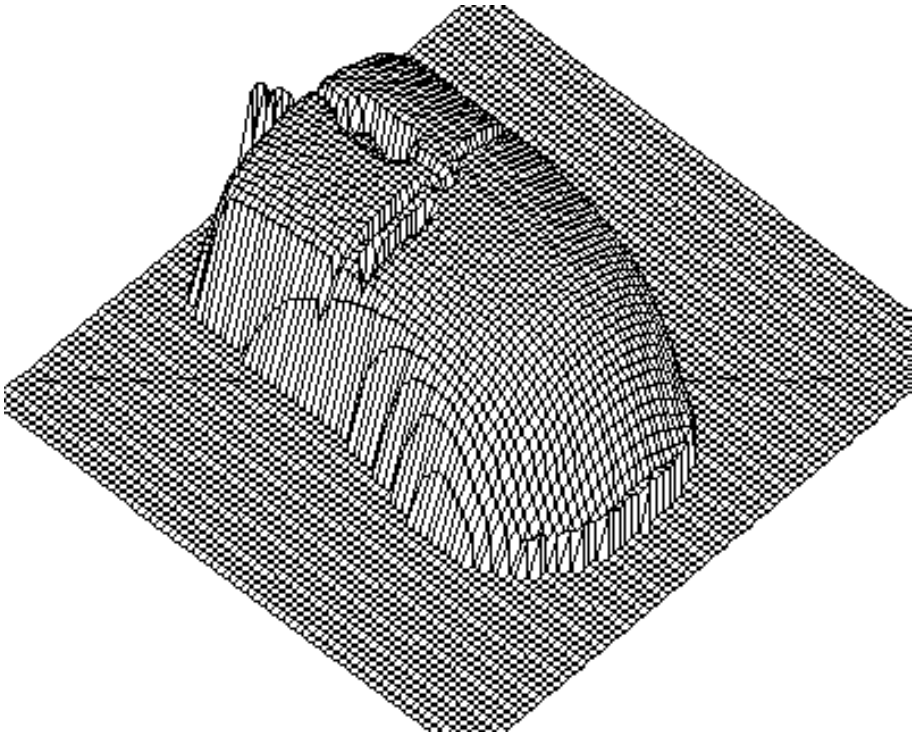

Figure 6.22: Reconstructed shape of mouse.

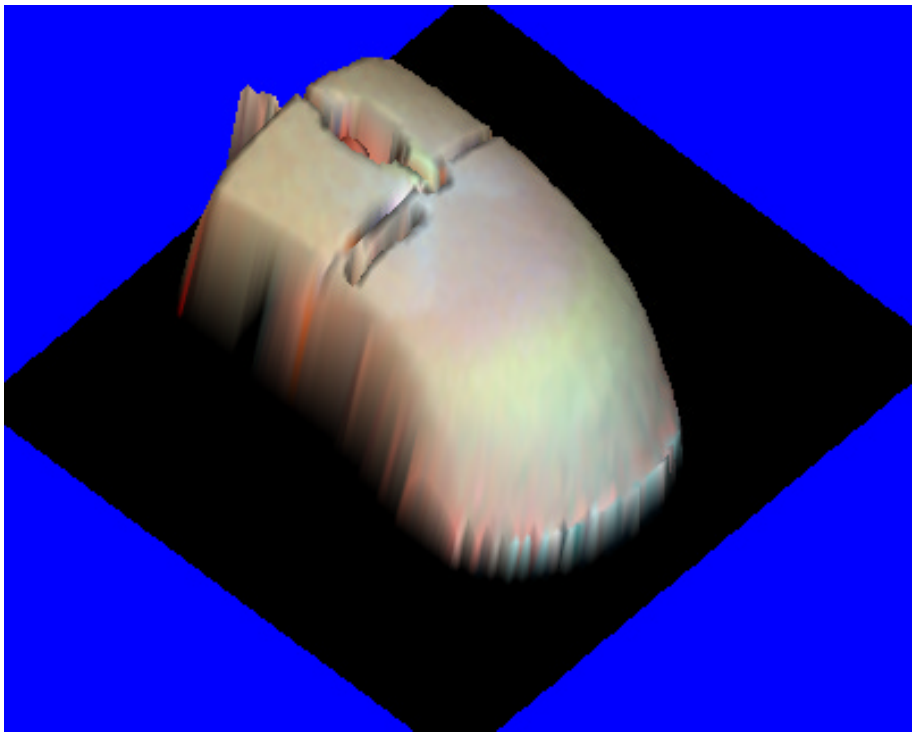

Figure 6.23: Restored texture mapped image of mouse.

6.6 Conclusion

In this chapter, we discuss the shape reconstruction method for an arbitrary shape from a scanned image. Since the arbitrary shape has no constraints for the object shape, it is difficult to apply the appearance-based model described in chapter 5 for the shape reconstruction. Hence, we employ the physically-based model for the shape reconstruction.

Because of the influence of the linear light source in the image scanner, shape parameters we must estimate are the surface normal vector and the distance from the light source to the object surface. These parameters are mutually dependent each other. This mutual relation is still remained, even if we use assumptions to simplify photometric characteristics, which are no interreflections, a Lambertian surface and an uniform albedo distribution. Therefore, to resolve the lack of conditions for shape parameters estimation, we use the color scanned image taken by three different light sources, red, green, and blue. In order to estimate mutual shape parameters efficiently and accurately, we proposed two step shape reconstruction algorithm; estimating initial values by the iterate computation and optimizing parameters by non-linear least squares. From the experimental results of the shape reconstruction using models and real objects, the proposed method is effective for the shape reconstruction not only the white object like a book surface but also the colored object under known albedo value.

The proposed method could estimate the depth from the light source to the object surface accurately, but it was difficult to recover the correct surface normal distribution.

To improve this problem, the objective functional for the parameter estimation should be reexamined. Also, we must discuss the method to recover the object with real world characteristics such as the interreflections, specular components, the difference of the albedo, and so on. In addition, the image scanner can recover only the one side shape, hence it is necessary to integrate partial 3D shapes to obtain the whole object shape.

Chapter 7

Conclusions

In this study, we discussed the problem of the 3D shape reconstruction for a scanned image taken by the image scanner. Here, we dealt with this problem as the shape-from-shading problem and we showed shape reconstruction methods taking account of the shape and shading relations and the photometric and geometric properties of objects.

As the relation between the shape and the shading, we dealt with the physically-based model of the reflection on the object surface and we also employ the appearance-based model constructed by the observed shape and shading profiles. Also, as the object for the shape reconstruction, we used the book surface shape and the 3D arbitrary shape. The geometric and photometric properties of these objects are different to each other. The photometric properties of the book surface is complex because of the interreflections, but since the cross section shape of the book surface can be assumed to be constant, geometric properties are simple. On the other hand, the 3D arbitrary shape has opposite properties because there are no restrictions about its shape, and we assumed no interreflections, a Lambertian surface and an uniform albedo distribution. In this study, we discussed the shape reconstruction methods under the combination of each model and object.

In chapter 2, we surveyed previous shape-from-shading studies from the viewpoint of the photometric and geometric characteristics for the shape reconstruction methods. And, we showed that real world characteristics were included in our study more than previous studies.

In next chapter 3, we described the characteristics of the image scanner. The characteristics of the linear light source in the image scanner make the photometric models complex. But, not only the surface normal vector but also the depth of the surface can be estimated from this characteristics. And, we also showed that the parallel projection along the scanning direction is effective for the shape reconstruction using the appearance-based model.

In chapter 4, the book surface shape reconstruction using the physically-based model was discussed. First, we formulated this shape-from-shading problem taking account of photometric complex properties in order. From this formulation, we could see that the whole book surface shape, depth and albedo distribution are mutually dependent. To recover the book shape under such complex situation, we proposed the iterative non-linear optimization method for the shape reconstruction taking account of geometric constraints of the book surface shape. Moreover, to compute this method effectively, we showed the piecewise approximation for the book surface cross section shape and the albedo

distribution. We also proposed the image restoration method for the geometric distortion and the shading in the scanned image. We confirmed that by using the proposed method, the cross section shape of the book surface could be recovered precisely and the readability of the scanned image could be improved.

In order to recover the book surface in practical time, we need more fast shape reconstruction method. In chapter 5, we discussed the problem of the book surface shape reconstruction using the appearance-based model. Here, a number of observed cross section shape profiles and shading profiles are used for the sample data to construct the relation between the shape and the shading, and they are preserved in eigenspaces to reduce their data size. We proposed the shape reconstruction method by using the local linear transformation between the shading and shape eigenspaces. To recover the book shape accurately, we took account of approximation errors in the linear transformation. And, in order to reduce the number of the sample profiles, we showed the profile normalization method to translate them to the shift-invariant profiles using Fourier transformation. By using the proposed method, the book surface shape could be recovered faster than the physically-based model method proposed in chapter 4, and the effectiveness of the consideration of the approximation error term and the profile normalization are also confirmed. But, in order to recover the various book surface shape, we must consider various properties, such as the reflectance property, the albedo distribution and the arrangement of the book surface on the scanning plane in the shape reconstruction method. This is a residual problem we must discuss.

In chapter 6, we discussed the shape reconstruction of the arbitrary shape by using the physically-based model because the arbitrary shape cannot be applied to the appearance-based model. In this problem, since the linear light source is used in the image scanner, we must estimate the surface normal vector and the distance from the light source simultaneously, so, we proposed the shape reconstruction method using the color scanned image taken by the color image scanner with three light sources. In the proposed method, since the surface normal and the distance are mutually dependent, to estimate these parameters effectively and precisely, parameters are estimated roughly by the iterative calculation and then, optimal parameters are estimated by non-linear least squares. In experimental results, we confirmed that the model and real objects can be recovered their shapes by the proposed method. In this problem, photometric properties are assumed to be simpler situation than the book surface shape reconstruction problem in chapter 4. To recover the various object shapes, we must consider real world photometric properties.

The shape reconstruction using the appearance-based model discussed in chapter 5 is more effective than the physically-based model in the view point of the computation costs. But, if the number of the variation of the object is increased, the number of the sample data also become increased extremely and we cannot apply this method to recover the object shape. To avoid such problem, we seem that the integration of the physically and appearance based model is necessary, for example, the acquisition of the synthesized sample data using the physically-based model.

In the shape reconstruction problem using the physically-based model in chapter 4 and 6, the linear light source in the image scanner makes this problem more difficult than previous shape-from-shading problems. In other words, we must estimate the distance (depth) between the light source and the object surface, but the physically-based model is non-linear with respect to the depth. However, the proposed methods, especially in

chapter 6, used this complex property as the constraint condition, and these methods showed the ability of the shape reconstruction using this condition. In the real world, various light sources are used rather than the parallel light source assumed in previous shape-from-shading problems. This study showed that the shape-from-shading problem can be solved even if under the complex situation in the real world.

To measure the object shape, many measurement devices have been developed such as the arm-typed digitizer, the laser range finder, multiple cameras based on the stereo method, and so on. These devices are usually large scale and expensive, thus everyone can not use such devices. But, the image scanner is not so expensive and can be used by easy operations, hence everyone can acquire the shape information. If the image scanner can be used as the shape scanner, it is useful not only the business use, such as the designs of CAD/CAM system and the virtual reality but also the home use. When the shape scanner become popular in many fields, we seem that the 3D shape information is used as the new media through Internet like texts, sounds, and image data. In future, we will discuss the shape reconstruction method for various objects, and construct the shape acquisition system using the image scanner.

Bibliography

[1] B.K.P.Horn and M.J.Brooks, Shape from Shading, MIT Press, Cambridge, 1989.

[2] O.Faugeras, Three-Dimensional Computer Vision —A Geometric Viewpoint—, MIT Press, Cambridge, 1993.

[3] N.Asada, H.Fujiwara, and T.Matsuyama, "Edge and Depth from Focus," Trans. IEICE D-II, Vol.J77-D-II, No.6, pp.1048–1058, Jun. 1994 (in Japanese).

[4] H.Ohge, H.Ito, and A.Kumamoto, "Image Correction of a Copy Machine Base on the Contour Information of Books," Journal of the Institute of Image Electronics Engineers of Japan, Vol.24, No.4, pp.397–404, Aug. 1998 (in Japanese).

[5] Y.Weng and Q.Zhu, "Nonlinear Shape Restoration For Document Images," Proceedings of IEEE Conference on Computer Vision and Pattern Recognition, pp.568–573, 1996.

[6] T.Araki, H.Guan, and K.Kojima, "Image Recovery Method for Scanned Book Images Using Lines and Characters," Proceedings of IEICE Information and System Society Conference 2001, p.169, 2001 (in Japanese).

[7] Y.Iwahori, H.Kamei, Y.Okugawa, and S.Yamaguchi, "Photometric stereo method considering the effect of interactive reflections," IEICE Technical Report (Image Engineering), IE86-130, pp.69–76, Mar. 1987 (in Japanese).

[8] B.K.P.Horn, "Obtaining shape from shading information," The Psychology of Computer Vision, P.H.Winston, ed., McGraw-Hill Book Co., New York, pp.115–155, 1975.

[9] K.Ikeuchi and B.K.P.Horn, "Numerical Shape from Shading and Occluding Boundaries," Artificial Intelligence, Vol.17, No.1–3, pp.141–184, 1981.

[10] B.K.P.Horn and M.J.Brooks, "The Variational Approach to Shape from Shading," Computer Vision, Graphics and Image Processing, Vol.33, No.2, pp.174–208, 1986.

[11] M.J.Brooks and B.K.P.Horn, "Shape and Source from Shading," Proceedings of the 1985 International Joint Conference on Artificial Intelligence, pp.932–936, 1985.

[12] R.T.Frankot and R.Chellappa, "A Method for Enforcing Integrability in shape from Shading," IEEE Transactions on Pattern Analysis and Machine Intelligence, Vol.10, No.4, pp.439–451, 1988.

[13] D.Lee, "A Provably Convergent Algorithm for Shape from Shading," Proceedings of IEEE Conference on Computer Vision and Pattern Recognition, pp.478–485, 1988.

[14] O.E.Vega and Y.H.Yang, "Shading Logic: A Heuristic Approach to Recover Shape from Shading," IEEE Transactions on Pattern Analysis and Machine Intelligence, Vol.15, No.6, pp.592–597, Jun. 1993.

[15] A.P.Pentland, "Local Shading Analysis," IEEE Transactions on Pattern Analysis and Machine Intelligence, Vol.6, No.2, pp.170–187, Mar. 1984.

[16] C.H.Lee and A.Rosenfeld, "Improved Methods of Estimating Shape from Shading Using the Light Source Coordinate System," Artificial Intelligence, Vol.26, No.2, pp.125–143, 1985.

[17] Q.Zheng and R.Chellappa, "Estimation of Illuminant Direction, Albedo, and Shape from Shading," IEEE Transactions on Pattern Analysis and Machine Intelligence, Vol.13, No.7, pp.680–702, Jul. 1991.

[18] M.Asada, "Cylindrical Shape from Contour and Shading without Knowledge of Lighting Conditions or Surface Albedo", Proceedings of International Conference of Computer Vision, pp.412–416, 1987.

[19] M.Asada and T.Nakamura, "Cylindrical Shape from Contour and Shading without Knowledge of Lighting Conditions or Surface Albedo," Transactions of Information Processing Society of Japan, Vol.34, No.5, pp.884–891, May 1993 (in Japanese).

[20] F.P.Ferrie and M.D.Levine, "Where and Why Local Shading Analysis Works," IEEE Transactions on Pattern Analysis and Machine Intelligence, Vol.11, No.2, pp.198–206, Feb. 1989.

[21] G.Q.Wei and G.Hirzinger, "Parametric Shape-from-Shading by Radial Basis Functions," IEEE Transactions on Pattern Analysis and Machine Intelligence, Vol.19, No.4, pp.353–365, Apr. 1997.

[22] W.Y.Zhao and R.Chellappa, "Symmetric Shape-from-Shading Using Self-ratio Image," International Journal of Computer Vision, Vol.45, No.1, pp.55–75, Oct. 2001.

[23] S.K.Nayar, K.Ikeuchi, and T.Kanade, "Shape from Interreflections," International Conference of Computer Vision, pp.2–11, 1990.

[24] J.Yang, N.Ohnishi, and N.Sugie, "Shape Recovery of Two Concavely Intersectiong Facets from a Single Image with Interreflections," Trans. IEICE D-II, Vol.J78-D-II, No.12, pp.1794–1805, Dec. 1995 (in Japanese).

[25] A.Blake, A.Zisserman, and G.Knowles, "Surface Descriptions from Stereo and Shading," Image and Vision Computing, Vol3, No.4, pp.183–191, 1985.

[26] S.Banerjee, P.S.Sastry, and Y.V.Venkatesh, "Surface Reconstruction from Disparate Shading: An Integration of Shape-from-Shading and Stereopsis," Proceedings of 11th International Conference on Pattern Recognition, pp.141–144, Jun. 1992.

[27] J.Malik and D.Maydan, "Recovering Three Dimensional Shape from a Single Image of Curved Objects," IEEE Transactions on Pattern Analysis and Machine Intelligence, Vol.11, No.6, pp.555–566, Jun. 1989.

[28] Y.Choe and R.L.Kashyap, "3-D Shape from a Shaded and Textural Surface Image," IEEE Transactions on Pattern Analysis and Machine Intelligence, Vol.13, No.9, pp.907–919, Sep. 1991.

[29] R.J.Woodham, "Photometric Method for Determining Surface Orientation from Multiple Images," Optical Engineering, Vol.19, No.1, pp.139–144, 1980.

[30] K.Ikeuchi, "Determining Surface Orientations of Specular Surfaces by Using the Photometric Stereo Method," IEEE Transactions on Pattern Analysis and Machine Intelligence, Vol.3, No.6, pp.661–669, Nov. 1981.

[31] K.Ikeuchi, "Determining 3D Shape from Shading Information Based on the Reflectance Map Technique," Trans. IECE Japan, Part D, Vol.J65-D, No.7, pp.842–849, Jul. 1982 (in Japanese).

[32] Y.Iwahori, N.Hiratsuka, H.Kamei, and S.Yamaguchi, "Extended Photometric Stereo for an Object with Unknown Reflectance Property," Trans. IEICE D, Vol.J71-D, No.1, pp.110–117, Jan. 1988 (in Japanese).

[33] S.K.Nayar, K.Ikeuchi, and T.Kanade, "Determining Shape and Reflectance of Hybrid Surfaces by Photometric Sampling," IEEE Transactions on Robotics and Automation, Vol.6, No.4, pp.418–431, Aug. 1990.

[34] H.D.Tagare and R.J.P.deFigueiredo, "Simultaneous Estimation of Shape and Reflectance Map from Photometric Stereo," Computer Vision, Graphics and Image Processing: Image Understanding, Vol.55, No.3, pp.275–286, May, 1992.

[35] H.D.Tagare and R.J.P.deFigueiredo, "A Framework for the Construction of Reflectance Maps for Machine Vision," Computer Vision, Graphics and Image Processing: Image Understanding, Vol.57, No.3, pp.265–282, May 1993.

[36] Y.Iwahori, H.Kamei, Y.Okugawa, and S.Yamaguchi, "Photometric Stereo Method Considering the Effect of Iteractive Reflections," IEICE Technical Report (Image Engineering), Vol.86, pp.69–76 (IE86–130), 1986 (in Japanese).

[37] S.I.Cho, H.Saito, and S.Ozawa, "Shape Recovery of Book Surface Using Two Shade Images Under Perspective Condition," Trans. of The Institute of Electrical Engineers of Japan, Vol.117-C, No.10, pp.1384–1390, 1997.

[38] R.Onn and A.Bruckstein, "Integrability Disambiguates Surface Recovery in Two-Image Photometric Stereo," International Journal of Computer Vision, Vol.5, No.1, pp.105–113, 1990.

[39] K.M.Lee and C.C.J.Kuo, "Shape from Shading with Perspective Projection," Computer Vision, Graphics and Image Processing: Image Understanding, Vol.59, No.2, pp.202–212, Mar. 1994.

[40] J.Yang, N.Ohnishi, and N.Sugie, "Shape Recovery and Reflectance Estimation of a Polyhedron by Two-Image Photometric Stereo," Trans. IEICE D-II, Vol.J78-D-II, No.2, pp.292–301, Feb. 1995 (in Japanese).

[41] Y.Iwahori, H.Sugie, and N.Ishi, "Photometric Stereo under Illumination from Unknown Zenith Angles," Trans. IEICE D-II, Vol.J74-D-II, No.3, pp.321–329, Mar. 1991 (in Japanese).

[42] Y.Iwahori, H.Kamei, and S.Yamaguchi, "Point Source Illumination Stereo for Objects with Uniform Reflectance," Trans. IEICE D, Vol.J71-D, No.10, pp.2086–2094, Oct. 1988 (in Japanese).

[43] H.Kamei and S.Yamaguchi, "A Method for Reconstructing the Shape of an Object from Two Images Taken under Point Light Source Illumination," Trans. IEICE D, Vol.J71-D, No.11, pp.2319–2326, Nov. 1988 (in Japanese).

[44] B.Kim and P.Burger, "Depth and Shape from Shading Using the Photometric Stereo Method," Computer Vision, Graphics and Image Processing: Image Understanding, Vol.54, No.3, pp.416–427, Nov. 1991.

[45] C.Cho and H.Minamitani, "A New Photometric Method Using 3 Point Light Sources," IEICE Trans. on Inf. & Syst., Vol.E76-D, No.8, pp.898–904, Aug. 1993.

[46] S.Kaneko, Y.Tomita, and T.Honda, "Photometric Stereo by Simultaneous Illumination with Three Colored Lights," Trans. IEICE D-II, Vol.J76-D-II, No.10, pp.2243–2246, Oct. 1993 (in Japanese).

[47] P.H.Christensen and L.G.Shapiro, "Three-Dimensional Shape from Color Photometric Stereo," International Journal of Computer Vision, Vol.13, No.2, pp.213–227, 1994.

[48] T.Okatani and K.Deguchi, "Reconstructing Surface Shape from Shading Using Eigenspace Method," IPSJ SIG Notes (Computer Vision), Vol.95, No.93, pp.1–7 (CV93-1), Mar. 1995 (in Japanese).

[49] R.Zhang, P.S.Tsai, J.E.Cryer, and M.Shah, "Shape from Shading: A Survey," IEEE Transactions on Pattern Analysis and Machine Intelligence, Vol.21, No.8, pp.690–705, Aug. 1999.

[50] B.K.P.Horn and R.W.Sjoberg, "Calculating the Reflectance Map," Applied Optics, Vol.18, No.11, pp.1770–1779, 1979.

[51] S.K.Nayar, K.Ikeuchi, and T.Kanade, "Surface Reflection: Physical and Geometrical Perspectives," IEEE Transactions on Pattern Analysis and Machine Intelligence, Vol.13, No.7, pp.611–634, Jul. 1991.

[52] S.Tominaga and S.Ohhashi, "A Color Reflection Model for Object Surfaces," Transactions of Information Processing Society of Japan, Vol.33, No.1, pp.37–45, Jan. 1992 (in Japanese).

[53] B.T.Phong, "Illumination for computer generated pictures," CACM, Vol.18, No.6, pp.311–317, Jun. 1975.

[54] K.E.Torrance and E.M.Sparrow, "Theory of off-specular reflection from roughened surfaces," Journal of the Optical Society of America, Vol.57, No.9, pp.1105–1114, Sept. 1967.

[55] M.S.Langer and S.W.Zuchker, "Casting Light on Illumination: A Computational Model and Dimensional Analysis of Sources," Computer Vision and Image Understanding, Vol.65, No.2, pp.322–335, Feb. 1997.

[56] H.D.Ballard and C.M.Brown, "Computer Vision," Prentice Hall, Inc., Englewood Cliffs, New Jersey, pp.93-102, 1982.

[57] J.Rissanen, "Modeling By Shortest Data Description," Automatica, Vol.14, pp.465–471, 1978.

[58] S.Ullman and R.Basri, "Recognition by Linear Combinations of Models," IEEE Transactions on Pattern Analysis and Machine Intelligence, Vol.11, No.10, pp.992–1006, Oct. 1991.

[59] H.Murase, F.Kimura, M.Yoshimura, and Y.Miyake, "An Improvement of the Auto-Correlation Matrix in the Pattern Matching Method and Its Application to Hand-printed "HIRAGANA" Recognition," Trans. IEICE D, Vol.J64-D, No.3, pp.276–283, Mar. 1981 (in Japanese).

[60] M.A.Turk and A.P.Pentland, "Face Recognition Using Eigenfaces," Proceedings of IEEE Conference on Computer Vision and Pattern Recognition, pp.586–591, Jun. 1991.

[61] S.Akamatsu, T.Sasaki, H.Fukamachi, and Y.Suenaga, "Robust Face Identification by Pattern Matching Based on KL Expansion of the Fourier Spectrum," Trans. IEICE D-II, Vol.J76-D-II, No.7, pp.1363–1373, Jul. 1993 (in Japanese).

[62] A.Pentland, B.Moghaddam, and T.Starner, "View-Based and Modular Eigenspaces for Face Recognition," Proceedings of IEEE Conference on Computer Vision and Pattern Recognition, pp.84–91, 1994.

[63] H.Murase and S.K.Nayar, "3D Object Recognition from Appearance —Parametric Eigenspace Method—," Trans. IEICE D-II, Vol.J77-D-II, No.11, pp.2179–2187, Nov. 1994 (in Japanese).

[64] H.Murase, "CVCV-WG Reports: Technical Review and Views in Computer Vision (VI) – Image Recognition in Eigenspace –," IPSJ SIG Notes (Computer Vision), Vol.95, No.108, pp.59–66 (CV97-9), Nov. 1995 (in Japanese).

[65] S.K.Nayer, S.A.Nene, and H.Murase, "Subspace Methods for Robot Vision," IEEE Transactions on Robotics and Automation, Vol.12, No.5, pp.750–758, Oct. 1996.

[66] J.W.Kim, K.Okazaki, Y.Sato, and S.Tamura, "Pose estimation of an image using parametric eigen spaces of edge images," IPSJ SIG Notes (Computer Vision and Image Media), Vol.96, No.115, pp.33–40 (CVIM102-5), Nov. 1996.

[67] Y.Fujimoto, H.Iwasa, N.Yokoya, and H.Takemura, "Retrieval of Image Sequences Base on Similarity of Trajectories in Eigenspaces," IEICE Technical Report (Pattern Recognition and Media Understanding), Vol.96, No.435, pp.49–56 (PRMU96-110), Dec. 1996 (in Japanese).

[68] S.Maeda, Y.Kuno, and Y.Shirai, "Mobile Robot Localization Based on Eigenspace Analysis," Trans. IEICE D-II, Vol.J80-D-II, No.6, pp.1502–1511, Jun. 1997 (in Japanese).

[69] A.Watanabe and H.Saito, "Estimation of Face Pose from Grayscale Image using Eigenspace Method," IEICE Technical Report (Pattern Recognition and Media Understanding), Vol.97, No.204, pp.111–116 (PRMU97-71), Jul. 1997 (in Japanese).

[70] K.Yagishita and M.Yamamoto, "Estimation of Human Pose from A Single Camera View by Inverse Kinematics and Eigenspace," IEICE Technical Report (Pattern Recognition and Media Understanding), Vol.99, No.306, pp.53–60 (PRMU99-85), Sep. 1999 (in Japanese).

[71] K.Deguchi and T.Noguchi, "On the Optimal Sub-Space Construction for Visual Servoing by the Eigen Space Method," Trans. IEICE D-II, Vol.J80-D-II, No.6, pp.1522–1529, Jun. 1996 (in Japanese).

[72] G.Strang, Linear Algebra and its Applications, Academic Press, New York, 1976.

[73] T.F.Chan and C.K.Wong, "Convergence of the alternating minimization algorithm for blind deconvolution," Linear Algebra and its Applications, Vol.316, No.1-3, pp.259–285, Sep. 2000.

[74] W.H.Press, et al., Numerical Recipes in C, Cambridge University Press, 1988.

Related Works

Papers

1. T.Wada, H.Ukida, and T.Matsuyama, "Recovering 3D Shape of Unfolded Book Surface from a Scanner Image (I) — Shape from Shading under Proximal Light Source —," Trans. IEICE D-II, Vol.J77-D-II, No.6, pp.1059–1067, Jun. 1994 (in Japanese).

2. T.Wada, H.Ukida, and T.Matsuyama, "Recovering 3D Shape of Unfolded Book Surface from a Scanner Image (II) — Shape from Shading with Interreflectons under Proximal Light Source —," Trans. IEICE D-II, Vol.J78-D-II, No.2, pp.311–320, Feb. 1995 (in Japanese).

3. T.Wada, H.Ukida, and T.Matsuyama, "Shape from Shading with Interreflections Under a Proximal Light Source: Distortion-Free Copying of an Unfolded Book," International Journal of Computer Vision, Vol.24, No.2, pp.125–135, Sep. 1997.

4. H.Ukida, K.Konishi, T.Wada, and T.Matsuyama, "Recovering 3D Shape of Unfolded Book Surface from a Scanner Image Using Eigenspace Method," Trans. IEICE D-II, Vol.J83-D-II, No.12, pp.2610-2621, Dec. 2000 (in Japanese).

5. H.Ukida and K.Konishi, "3D Shape Reconstruction Using Three Light Sources in Image Scanner," IEICE Trans. on Inf. & Syst., Vol.E84-D, No.12, pp.1713–1721, Dec. 2001.

International Conferences

1. H.Ukida, T.Wada, and T.Matsuyama, "3D Shape Reconstruction of Unfolded Book Surface from a Scanner Image," Proceedings of IAPR Workshop on Machine Vision Applications, pp.409–412, 13-15 Dec. 1994, Kawasaki, Japan.

2. T.Wada, H.Ukida, and T.Matsuyama, "Shape from Shading with Interreflections under Proximal Light Source, — 3D Shape Reconstruction of Unfolded Book Surface from a Scanner Image —," Proceedings of 5th International Conference of Computer Vision, pp.66–71, 20-23 Jun. 1995, Boston, USA. (Marr Prize)

3. H.Ukida and K.Konishi, "3D Shape Reconstruction using Three Light Sources in Image Scanner," Proceedings of IAPR Workshop on Machine Vision Applications, pp.201–204, 28-30 Nov. 2000, Tokyo, Japan.

4. H.Ukida, K.Konishi, T.Wada, and T.Matsuyama, "Recovering Shape of Unfolded Book Surface from a Scanner Image usign Eigenspace Method," Proceedings of IAPR Workshop on Machine Vision Applications, pp.463–466, 28-30 Nov. 2000, Tokyo, Japan.

Domestic Conferences

1. H.Ukida, T.Wada, and T.Matsuyama, "Shape from Shading under Attenuating Illumination —Restoring Distorted Scanner Image of Unfolded Book Surface —," IPSJ SIG Notes (Computer Vision), Vol.93, No.7, pp.9–16 (CV81-2), Jan. 1993 (in Japanese).

2. H.Ukida, T.Wada, and T.Matsuyama, "3D Shape Reconstruction of Unfolded Book Surface using an Image Scanner (II) — Shape from Shading with Interreflections under Proximal Light Source —," Proceedings of Meeting on Image Recognition and Understanding (MIRU'94) , pp.I-91–I-98, Jul. 1994 (in Japanese).

3. H.Ukida and K.Konishi, "Recovering 3D shape of Unfolded Book Surface from a Scanner Image usign Eigenspace Method," IEICE Technical Report (Pattern Recognition and Media Understanding), Vol.99, No.380, pp.23–30 (PRMU99-91), Oct. 1999 (in Japanese).

4. H.Ukida and K.Konishi, "3D Object Shape Reconstruction using Three Light Sources in Image Scanner," Proceedings of JSME Chugoku-Shikoku Branch Symposium in Tokushima, No.005–2, pp.223–224, Oct. 2000 (in Japanese).